Towards understanding and improving the safety of informal public transport in Sub-Saharan Africa: A real-time sensing and reporting system for minibus taxis

by

Adriaan Siebrits Zeeman

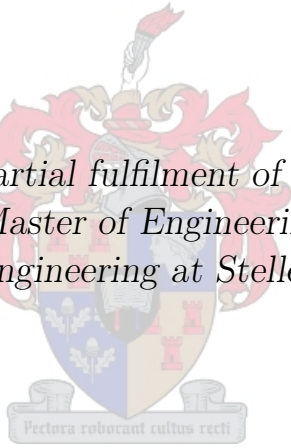

Thesis presented in partial fulfilment of the requirements for the degree of Master of Engineering (Research) in the Faculty of Engineering at Stellenbosch University

Supervisor:
Mr. M.J. Booysen
Department of Electrical & Electronic Engineering,
Stellenbosch University.

December 2013

Declaration

By submitting this thesis electronically, I declare that the entirety of the work contained therein is my own, original work, that I am the sole author thereof (save to the extent explicitly otherwise stated), that reproduction and publication thereof by Stellenbosch University will not infringe any third party rights and that I have not previously in its entirety or in part submitted it for obtaining any qualification.

Date: December 2013 .....

Abstract

Developed countries have led the way in the implementation of Intelligent Transport Systems (ITS), with the main objectives of improving road safety and efficiency. Current ITS solutions are heavily dependent on advanced and expensive technologies, and do not necessarily meet the unique requirements of public transportation in Sub-Saharan Africa (SSA). The informal minibus taxi sector dominates public transport in SSA in general, and in South Africa in particular, and is notoriously dangerous – leading to many fatalities annually.

This work presents the design and testing of a sensing and reporting system for public transport in SSA. The system contributes to improving the safety and efficiency of minibus taxis in SSA. The system provides three core functions, namely, reckless driving detection, multiple occupancy detection, and wireless reporting to a visualised online platform.

The reckless driving detection system implements a novel model that augments inertial vehicle acceleration data with GPS speed information. The model is based on standards used in road design, and takes into account the relationship between a vehicle's tyres and the road surface. A lateral acceleration threshold, which is speed dependant, and a longitudinal acceleration threshold are suggested to detect reckless driving. Acceleration data is filtered to remove both high-frequency noise and zero-frequency offset, and compared to the thresholds to detect reckless driving events.

The occupancy detection system detects multiple occupants in the minibus taxi using low-cost capacitive sensor electrodes, which utilise the electrical field properties of a human body for presence detection. A simplified mathematical model was created to calculate the expected capacitance on the occupancy sensor electrode, and was compared to the measured capacitance in the minibus taxi. The theoretical and empirical results demonstrate that the capacitance of an occupied seat is more than double that of an unoccupied seat. Occupants were clearly detected in various scenarios, such as different occupant sizes, water on seat, various seated positions on the sensor, etc.

The wireless reporting inside the vehicle is implemented using a ZigBee network on an Arduino platform. The extra-vehicle wireless reporting uses the existing SSA cellular network, and the online data visualisation is implemented on Trinity Telecoms' SMART platform. The complete sensing and reporting system is implemented as a prototype, and tested in South African and Ugandan minibus taxis.

The results demonstrate that the system achieves the set goals, and could be used to make transport in SSA safer and more efficient.

Uittreksel

Ontwikkelde lande neem die voortou met die implementering van Intelligente Vervoer Stelsels (IVS) met die hoof doelwit om padveiligheid en vervoerstelsels se effektiwiteit te verbeter. Huidige stelsels wat ontwikkel is vir IVS is baie afhanklik van duur en gevorderde tegnologieë en bevredig dus nie die huidige vereistes binne die openbare vervoer stelsel van Sub-Sahara Afrika (SSA) nie. Die minibus taxi sektor domineer die openbare vervoer stelsel in SSA en meer spesifiek in Suid-Afrika, en daar is jaarliks duisende ongelukke waarvan baie tot sterftes lei.

In hierdie werkstuk word daar 'n stelsel voorgestel wat minibus taxi's in SSA kan monitor. Die doel van die stelsel is om die openbare vervoerstelsel se effektiwiteit en padveiligheid te verbeter. Die stelsel bestaan uit: roekelose bestuur opsporing, veelvoudige-passasier waarneming (monitor van aantal passasiers in voertuig) en network verslagdoening na 'n aanlyn platform.

'n Nuwe model is ontwikkel om roekelose bestuur op te spoor – deur die voertuig se versnelling en spoed te kombineer in berekenings. Die model se berekenings is ook gebasseer op die verwantskap tussen die voertuig se bande en die padoppervlak. Roekelose bestuur word bespeur deur 'n laterale en longitudinale drempel wat spoed afhanklik is. Versnellingsdata word gefilter om hoë-frekwensie geraas en nul-frekwensie afwykings te verwyder. Gefilterde data word dan met die gepaste drempel vergelyk om te bepaal of die bestuurder 'n roekelose beweging uitgevoer het.

Die veelvoudige-passasier waarnemingstelsel is getoets in 'n minibus taxi en bestaan uit 'n lae-koste kapasitiewe sensor stelsel. Die stelsel meet 'n passasier se liggaamlike elektriese lading. 'n Wiskundige uitrukking van die kapasitiewe sensor stelsel is bepaal wat 'n teoretiese kapasitansie waarde gee. Dié waarde is met die gemete kapasitansie op die sensor elektrode vergelyk. Die resultate bevestig dat die ontwikkelde stelsels duidelik 'n sittende passasier kan identifiseer. Verskeie toetse is gedoen om te verseker dat die kapasitiewe stelsel gepas is vir die heterogene minibus taxi omgewing.

Draadlose verslagdoening word binne die voertuig uitgevoer met behulp van 'n ZigBee netwerk wat geïmplementeer is op 'n Arduino platform. Die buite-voertuig verslagdoening stelsel gebruik bestaande sellulêre kommunikasie netwerke en die inligting word dan op Trinity Telecoms' SMART platform visueel vertoon. Die volledige ontwikkelde stelsel is as 'n prototipe geïmplementeer en getoets in Suid-Afrikaanse en Ugandese minibus taxi's.

Die resultate toon aan dat die stelsel die doelwitte bereik en dat dit gebruik kan word om die vervoer stelsel in Suid Afrika veiliger en meer doeltreffend te maak.

Publications

Work in this manuscript has been accepted for publication as follows:

- A.S. Zeeman, M.J. Booysen, G. Ruggeri, and B. Laganá, "Capacitive seat sensors for multiple occupancy detection using a low-cost setup", *2013 IEEE International Conference on Industrial Technology (ICIT)*, pp.1228-1233, 25-28 Feb. 2013, Cape Town, South Africa.
- A.S. Zeeman, and M.J. Booysen, "Combining speed and acceleration to detect reckless driving in the informal public transport industry", *16th International IEEE Conference on Intelligent Transportation Systems*, 6-9 Oct. 2013, The Hague, The Netherlands.
- M.J. Booysen, S.J. Andersen, A.S. Zeeman, "Informal public transport in Sub-Saharan Africa as a vessel for Novel Intelligent Transport Systems", *16th International IEEE Conference on Intelligent Transportation Systems*, 6-9 Oct. 2013, The Hague, The Netherlands.

Acknowledgements

First and above all, I praise God, the almighty for providing me with this opportunity and giving me the ability to proceed successfully. This thesis appears in its current form due to the assistance and guidance of several people. I would therefore like to offer my sincere gratitude to the following people and organisations:

- Mr. Thinus Booysen for accepting me as a Masters student, his thoughtful guidance, critical comments, and correction of the thesis. I would also like to thank him for opening a lot of doors to me, giving me exposure to interesting meetings, organising incredible study opportunities abroad, and his accessibility and willingness to help me at any time.
- Mr. Roodt for giving me insight into the civil engineering aspect of this thesis, and providing me with valuable information on road design and vehicle dynamics.
- Dr. De Villiers for all his assistance regarding the mathematical model of the capacitive occupancy sensor.
- The Electrical & Electronic Engineering department at Stellenbosch University for their financial assistance towards this research.
- MTN and Trinity Telecomms, who supported this work with their technical and financial assistance.
- Professor Antonella Molinaro and the Università degli Studi Mediterranea di Reggio Calabria for the opportunity and financial assistance to visit your university.
- All the members of the Electronic Systems Laboratory who created a pleasant working environment over the past two years.
- Family for their support, willingness to help, and late night hours of language reviewing.

Contents

List of Figures

List of Tables

Nomenclature

Abbreviations and acronyms

ITS	Intelligent Transport Systems
SSA	Sub-Saharan Africa
GPS	Global Positioning System
CVO	Commercial Vehicle Operations
ARTS	Advanced Rural Transportation Systems
APTS	Advanced Public Transportation Systems
TIS	Traveller Information Systems
IVI	Intelligent Vehicle Initiative
ETC	Electronic Toll Collection
ISO	International Organization for Standardization
IT	Information Technology
FMS	Freeway Management System
WHO	World Health Organization
NHTSA	National Highway Traffic Safety Administration
IVDR	In-Vehicle Data Recorder
WiMAX	Worldwide Interoperability for Microwave Access
3G	3rd Generation International Mobile Telecommunications
LTE	Long Term Evolution
V2I	Vehicle to Infrastructure
M2M	Machine-to-Machine
OBU	On-Board Unit
V2I	Vehicle to Infrastructure
ISA	Intelligent Speed Adaptation
ESC	Electronic Stability Control
ECU	Electronic Control Unit
EDR	Accident Data Recorder
TPMS	Tyre Pressure Monitoring Systems

Lidar	Light detection and ranging
LDW	Lane Departure Warning
BSD	Blind Spot Detection
HMM	Hidden Markov Model
DTW	Dynamic Time Warping
GSM	Global System for Mobile communications
CAN	Controller Area Network
IDRES	Intelligent Driving Recognition with Expert System
3D	Three-dimensional
SMA	Simple Moving Average
SD	Secure Digital
CSMA/CA	Carrier Sense Multiple Access with Collision Avoidance
IEEE	Institute of Electrical and Electronics Engineers
LED	Light-Emitting Diodes
GND	Common Electrical Ground
OCC	Occupied
UNOCC	Unoccupied
LPF	Low Pass Filter
EMA	Exponential Moving Average
HPF	High Pass Filter
pF	Picofarad
Hz	Hertz
km/h	Kilometres per hour
AASHTO	American Association of State Highway and Transportation Officials
cm	Centimetres
ODP	Occupancy Detection Prototype
Occ.	Occupant

List of symbols used

μs	Micro seconds
P_S	Stimulus digital pin
P_R	Response digital pin
R	Resistor
Ω	Ohm
V_{CC}	Microcontroller's logical high
V_{IH}	Microcontroller's threshold logical high
V_{IL}	Microcontroller's threshold logical low
V_{OL}	Microcontroller's logical low
V	Voltage
C	Capacitance
τ	Resistor-Capacitor time constant
S_1	Capacitive sensor 1
V_S	Stimulus pin's output voltage
V_R	Response pin's output voltage
A	Plate area
d	Distance between plates
ϵ_o	Permittivity of free space
ϵ_r	Relative permittivity of a dielectric substrate
ϵ_e	Effective relative permittivity
w	Conductive strip width
h	Conductive strip hight
γ	EMA smoothing factor
N	Number of EMA samples
T_s	Sampling period of jerk differentiator
n	Current sample
W_n	Window width of the EMA
W	Weight of vehicle
α	Horizontal incline
f_s	Side friction coefficient
F_c	Centrifugal force
a_c	Acceleration for curvilinear motion
u	Speed in m/s
r	Radius of road curve
g	Acceleration of gravity
e	Rate of superelevation
U	Speed in km/h
G	g-force
t_C	Capacitive sensor electrode charge time
t_D	Capacitive sensor electrode discharge time

Chapter 1

Introduction: Intelligent Transport Systems

The term Intelligent Transport Systems (ITS) refers to information and communication technology applied to transport infrastructure and vehicles. ITS can be interpreted in a broad or narrow way. "Transport Telematics" is a term used in Europe for the group of technologies that support ITS [1]. ITS represent the next step in the evolution of the entire transportation system; with the latest technology in communication, electronics, and safety systems. These technology systems are applied to improve productivity, system performance, environmental impacts, productivity, energy consumption, efficiency, transport safety, service quality and mobility of transportation.

Research on ITS covers a wide field, and apply to all transport modes. ITS are generally organised in three application areas: commercial vehicle operations (CVO), advanced rural transportation systems (ARTS), and advanced public transportation systems (APTS) [2]. CVO applications are intended to assist the operations of commercial vehicles, whether on land or sea (e.g., motor carriers, buses, or ships) in moving freight or passengers. The interferences in the flow of commercial vehicles are minimized through the reduction of administrative barriers. Examples of CVO activities include: weigh-in-motion systems, fleet administration, freight administration, electronic clearance, automatic vehicle location system, and international border crossing clearance.

ITS applications that fall under ARTS, are generally implemented in rural areas with lower population densities and lesser transport demand (communities or areas with less than 50,000 residents). The motivation for systems that fall under ARTS is the unique set of attributes, such as steep slopes, blind corners, road curves, few navigational signs, mix of users, and few alternative routes [3]. The ARTS applications are not so much targeted

areas for future development, but rather a classification of the work already being done. They are systems that assist with route guidance, communications, emergency signalling, incident detection, as well as automatic vehicle location systems and road warning systems [2].

The APTS area uses advanced technologies to improve the efficiency and safety of public transit operations, and offer users greater access to information on system operations. APTS can be categorised into five transit applications: fleet management systems, traveller information systems, electronic payment systems, transportation demand management, and the transit intelligent vehicle initiative [4].

In fleet management systems the efficiency and productivity of vehicle (e.g., cars, ships, and trucks) transit is optimised. They include the use of automatic vehicle location systems, communications systems, geographic information systems, automatic passenger counters, and traffic signal priority systems. Traveller information systems (TIS) assist travellers in making pre-trip and en route travel choice decisions (e.g., avoiding traffic congestions). Technologies used for TIS are pre-trip transit and multi-modal traveller information systems, in-terminal/wayside transit information systems, and in-vehicle transit information systems. Electronic payment systems are installed to offer public transport operators more flexible ticketing, lower administrative costs, and better management and marketing information. It also provides passengers with the convenience of cash-free travel since smart card based technology is used. Transportation demand management consist of dynamic ride-sharing, automated service coordination and transportation management centres. They are therefor programs employed by transportation agencies to effectively manage and utilize existing infrastructure. The transit intelligent vehicle initiative (IVI) is research efforts to improve road safety by developing technologies that help prevents accidents. These technologies include lane change and merge collision avoidance, forward collision avoidance, rear impact collision mitigation, and tight manoeuvring or precision docking.

ITS cover a wide spectrum of transit, but the main drivers for ITS adoption are safety, efficiency, and environmental impact reduction.

1.1 ITS in sub-Saharan Africa

Developed countries like the United States, Australia, Japan, and a number of countries in Europe, are leading the way in ITS. Initially, these countries applied ITS for simple traffic control (e.g. traffic light coordination) and later Electronic Toll Collection (ETC), but has since evolved. To a large extent, every region decided on a different approach, and proprietary technologies were used. Since the late 1980's, most of the above countries developed national architectures to ensure a stable implementation environment. The ITS standards committee is also quite active and ITS are addressed under the TC204 committee of international organization for standardization (ISO) [5]. The major role

players across the globe participate in this committee.

Because of its dependence on wireless communications, electronic sensing, and computer-based data aggregation and visualization, successful deployment and maintenance of ITS is heavily dependent on advanced, and expensive technology and Information Technology (IT). Developing regions in general, and Sub-Saharan Africa (SSA) in particular, have lagged behind in the implementation of ITS solutions, with the exception of some cities in South Africa. These exceptions include, Freeway Management System (FMS) projects in Gauteng, Cape Town, and Durban [6], and Bus Rapid Transit programmes that are rolled out in the major metropoles, including Johannesburg, Cape Town, Tshwane, Durban, Rustenburg, Nelson Mandela Metropolitan Municipality, Buffalo city Municipality, etc. The focus of these exceptional systems is largely the provision of high quality public transport services, and has a large technology component to enable the improved focus on user satisfaction. They include fleet management systems, passenger information systems, on board surveillance and at stations to ensure passenger safety, electronic fare collection, etc.

Apart from these exceptions, the SSA region seriously lack guidance with regards to national ITS architecture. These countries are most vulnerable to ad-hoc deployments, technology/product dumping, etc. The solutions realised by ITS address the needs of the developing world as if tailor-made. Investment into infrastructure has been crippled by monetary constraints and mismanagement, which might prevent successful ITS deployment. The bleak reality is that the developing world desperately needs ITS.

An area with substantial potential for ITS implementation in the developing world is the informal public transport system in SSA. The key differences between the transportation modes in the developed world and those in SSA are listed in Table 1.1. The advent of the taxi industry was in the late 1970s early 1980s – Little attention was given to the transport needs of the poor, hence the rise of the taxi industry, which was initially unregulated. Although many routes are regulated (permits provided), driver behaviour remains a big challenge.

Table 1.1: Differences between public transportation in developed countries and Sub-Saharan Africa.

Aspect	Developed world Metered taxi	Developed world Bus	Sub-Saharan Africa Minibus
Payment type	Cash/card	Cash/card/free	Cash/ limited card use
Payment event	After ride	Before ride	After middle of the journey
Ownership	Private	Government or national industry	Many private owners
Schedule	On demand	Predetermined, fixed, publicly available	Departs when full, peak times tacitly known
Routes	On demand	Fixed	Partially fixed
Vehicle	Small	Large	Small
Number of passengers	Individual or small group	Many passengers	Many passengers
Safety	Considered safe	Considered safe	Considered unsafe
Stops	Taxi stops anywhere	Bus stops and designated stops on route	Taxi ranks, organically determined stops

1.1.1 Informal public transport in SSA

The focus on ways to start regulating the informal public transport system in SSA, based on demand per route as well as vehicle fitness, was started in the late 1980s. The informal taxi industry has since sprawled into a vibrant industry. A recent study by the Trans-Africa consortium found Lagos alone had 80,000 informal minibuses. According to the Arrive Alive campaign, South Africa alone has more than 200,000 minibus taxis [7]. The story is similar for other countries in SSA; consider for example the ubiquitous Dala-Dalas in Tanzania, Ndiaga Ndiaye from Senegal, and Boda-bodas from Uganda.

The World Health Organization (WHO) African region has some of the world's highest road traffic fatalities globally with more than 32 deaths per 100,000 population annually making it the 9th leading cause of death in the region [8]. An 80% increase in traffic deaths between 2000 and 2020 is predicted [9]. The African region has less than 2% of the world's registered vehicles, but almost 20% of the global traffic deaths. According to the Trans-Africa study, the majority of taxi owners in SSA manage to cover their operation costs, but cannot afford to adequately maintain and upgrade their fleets, compromising on safety and quality. Both Senegal and South Africa have introduced fleet renewal programs, with varying levels of success [10].

In SSA in general, and South Africa in particular, the minibus taxi sector dominates the informal public transportation system and has grown enormously in the last 20 years. Not only is it the most available mode of transport, it is also affordable to the public. In 2008 it held 67.9% of the collective transport market share [11]. The taxi industry accounts for 65% of all public transport (more than 14 million passengers every day), while buses and trains account for 21% and 14% respectively [12]. A passengers spends an average of 65 minutes daily in a minibus taxi [13].

There are five distinct role players that make up the informal transport industry, namely the owners, the drivers, the passengers, the taxi associations, and the regulation authorities. The drivers lease the vehicles from the owners, and have to earn a certain sub-minimum to make the business viable. The owners have very little control over the way their vehicles are used, and have no control over the flow of cash. There are over 80,000 minibus taxi owners in South Africa, and the industry employs around 300,000 people, mostly drivers. A taxi driver spends on average 8.8 hours per day on the road, drives an average of 8,000 kilometers per month, and works an average of 6.33 days per week [13]. This is 10 hours per week more than the average legal limit in the EU [14]. 1,408 of the minibuses were involved in fatal crashes during 2010-11 with 1,795 fatalities. Of that number, 57% were passenger fatalities and 30% pedestrian fatalities.

This study will focus on the most prominent segment of the informal public transportation industry in South Africa, namely the minibus taxi sector. A short video of a trip in a taxi can be found in [15]. The minibus taxi sector performs a vital function in people's mobility in SSA and yet little is known about this sector. The sector originally evolved to meet the demand of mobility, but unfortunately, a crucial obligation has fallen victim

to the incentive of personal wealth, namely personal safety. What makes this tragedy especially unjust is the victims – the poor have few other options due to the inadequate public transport network in SSA. The damage is not limited to "the bodies of loved ones scattered on our roads" (Arrive Alive Campaign on taxi deaths [7]). It extends to other vehicles involved in minibus accidents, and more broadly affects the economy through the large number of employees and breadwinners lost in the senseless carnage.

1.1.2 Challenges and issues

Key challenges that face the informal public transport industry in Sub-Saharan Africa are highlighted here. It is especially significant because this informal industry operates on principles foreign to the developed world.

Implementation of ITS solutions from the developed world is not always feasible in developing countries. Some of the main reasons for this are

- cost of implementation,
- cost of maintenance and operations,
- intermittent supply of electricity,
- lack of technical skills in country, and
- remote roads and distance to cities.

The main challenges to the informal transportation industry, in likeness to the main objectives of ITS, are safety and efficiency. Each of these challenges is discussed below.

1.1.2.1 Safety

Being a safe alternative in the developed world, public transport is considered to be a dangerous option in SSA. This fact is best illustrated by the numerous night vigils that are held by would-be passengers the night before a long-distance journey, but also substantiated by the high number of fatal taxi accidents. The root cause for the unsafe nature of this form of travel can be found in the financial incentives and lack of policing. The drivers have a clear incentive to generate as much money as possible, which can be done by accommodating more passengers per trip, or by completing more trips. The taxis are therefore overloaded, or the drivers speed and perform dangerous stunts between destinations, both of which lead to dangerous driving conditions.

Often, the owners are not in a financial position to adequately maintain their vehicles and keep them road worthy. This problem is compounded by the owners not having control over the way the vehicles are driven. Authorities also do not have the capacity to effectively police compliance to legislation relating to driving speed, occupancy, and responsible driving. Moreover, the long-distance taxis travel after hours, when policing is reduced.

1.1.2.2 Efficiency

SSA's taxis are much more demand driven and organic with more discretion, but also with more uncertainty than the developed world. Despite the organic optimisations that have evolved in the industry, various inefficiencies are still apparent. The biggest inefficiency is the time that is spent waiting, by both the passengers as well as the drivers. People have to wait for the taxi to fill, or have to wait at allocated points for the taxi to turn up, both of which can take hours.

1.2 Proposed ITS support for minibuses in SSA

ITS solutions for improving road safety can be categorised into systems that prevent unsafe traffic participation (e.g., seatbelt reminders), prevent unsafe situations or actions while driving (e.g., lane keeping systems), and systems that reduce injury severity (e.g., airbags) [16]. In order to contribute to a safer public transportation system, this work is focused on solutions to prevent unsafe driving. Other examples of ITS solutions that prevent unsafe situations or action while driving include: electronic stability control [17], electronic vehicle identification [18], collision avoidance systems [19], and night time vision systems [20]. The above named solutions depend on advanced and expensive technology.

An intelligent transportation system that contributes to safer driving, which applies more to SSA, are electronic devices that monitor driver behaviour. A high correlation between driver behaviour and accidents were found by the National Highway Traffic Safety Administration (NHTSA) [21]. Many driver behavioural devices and models have been developed to detect reckless driving manoeuvres. The models developed are based on pattern recognition algorithms that continuously monitor the driver's behaviour. Almost all of the developed systems are based on self-reported scales which can be too general and biased. The alternative, in which references for driver behaviour has been established, comes from experiments involving driving simulators [22], which has a limited scope. More accurate behaviour modelling systems have been developed from past road crash data [21, 23]. In [23] an in-vehicle data recorder (IVDR) system was evaluated and risk indices developed, which showed high correlation with past crash involvement. A shortcoming of all these models is that they do not include speed directly into their behavioural algorithm. Speed effects the severity of a vehicle accident, and also increases the probability of being involved in a crash [24]. A number of studies have investigated the relationship between speed and crash rate, finding evidence for an exponential function and a power function between speed and crash rate [25]. A behavioural model must be developed to include speed in the detection of dangerous driving manoeuvres.

ITS for the improvement of efficiency, as previously stated, include many solutions. Their main goal is to relieve road congestion and do not satisfy the needs of public transportation in SSA. A system that can inform passengers of the minibus taxi's current occupancy status, the taxi's location, and the drivers' driving history (if he is a safe driver,

or not) would improve efficiency since the public can make informed decisions based on a taxi's whereabouts.

Despite the financial challenges, being on the wrong side of the digital divide provides an opportunity for SSA to leapfrog some of the ITS technical development phases, especially the wireless communications technologies. If the decision makers are therefore empowered and knowledgeable, they could avoid many of the mistakes made, and unnecessary expenses incurred during initial implementation in the developed countries. An option in reducing the cost of implementation is to move away from standards specifically developed for ITS, and instead use existing cellular communications such as Third generation (3G), WiMAX, and Long Term Evolution (LTE). The data rates of modern cellular networks can support a large number of the applications foreseen for ITS, including Vehicle to Infrastructure (V2I) communications – in V2I communications, vehicles (as opposed to the passengers in it) communicate with the ITS in a Machine-to-Machine (M2M) configuration.

It is evident from the preceding sections that, to fully embrace the unique challenges and opportunities of ITS in the developing world, one almost has to unlearn what ITS means in the developed world.

1.3 Dissertation statements and hypotheses

Dissertation statement 1:
The number of occupants in a taxi can be detected with high degree of certainty using a cost-effective electronic system.

A robust and low-cost sensing system is designed that can detect multiple occupants in the heterogeneous minibus taxis environment. This work implements a capacitive sensing system for the detection of occupants. Capacitive sensing systems use electrodes to detect the electrical field properties of a human body and consists of a low-cost electronic setup with high sensitivity.

Hypothesis 1.1:

The capacitive effects of passengers can be modelled mathematically.

Hypothesis 1.2:

There is a significant difference between the capacitance with an occupant present and without an occupant present.

Hypothesis 1.3:

The presence of multiple bodies can be individually detected using capacitive coupling

and sensing.

Hypothesis 1.4:
Multiple passengers can accurately be detected using a low-complexity capacitive sensing system.

Hypothesis 1.5:
Capacitive coupling and sensing can distinguish between a human body and a non-human body (e.g. a bag) on a seat.

Hypothesis 1.6:
A capacitive sensing system can endure the heterogeneous minibus taxi environment.

Dissertation statement 2:
Reckless driving can be detected successfully by implementing standards used for road design – based on the relationship between inertial vehicle dynamics and the road's friction coefficient.

A reckless driving detection system is developed utilising acceleration and speed data. Acceleration is used to measure the vehicle's dynamics, and is generated from an accelerometer installed in the vehicle. Speed is measured with a GPS device, and the generated information processed with the model based on road design standards. Minibus taxis are also fitted with tracking systems to study their behaviour.

Hypothesis 2.1:
Acceleration and speed provide a measure of recklessness.

Hypothesis 2.2:
Sensors can be sampled fast enough to detect recklessness from accelerometers and GPS speed detection.

Hypothesis 2.3:
Acceleration measurements can be filtered successfully to remove unwanted variances and offsets.

Hypothesis 2.4:
Minibus taxis travel at excessive speeds and ignores the national speed-limit.

Hypothesis 2.5:
There are substantial differences in the driving patterns of minibus taxis in urban and

highway scenarios.

Hypothesis 2.6:
Occupancy information can be used to improve a reckless driving detection system.

Dissertation statement 3:
A system can be developed that makes real-time sensing information, of reckless driving and occupancy, in a minibus taxi graphically available online.

A prototype is developed from the designed system, and tested on South African and Ugandan roads.

Hypothesis 3.1:
The system is integrable with the existing cellular network in SSA.

Hypothesis 3.2:
Minibus taxis can be tracked in real-time, and information of recklessness and occupancy combined with location information.

1.4 Research objectives

Research objective 1:
To develop a realisable system that improves the safety and efficiency of minibus taxis in SSA. The system must be robust, integrable with the existing cellular network in SSA, provide black box functionality, cost-effective, and have simple installation in minibus taxis.

Research objective 2:
To develop a detection system that can detect and count multiple occupants in a minibus taxi. The system must distinguish between a human body and non-human body.

Research objective 3:
To develop a system that determines when a minibus taxis drives recklessly. The system must make use of available technology.

Research objective 4:
To develop an online graphical user interface that displays real-time information of

the minibus taxi.

1.5 Scope of work

This dissertation focuses on minibus taxis in SSA. A system is developed that detects reckless driving manoeuvres performed by minibus taxi drivers. The detection system is based on a novel model that augments inertial vehicle acceleration data with GPS speed information. The model is based on the relationship between a vehicle's tyres and the road surface, which comes from standards used for road design (Traffic and highway engineering [26]). A second system, which is integrated with the previous, detects the number of occupants in a minibus taxi using a cost-effective electronic system. The occupancy detection system measures the electrical charge on the seat, which increases with the presence of an occupant, and is called capacitive sensing. This sensing technique is designed to be robust, low-cost, and enables the distinction between passengers and their luggage (typically placed on seat next to them) as appose to traditional pressure sensors. A system is then developed, that uses the above collected information from the minibus taxi, and makes it graphically available on an online dashboard for users to utilize. Although most of the data was collected on South African roads, the work in this dissertation also applies to the rest of SSA. Data was also collected in a central African country, Uganda, which showed similar results.

1.6 Dissertation structure

Chapter 2 presents a comprehensive review of the literature for improving road safety, and the detection of occupants in a vehicle. Many systems have been developed that improves road safety by decreasing the risk of accidents, and decreasing injury severity. Several different systems have also been developed for occupancy detection in vehicles. These system are discussed with with regard to public transportation in SSA.

Chapter 3 describes the design of two integrated sensing systems that form the sensing and reporting systems. The sensing system monitors the number of occupants in the minibus taxi and detects reckless driving manoeuvres performed by the driver. The information is then reported by storing it on a SD-card that acts as a black box, and is also uploaded onto an online platform. An overview of the complete sensing and reporting system is discussed and is given by Figure 3.1 on page 25. The occupancy detection system (section 3.1) calculates the electrical charge on a seat before and after a passenger occupied it. The difference in capacitance, which increases in the presence of an occupant, gives an indication of the seat's occupancy status, which can be either occupied or unoccupied. The reckless driving system (section 3.2) utilises

acceleration data from an accelerometer, filters it, and then compares it to a threshold. A lateral and longitudinal threshold is designed, which is based on standards set for road design. The lateral threshold is dynamic and reduces with an increase in speed, and the longitudinal threshold remains constant with regards to speed. An additional occupancy dependant threshold is proposed which deceases the threshold, for both lateral and longitudinal acceleration, with an increase in the number of occupants in the minibus taxi. In section 3.3 the implementation of the designed system as a prototype is introduced, where the components used for the prototype, and the software developed for the system are discussed.

Chapter 4 presents the results of the designed sensing and reporting system described in Chapter 3. The experiments were conducted on South African and Ugandan roads, in both urban and highway environments.

Chapter 5 concludes the work by validating the hypotheses from Chapter 1 using the results from Chapter 4. The main findings and contributions of the work in this dissertation are provided.

Chapter 2

Literature Survey

This chapter firstly provides a detailed survey of the literature on approaches and systems used for increasing road safety, which is followed by a description of systems used to detect occupants in vehicles.

2.1 Road safety

Improving road safety received a lot of attention in ITS, and a number of systems have therefore been developed to improve road safety [27, 28, 29, 30]. The improvement of road safety decreases the number of fatalities and injuries that occur on roads. These fatalities and injuries affect pedestrians, passengers, and drivers. Systems that improve safety include the enforcement of existing rules, improving infrastructure, and introducing new technologies and driver information systems to vehicles.

Technologies and driver information systems can be vehicle-based, infrastructure-based, or co-operative (a combination of the two). Vehicle-based systems use on-board sensors to collect information from the vehicle, such as speed, tyre pressure, acceleration, or location, which is then sent to the on-board units (OBUs) of the vehicle. The OBU can issue warnings or even take partial control over the vehicle. An example of such a system, where partial control is taken over by the OBU, is electronic stability control, which will be discussed later in section 2.1.3. Infrastructure-based systems are roadside sensors that collect and display information or issue warnings to all vehicles in the vicinity. Examples of these sensors are, inductive loop detectors, magnetic detectors, ultrasonic detectors, microwave detectors, infrared detectors, and image detectors [31]. A problem in ITS with infrastructure-based systems is that the data must be standardised to improve driver's understanding of provided information; also expensive to install and even more so to main-

tain. Drivers are also not compelled to follow or obey the information. In co-operative systems, infrastructure-based systems communicate with vehicles through Vehicle to Infrastructure (V2I) communication networks. The information received by the vehicle is processed on the vehicle's OBD and provided dynamically to the individual in the vehicle, such as speed limits, traffic and road conditions Information is also transmitted from the vehicle to the infrastructure.

Vehicle-based technologies for ITS can be further categorised into systems that prevent or warn drivers before participating in traffic, reduce injury severity in the case of an accident, and preventing unsafe situations or actions while driving. Some typical representatives of these categories are presented in the following, with special attention given to systems that monitor the task of driving.

2.1.1 Prevent or warn drivers before participating in traffic

The implementation of seat belt reminders fall under the prevention of unsafe traffic participation. From a cost-benefit assessment conducted by the European Transport Commission of 21 existing vehicle safety technologies, seat belt reminders showed to be the most cost-effective solution for improving road safety [29]. Wearing a seat belt is compulsory in many countries. Statistics from a 2011 WHO review for South Africa state that 67% of front seat occupants and 58.6% of drivers wear seatbelts.

Another cost-effective solution for the prevention of unsafe traffic participation is an alcohol ignition interlock device (alcolock) [27]. This device showed very promising results and has been used in various developed countries, especially for drivers that have been caught while driving under the influence. The alcolock device acts as an immobiliser for the vehicle. Drivers have to exhale into a device on the dashboard that calculates the alcohol level in the person's breath, before the vehicle can be started.

2.1.2 System that reduce injury severity

A pre-crash sensing system is an example of a system that reduces injury severity [32]. The pre-crash sensing system is designed to predict an unavoidable collision and activate pre-crash brake assistance, and increase the effectiveness of passive safety instruments (seatbelt or airbags) well in advance of the collision to mitigate occupant injury caused by the collision.

Furthermore, a European initiative named eCall speeds up the arrival of medical response assistance to motorists involved in a collision by automatically reporting the exact location to an emergency centre. The eCall service has been introduced in European countries with the aim to render the service fully operational in 2015 [33].

2.1.3 Preventing unsafe situations or actions while driving

Technologies designed to prevent unsafe situations or driving actions are known as collision avoidance systems. Collision avoidance systems encompass a wide variety of vehicle features designed to help drivers operate the vehicle safely. These systems monitor the vehicle and the environment around the vehicle – warning the driver if it detects a potential collision.

Two of the most popular driver assistance systems are intelligent speed adaptation (ISA) and electronic stability control (ESC). Results show that they are cost-effective solutions [29]. The ISA system constantly monitors the vehicle's speed and compares it to the local speed limit to determine if the speed limit is exceeded. In an advisory system, the driver is notified of the infringement, but has the option of obeying or ignoring the warning. For a mandatory system, the system has the ability to control the vehicle's speed and does not permit the speed limit to be exceeded at any time. In some applications the system is voluntary; drivers are provided with an option where they can switch the ISA system on or off. European studies have shown that ISA can have a reduction of 36% in injury accidents and 59% in fatal accidents [34].

ESC systems improve the safety of a vehicle's stability by detecting and reducing loss of traction. The system then automatically intervenes when there is yaw instability or a high risk of rollover. In current ESC systems, wheel speed sensors and lateral yaw and steering angle sensors send data to the vehicle's electronic control unit (ECU). The vehicle's actual movement is then compared to performance models, and if the vehicle shows a tendency to leave an appropriate travel path, the system will intervene. The system automatically reduces throttle and applies appropriate braking to reduce the vehicle's speed below the rollover risk. When the vehicle slides from either under-steer or over-steer, the system automatically reduces throttle and selectively applies individual braking to the appropriate wheels to better align the vehicle for the appropriate path of travel [28]. ESC does not increase traction or cornering performance, but instead minimises loss of control.

Event or accident data recorder (EDR) systems have also been identified by [29] as a cost-effective ITS solution with high potential for improving road safety. EDR systems record information from the vehicle shortly before and after an accident and are used to reconstruct the accident. These devices are commonly known as black boxes. The information is especially of importance to researchers, crash investigators and manufacturers. Although these systems are not directly responsible for preventing accidents, studies have shown that awareness of being monitored leads to safer driving [35, 36, 37].

According to [38], approximately 3 out of 4 vehicles operate with at least one underinflated tyre. Underinflation increases braking distance, reduces handling, decreases tyre life, and creates overheating that can lead to accidents. Tyre pressure monitoring systems (TPMS) have therefore been developed to monitor the tyre pressure of a vehicle. An example of a low-cost TPMS system consists of a sensor fitted on the tyre valve stem,

which changes its colour when the pressure drops. A more sophisticated TPMS system gives audible notifications to the driver inside the vehicle when the pressure falls below the specified level. Other TPMS technologies monitor wheel rotational speed and other signals outside the tyre itself. These systems were not identified as cost-effective solutions for road safety [29].

Night time vision systems installed in vehicles increase a driver's perception in darkness, bad light or poor weather conditions. These systems do not only increase the safety of the driver, but are especially important for the safety of pedestrians and cyclists. Many techniques have been developed to detect and recognise vehicles and obstacles [39, 40, 20]. These techniques are also used for traffic surveillance. Technologies utilized for these systems include acoustic, infrared, magnetic, laser, radar, microwave, and optical systems such as video processing devices [41, 42]. The implementation of these technologies is popular in more advanced modern-day vehicles.

Warning systems have been developed that monitor driver fatigue. An example of such a system is the Copilot that measures slow eyelid closures [43]. This system measures the duration a subject's eyes are closed which is expressed as a percentage; a warning alarm notifies the driver when a resting break should be taken. Interesting results from [43] showed that drowsiness increases slowly over a period of hours and that a short resting break has a significant effect on eyelid closure.

Forward collision avoidance systems alert the driver when the vehicle is getting too close to the one in front of it. The system gives audible warnings, or in more advanced systems applies the brakes automatically, to prevent a crash or reduce the impact. In most systems the brakes are precharged to maximise their effect. Sensors used for these systems include, radar [44], cameras [45], or light detection and ranging (Lidar). A similar system is adaptive cruise control, which automatically adjusts the vehicle's speed in relation to the vehicle ahead of them in order to maintain a safe distance [46]. These systems are mainly found in high-end vehicle models.

Lane departure warning (LDW) and prevention systems use cameras to monitor the road lines and give a warning to the driver when the vehicle strays over the lines. Audible and visual warnings notify the driver if the vehicle is drifting across the lane. In some systems, haptic warnings vibrate the steering wheel or seat, or send pulses through the seatbelt. Light braking and minor steering adjustments are used in some systems to automatically help drivers remain on the road in their lanes. Turning on the indicators temporarily disable the system. According to [47], LDW systems do not necessarily reduce accidents, but their results showed that crashes actually increased by 10%.

Blind spot detection (BSD) systems monitor the side of the vehicle for vehicles approaching blind spots. For typical BSD systems, audible and visual warnings are enabled if the driver attempts to change lanes and a vehicle is on the turning side. Cameras are used in [48] to continuously monitor the side of the vehicle; their results showing an accuracy of 91%.

Curve warning systems have been developed to warn drivers of oncoming sharp turns.

In some systems, they automatically reduce the vehicle's speed. A combination of GPS speed and location information and digital maps are used to determine if the driver is travelling at an excessive speed for the particular road bend. An advanced curve warning system was proposed by [49]. Their system determines the characteristics of the coming road bend, computes a safe speed for the driver, and then imposes speed control on the vehicle in order to achieve a safe speed around the road bend. In order to develop such a system, a complete set of upcoming road geometry is required to regulate the vehicle's speed.

The above discussed systems can unfortunately have a negative indirect impact on driver behaviour [28]. The addition of driver assistance devices will increase the safety of the minibus taxis, which enable them to drive at higher speeds. The increased speed increases the risk of other vehicles on the road that are not equipped with assistance devices, as well as pedestrians and cyclists. Since public transit drivers in SSA has a clear incentive to generate as much money as possible, they may adapt to the driver assistance systems and drive more aggressively assuming better protection and assistance from the device. Another possible side effect is that vehicles not equipped with driver assistance devices may imitate other vehicles that have such devices, which can relate to an increased accident risk.

2.1.4 Driver behaviour models

Driver behaviour can be modelled as descriptive models or functional models. Descriptive models describe the driving task in terms of what the driver does, and functional models attempt to explain why drivers behave the way they do [50]. We focus on descriptive models, using vehicle based sensors, to describe and comment on a driver's driving.

Numerous studies have been completed on driving behaviour and descriptive modelling thereof. The main differences between these studies are in the specific application area and the sensing method employed. Driver behaviour modelling is often the backbone for the design of on-board controls that influences vehicle dynamics and stability. Their implementation is therefore typically found in ITS technologies described in the previous section. An overview of the work done on driver modelling over the past few decades is given in [30]. Their overview focused on automatic vehicle control and driver assistance, such as path following, lane change assist, and overtake assistance. From their study it is apparent that vehicle acceleration plays an especially significant role in driver modelling.

In the remainder of this section we investigate the different behaviour modelling techniques used to detect driving manoeuvres. A summary of the literature on driver behaviour detection can be seen in Table 2.1, with their research goal and modelling technique. A summary of the sensors used by each approach is shown in Table 2.2.

Table 2.1: Summary of goals and techniques of driver behaviour systems.

Goals of behaviour modelling system	Behaviour modelling technique	Ref.
Machine learning framework for modelling and recognizing driver manoeuvres	Graphical models and HMM	[51]
Adaptive assistance system to determine and predict drivers' behaviour	HMM	[52]
Intelligent driving recognition with expert system (IDRES)	Rule based	[53]
Classify driving patterns using neural networks	Neural networks	[54]
Record driving events and detect unsafe driving behaviours	Fuzzy Logic	[55]
Monitor road and traffic conditions using mobile Smartphones	Threshold detection	[56]
Understand the driver behaviour using Smartphone sensors	Endpoint detection, DTW, Bayesian classification	[57]
Detect and alert dangerous vehicle manoeuvres related to drunk driving	Pattern recognition	[58]
Investigate driver behaviour as safe or unsafe	DTW, Bayesian classification	[37]
Evaluate the comfort in public transportation	Three algorithms: Threshold detection, jerk detection and Comfort index measurement	[59]

Table 2.2: Summary of sensors used by related driver behaviour systems.

Sensor	[53]	[51]	[52]	[54]	[59]	[55]	[56]	[57]	[58]	[37]
Accelerometer	-	✓	-	✓	✓	-	✓	✓	-	-
Gyroscope	-	-	-	-	-	-	-	✓	✓	✓
Magnetometer	-	-	-	-	-	-	-	✓	-	✓
GPS	-	-	-	✓	✓	✓	✓	✓	✓	✓
Camera	✓	-	✓	-	-	✓	-	-	-	-
GSM module	-	-	-	-	-	-	✓	-	-	-
Speedometer	-	✓	✓	-	-	-	-	-	-	-
Acceleration throttle	-	✓	✓	-	-	-	-	-	-	-
Brake pedal	-	✓	✓	-	-	-	-	-	-	-
Steering wheel	-	✓	✓	-	-	-	-	-	-	-
CAN-bus reader	-	-	-	-	-	✓	-	-	-	-

Driving pattern classification using Hidden Markov Models (HMM) is proposed by [51] as a framework for machine learning for modelling and recognising driver behaviour. Information sensed from a steering wheel angle sensor, brake pedal, speedometer, acceleration throttle, gear and GPS unit is used as inputs for the HMM. An adaptive assistance system to determine or predict driver's behaviour using HMM has been developed by [52]. Four cameras are installed in the vehicle (view of front, rear, driver head, and driver feet) to monitor the vehicle's sensors (speedometer, steering wheel, acceleration throttle and brake pedal) and the driver.

In [53] a system named Intelligent Driving Recognition with Expert System (IDRES) was proposed, utilizing vehicle mounted cameras that face the road to determine lateral position delimiting the lanes of the road. The IDRES system is complex and takes into account high-level information such as the intent of the driver.

Research focus has recently shifted from visual monitoring to the use of vehicle-mounted motion sensors. Visual monitoring makes use of cameras, radar and/or lasers to

monitor the driver's behaviour and determine the vehicle's speed and position relative to obstacles in the road. Motion sensors such as accelerometers, gyroscopes and magnetometers measure the vehicle's acceleration and orientation. The popularity of these sensors is mostly due to their simplicity, robustness, and low cost.

A neural network based model is proposed by [54] for driving pattern classification. Bi-axial accelerometer and GPS data are combined to characterize driving patterns using neural networks. Neural networks are efficient and complex networks that are capable of machine learning and pattern recognition, as opposed to ordinary rule-based systems. A geo-referenced database was developed empirically to compare positioning data to disregard outliers and anomalies.

In [55] a hazardous driving detection system is proposed based on fuzzy logic inference. The system consists of a 3-axis accelerometer, a camera and an engine control unit reader that provides the fuzzy logic inference system with speed and engine readings. The system produces as an output, a driving-risk level ranging from 1 to 3. In order to verify the system's output, a driver was instructed to drive a vehicle at different risk levels. Three passengers had to complete questionnaires to indicate each round's safety level. They compared the passengers' experience to the fuzzy logic output, and a 60 - 70% correlations between the results were found. They regarded the anomalies due to passengers having different personal hazardous driving thresholds.

A system that monitors road and traffic conditions using smartphones, was proposed by [56]. Their system, called Nericell, is installed on a smartphone and uses the phone's internal sensors. These sensors include an accelerometer, microphone, cellular modem, and a GPS to detect braking, potholes, speed bumps, and honking. The device can also automatically detect the smartphone's orientation. Another smartphone based system utilizing the phone's sensors was proposed by [57], and monitors driver behaviour. An empirically determined threshold determines the occurrence of an event and a dynamic time warping (DTW) algorithm compares the occurred event to a set of predefined templates to find an optimal path, which represents a certain driving manoeuvre. A Bayesian classification system is used to determine how hazardous the driving habits of the driver are.

A smartphone based system, developed by [58], detects drunk driving manoeuvres by comparing a driver's driving to typical predefined drunk driving patterns. The pattern recognition algorithm receives data input from a smartphone's accelerometer and gyroscope.

A driving style recognition system, also implemented on a smartphone, is given by [37]. Their system also uses the smartphone's sensors and a dynamic time warping algorithm to detect driving manoeuvres, but the data from multiple inter-axial sensors are then combined into a single classifier. An Euler representation aids in the classification process in order to distinguish between safe and unsafe driving behaviour.

An embedded sensor system to measure comfort in public transportation systems was developed by [59]. The system consists of a tri-axial accelerometer, GPS receiver, temper-

ature sensor and SD Card storage (acting as a black box). The comfort level is determined by detecting jerky manoeuvres and vertical, longitudinal and lateral acceleration peaks. These values are compared to an empirically determined threshold and then entered into an index system (based on ISO 2631-1 comfort standards), which produces a comfort index measurement. Lateral and longitudinal acceleration values over 0.229G (g-force) and vertical acceleration over 0.5G is regarded as "extremely uncomfortable", and lateral and longitudinal acceleration values under 0.032G is regarded as "not uncomfortable".

2.2 Occupancy detection systems in vehicles

Several different systems have been developed for occupancy detection in vehicles. Some systems detect occupants using sensors installed on strategic locations next to the road, e.g. intersections or high occupancy lanes, and other systems are installed within the vehicle to detect the occupants. An example of a system that is installed on the road side is a real-time vision system called Visatram. Their system is used for automatic traffic monitoring, usually along highways [60]. Occupancy detection systems that are installed within the vehicle itself can be categorised into the three most common sensor systems used for occupancy detection: pressure sensors, video sensors and capacitive sensors. Most of the vehicle mounted sensors are used for smart air-bag control systems. In the following three sub-sections, each of the three in-vehicle occupancy detection systems is discussed.

2.2.1 Pressure sensors

Most pressure sensors consist of a variable resistance membrane that changes resistance with a load placed on the sensor. The change in resistance is as a result of an increase in weight from a load placed on the sensor. For vehicle occupancy detection, the load is an occupant that occupies the seat. Most of the pressure sensor systems installed in vehicles is used to notify occupants to fasten their seatbelt, or inhibit airbags if the seat is vacant or an infant is on the seat. If an adult is on the seat, the increased weight load enables airbag deployment.

The sensor system in [61] consists of eight variable resistance pressure sensors installed in the seat cushions. The sensors are connected to and monitored by a microcontroller that calculates the weight distribution. This sensor configuration enables the system to distinguish between an occupied infant seat, an occupied adult seat, and an unoccupied seat. Their system also determines if an infant seat is forward or rear facing. This system is used to determine if the airbags must be deployed in the case of an accident.

A similar system that inhibits airbag release when a seat is unoccupied has been developed in [62]. The sensor system also has a resistive membrane pressure sensor that is integrated into the seat cushion. The system prevents the vehicle from unnecessary damage in the case of an accident when no occupant is present in the passenger seat. The sensor system is divided into a front sensing region and a rear sensing region. Another

system described in [62], consists of two contact bands that are integrated into the seat cushion. The two sensors come into contact when loaded. Different sensitivities are achieved by using alternative contact bands of various patterns. Their sensor system is also able to detect occupants that sit on the side or front of the seat.

In [63] a system is developed to detect a load at the backrest using multiple sensitive contact points. The pressure points are installed on a rubber sheet that changes resistance with load applied to them.

An alternative pressure sensor system has been developed by Delphi [64]. Their passive occupant detection system relies on a fluid-filled bladder to classify the occupant. The setup is low-cost and is used to aid the airbag system.

Unfortunately a reoccurring problem for pressure sensors is that their systems cannot distinguish between an occupant and a heavy object (e.g. a heavy bag). Since the system is resistor based, the components will wear out after continues usage.

2.2.2 Video based sensors

An alternative solution for occupancy detection is vision based systems. Vision based sensors also provide the detection system with additional functionalities like dynamic occupant position analysis or determining child seat orientation. Typical sensors used include: video, ultrasonic, stereo camera, or range camera.

An occupancy detection system that utilizes stereo cameras for occupant classification was designed in [65, 66, 67]. The system in [65, 66] is called stereovision and is used to control the airbag firing. A 3D vision system is generated from their camera configuration and they were able to detect a wide variety of situations, such as a child on a passenger's knee or different objects on the seat. In [67], a similar system was developed, but low performance was observed with only a 70% success rate.

A technology that is based on thermal long-wavy infrared cameras was evaluated in [68], but the focus was mainly on dynamic occupant-posture analysis. The system can easily be adopted for occupancy detection in vehicles. The occupancy detection system developed in [69] also uses infrared imaging to detect occupants. A cumulative histogram is created from the captured infrared image and compared to a predefined image of a "standard" human head. In [70], a static occupant classification system was developed. Their system used low-resolution range cameras for the classification process.

Ultrasonic occupancy detection systems are available, but very uncommon since the sound waves are easily blocked by objects (e.g. newspapers) and it requires a lot of processing. According to [71], the ultrasonic system will be affected by environmental conditions, such as temperature, altitude, or humidity. The sensing systems must have a clear line of site to be able to detect occupants, which means that the sensor setup is clearly exposed to the occupant. Many people in a minibus taxi, seated behind one another, makes visual detection problematic.

2.2.3 Capacitive sensors

Capacitive sensing describes a number of techniques to measure the electrical field between an electrode and its surroundings [72]. These sensors are proving to be one of the most attractive technologies for any kind of environmental monitoring systems and non-contact control elements. A background on capacitive sensors is given by [73]. From their study it can be seen that sensing with electric fields is not a new concept, and that it is used in many different applications. An example of an alternative sensing application can be found in [74], where electric field sensing is used for three-dimensional position measurements of a hand. The measurements are used to provide three dimensional positional inputs for computer graphics.

Capacitive sensing technology to detect human presence has proven to be a robust and reliable measurement technology with low power consumption that is ideal for the automotive environment. Numerous studies have therefore researched capacitive sensors for seat occupancy detection with several prototypes developed. These systems are mostly used for airbag inhibition if no occupant is detected on the seat. In [75, 76] a capacitive sensor array is installed above the passenger in the roof of the vehicle. The roof-mounted sensor array detects the distance to and proximity of the occupant by means of triangulation analysis, and enables the airbags for deployment when necessary. Their system also determines lateral and diagonal passenger motion.

Electrodes are incorporated into the base and backrest of the seat in [77]. Their system has been designed to discriminate between human occupants and animals or packages resting on an automobile seat.

The capacitive sensing systems developed for airbags are required to have a very fast response time. The capacitive sensing system developed in [78] has a very fast response time, since it only take 200μ seconds to complete a set of measurements. Multiple electrodes are placed on the seat and backrest to detect an occupant. Their system is a typical example of how capacitive sensors are implemented on vehicle seats. The sensor configuration for [78] can be seen in Figure 2.1. The system also detects the type (infant

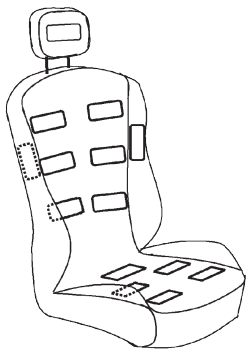

Figure 2.1: Capacitive occupancy detection system with multiple sensors installed on a single seat. The image is from [78] showing the sensor distribution on the seat. Typical setup for most capacitive occupancy sensor systems in vehicles.

or adult) and position of the occupant. Very accurate results were reported, which is crucial for airbag inhibition systems.

The system developed in [79], installed 16 capacitive sensor electrodes on the backrest and seating surface area for the detection of a single occupant. The system setup is complex with multiple sensors and relays. Their system is also integrated with the airbag deployment system. They reported that their detection system worked inaccurately when a passenger touched the chassis during measurements – the system reports an empty seat, although an occupant was present.

An alternative occupancy detection sensor was introduced by [80], which is an extension of their previous design in [78]. Their research showed that conductive objects (e.g., laptop) placed on a capacitive sensor will result in positive occupancy readings, i.e. the object is seen as an occupant. The new sensor system combines inductive and capacitive sensing principles for proximity detection. The capacitive detection part of the sensor is similar to previously discussed systems, but the additional inductive feature senses the presence of conductive objects (e.g., laptop) placed on the seat. Their inductive-capacitive proximity sensor improved the reliability of occupancy sensing since the system can distinguish occupants from conductive objects.

It is stated in [72] that capacitive sensors suffer from two sources of errors: random noise and sensor drift. Random noise is inherent to all analog sensors. The noise increases with an increasing distance away from the sensor and it is therefore recommended that the sensed item is as close to the sensor as possible. They recommend a simple moving average filter which works well against such random noise. A simple moving average (SMA) calculates the sum of N samples and then divides the total by N. One disadvantage of a SMA is that it delays the attenuating effects of capacitance changes. Sensor drift is a slow increase in the sensor reading and is especially problematic for capacitive sensors (according to their research). This slow increase can be misinterpreted as a slow movement of an object towards the sensor, but is usually clearly distinguished from movements, since the increase is so slow. Another problem that [71] commented on, is that capacitive occupant sensing systems have significant problems when the sensor is wet – water beneath and above the seat cushion or cover. The water results in inconsistent capacitive coupling between the sensor and circuit ground which leads to inconsistent sensor readings.

2.3 Conclusion

In this Chapter a number of ITS solutions for improving road safety and occupancy detection were discussed. ITS solutions developed for improving road safety depend on advanced and expensive technology. Although they show promise in developed countries, they are not necessarily a sustainable solution for public transit in SSA. Minibus taxi drivers' have a clear incentive to generate as much money as possible; they speed and perform dangerous stunts between destinations in order to reduce the duration of a trip

to complete more trips. Even though the implementation of many of the safety systems could improve the safety of the driver and passengers, a high accident risk still remains to other vehicles, cyclists and pedestrians on the road. Various contributions have been made in the field of modelling driver behaviour, but shortcomings still exist. Most of the developed systems that detect reckless driving manoeuvres are based on self-reported scales which can be too general and biased. Previously developed approaches also lack an algorithm where the relationship between speed and acceleration are taken into account to accurately identify reckless driving.

For occupancy detection, visual based systems require expensive technologies and often do not perform well if the sensors do not have line of site of the occupants – they can easily be blocked by objects. Pressure sensors is a common sensing technique for occupants in vehicles, but is not suitable for the public transit environment since the system can't distinguish between a heavy bag and an occupant. Pressure sensors also contain parts that will wear out after continues usage. It is therefore apparent that capacitive detection is the most robust and low-cost system for the detection occupants in vehicles. In section 3.1.1 three different sensing techniques will be discussed in detail. The most important difference established between the techniques, is that two of the techniques requires multiple sensors to establish proximity. The plurality of the capacitive sensors is used to sense the distances to the occupant and triangulated the data to locate the position of the occupant. As an example, in the typical capacitive occupancy detection system in [78], their prototype uses 12 electrodes per seat, thus 192 electrodes would be required for a 16-seat minibus taxi. The sensor system setup is therefore complex since a large number of wires are needed to connect all the capacitive electrodes with a control unit. The distribution of the sensors in the vehicle will also cause difficulties. Therefore, a re-occurring shortcoming in the previous developed occupancy detection systems is that they require multiple sensors to detect a single occupant.

Chapter 3

Sensing and Reporting System

This chapter describes the design of a real-time sensing and reporting system which aims to make minibuses safer and more reliable. The system monitors the number of occupants in the minibus taxi and detects reckless driving manoeuvres performed by the driver. The information is stored on a SD-card, which acts as a black box, and is also uploaded onto an online platform. From previous work (chapter 2), and the background of the informal transportation system in Sub-Saharan Africa (chapter 1), it is evident that the developed system must have a low cost setup, and provide integration with existing cellular communications. The sensing and reporting system can be seen in Figure 3.1 on page 25. A broad overview of the sensing and reporting system follows.

The sensing system consists of a central microcontroller (Gateway unit), with multiple microcontrollers (end devices) connected to it, which also have multiple seat sensors connected. The ZigBee network (based on the IEEE 802.15.4 networking protocol) is used to provide wireless connectivity between the sensors' microcontrollers and the Gateway unit. Accurate data transmission is ensured, since ZigBee has built-in data-packet building and employs Carrier Sense Multiple Access with Collision Avoidance (CSMA/CA) to avoid packet collisions [81]. The topology of the network is a star arrangement [82], which means that in this configuration the Gateway unit acts as a coordinator at the centre, with end-devices connected around it and the end devices do not communicate with each other directly. The system is designed with wireless connectivity between the microcontrollers, since this enables the Gateway unit to be placed at the most convenient location in the minibus (usually in front) without affecting the other microcontrollers. This also enables sensors to be added or removed from the system without modifying or updating the wiring to the Gateway unit. Individual sensors in the integrated sensor system can be identified and monitored independently. Sensor electrodes, that are used

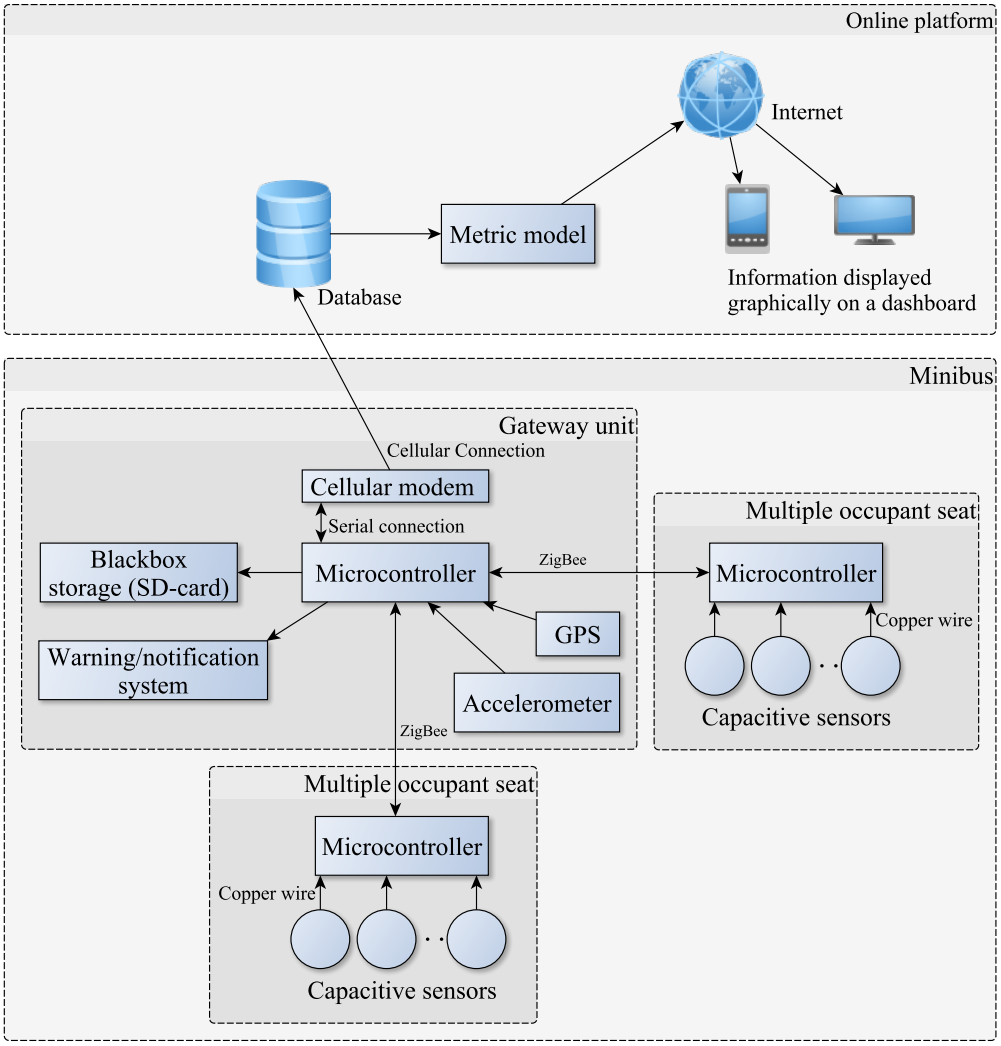

Figure 3.1: Overview of the sensing and reporting system. Multiple occupants are detected within the taxi and data transmitted via ZigBee network between the microcontrollers. The main microcontroller is the Gateway unit, that has a GPS modem, accelerometer, a warning and notification system, SD-card storage, and a cellular modem connected. The SD-card provides black box capability and the cellular modem enables real-time reporting of information. The uploaded real-time information is made graphically available on an online dashboard. The dashboard can be accessed from any device with internet access.

to detect occupants, are placed on the seat. The electrode is connected via a standard copper wire to the end device microcontroller. The electrode reports on occupancy, which is processed and collected on this microcontroller, and then sent to the Gateway unit.

For the reporting system, the Gateway microcontroller has a warning and notification system, SD-card storage device, and a cellular modem connected. The warning and notification system consists of light-emitting diodes (LEDs) and a buzzer to notify the driver or passengers of reckless driving manoeuvres and occupancy information. The SD-card provides the system with black box capability and the cellular modem enables real-time reporting of information. The uploaded real-time information is made graphically

available on an online dashboard. The dashboard can be accessed from any device with internet access. Since the reporting system consist of a cellular modem, it can easily be integrated with the existing cellular network in Sub-Saharan Africa. The microcontroller is also fitted with a GPS modem and accelerometer. The accelerometer provides acceleration data, which is filtered on the microcontroller to remove noise and offsets. The GPS modem provides the microcontroller with location, speed, and accurate date and time information.

In the rest of the chapter, the detailed sensing and reporting system design is investigated. The sensing system is dived into two main sections; capacitive sensing for occupancy detection, and the reckless driving detection system. Section 3.1 describes the detailed design of the capacitive sensing system for occupancy detection. Section 3.2 details the design of the reckless driving detection system, where a novel technique is discussed, to identify reckless driving manoeuvres in augmenting acceleration data with vehicle speed, and occupancy information. The hardware setup for the sensing and reporting system is discussed in section 3.3.

3.1 Capacitive sensing for occupancy detection

Previous work (Chapter 2) shows that the detection of an occupant in a vehicle is not a new concept, but that shortcomings exist for a realisable multiple occupancy detection system. In this chapter, a system is designed that can detect multiple occupants in a minibus taxi using a low cost setup.

The design of the sensor system, for public transportation vehicles, must be a robust setup. Capacitive sensors proved to be robust and inexpensive, and showed good performance in the past [83], it was therefore decided to investigate this sensing method for the implementation of a multiple occupancy detection system in minibus taxis.

In section 3.1.1, capacitive sensing in general is discussed, and three different sensing techniques investigated. The most suitable technique is adopted for the detection of multiple occupants. In section 3.1.2, the capacitive sensing system is designed and discussed, showing some expected results. In section 3.1.3, the system is discussed where the capacitive sensor readings are interpreted to determine if seat is occupied or unoccupied. In section 3.1.4, a simplified mathematical model for the designed capacitive sensor system is determined. The assumptions made for the mathematical model are also discussed. The analysis of the designed capacitive sensor follows in section 3.1.5. The capacitive occupancy detection system is concluded in section 3.1.6.

3.1.1 Capacitive sensing techniques

Capacitance is a quantity describing the charge stored between a set of electrodes where capacitive sensing (or electric field sensing) describes a number of modes to measure the capacitance between electrodes and its surroundings. These modes use electrodes to create electric fields, that induce potentials and displacement currents, which can be measured

to determine the intervening distribution matter between the electrodes. For proximity detection, the intervening matter is the human body. Smith [84] describes three distinct modes of capacitive sensing: loading mode, transmit mode and shunt mode. These modes correspond to the different possible electric current pathways.

In shunt mode, an oscillating voltage is applied at a transmit electrode and the induced displacement current measured on the receive electrode. When a human body enters the proximity of the electric field, the body effectively becomes grounded and screens the field, thereby reducing the current measured at the receiver electrode. This mode for capacitive sensing can be seen in Figure 3.2. In this method, however, two or more receiver electrodes have to be added in order to distinguish between a large mass far away and a small mass nearby.

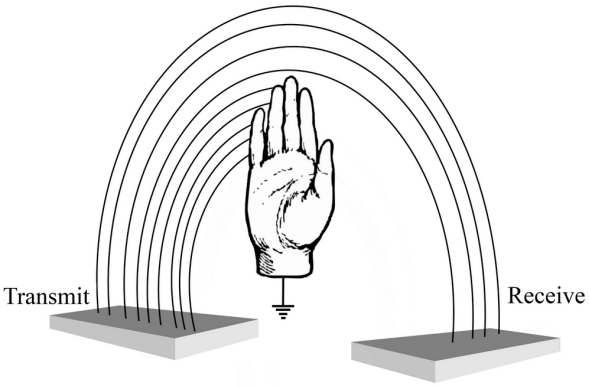

Figure 3.2: Shunt mode capacitive sensing.

Transmit mode capacitive sensing is where the body acts as a virtual extension or antenna of the transmitter to the receiver electrode. The body therefore prolongs the electric field of the transmitter electrode and since the received electric field is a function of distance between the body and the receive electrode, body position can then be estimated [85]. Figure 3.3 gives a schematic representation of this sensing technique. In this mode,

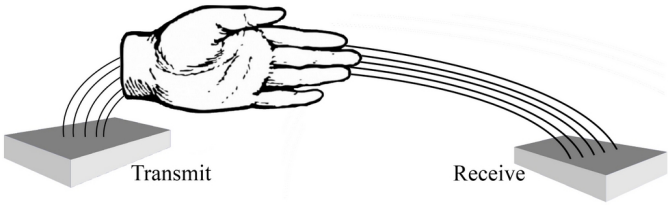

Figure 3.3: Transmit mode capacitive sensing.

the body is required to be connected to the electrode, either by direct contact or through capacitive coupling.

Loading mode capacitive sensing measures the change in capacitance between a single electrode and ground. This technique anticipates a certain capacitance in the circuit on

the transmitting electrode. A body entering the proximity of the sensor changes the total capacitance between the transmitting electrode and ground. The variation in capacitance then changes the frequency of the variable oscillator which is compared to a reference frequency. The frequency is determined from the time constant that is set by capacitive coupling. The loading mode capacitive sensing technique shown in Figure 3.4. A device that works on a similar principle, using this technique, is the Therminin, an electronic music instrument developed in 1919 [85].

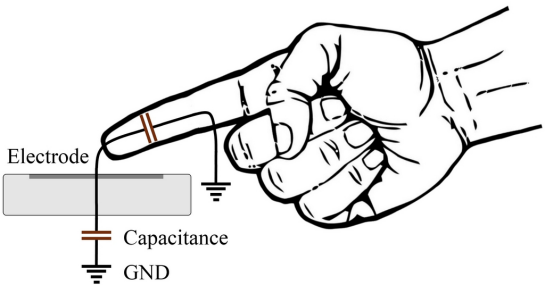

Figure 3.4: Loading mode capacitive sensing.

Shunt mode and transmit mode are popular modes for proximity detection in Smartphones. Although these two modes provide better accuracy than loading mode sensing, multiple sensors are required. In this paper a sensing and reporting system for the informal public transport sector, and particularly minibus taxis, is investigated. A typical minibus taxi has between 12 and 16 seats, which makes the implementation of multiple sensor capacitive sensing methods for the detection of a single occupant impractical. This is due to the increased complexity and cost for a high number of sensors. The loading mode technique is therefore implemented, since a single electrode can detect an occupant.

3.1.2 Design

Parallel plate capacitance can be defined as the amount of electrical charge, which changes with voltage, stored between two non-connected conductive plates. The capacitance depends primarily on the dielectric substrate of the objects, the size of the plates and the distance between them. A dielectric substrate is an electrically isolating material that provides isolation between the non-connected conductive plates. The loading mode capacitor configuration is therefore approximated by the parallel plate capacitor model, since the capacitance is effectively determined between two conductive mediums (that is, the electrode and ground) with a dielectric medium in between (consisting partially of air).

An electronic system that measures the capacitance directly or indirectly, using the loading mode capacitive sensing technique, is simply referred to as a capacitive sensor for the remainder of the paper. The implementation and design of the capacitive sensor's

electronic circuit follows in this section. The electronic circuit setup can be seen in Figure 3.5.

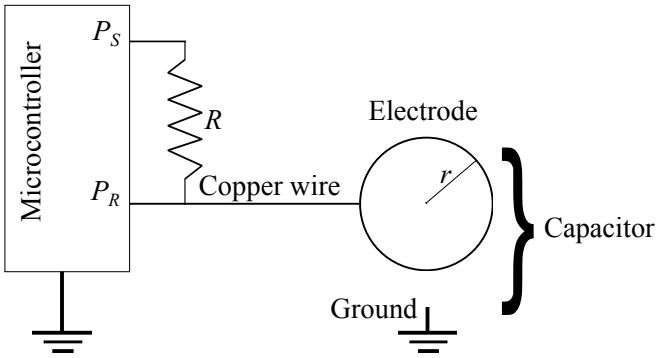

Figure 3.5: Capacitive sensor circuit diagram, with P_S and P_R the Stimulus and Response pin respectively, R is the resistor and r the electrode's radius.

The circuit requires a high value resistor (R) between the stimulus pin (P_S) and the response pin (P_R). The high value resistor ($10M\Omega$ - $50M\Omega$) ensures a sufficient charge/discharge time in the order of $500\mu s$. A higher R will result in a more sensitive capacitive sensor, but more susceptible to noise. The electrode is the sensor component to detect human proximity and is connected via a standard copper wire to the response pin. The sensor electrode is made from a thin circular metal plate covered by a piece of non-conducting material. This is the sensor component, which is installed on the surface area of the seat, and is occupied by the occupant. The placement of the electrode on the seat can be seen in Figure 3.8 on page 33.

The two digital pins are set up to be in one of two modes; the *stimulus* pin, which changes to a new state and waits for the *response* pin to change to the same state as the stimulus pin. The following sequence describes how the capacitive sensor is measured:

1. The stimulus pin is set as output and response pin as input.

2. A timer is started and the stimulus pin is set to logical high (V_{CC}) which charges the capacitor until the response pin crosses the threshold logical high (V_{IH}). The timer is then momentarily stopped (paused) while the response pin is charged completely to V_{CC} by setting the response pin to V_{CC}.

3. The timer is resumed when the stimulus pin is set to logical low (V_{OL}) which discharges the capacitor until the response pin crosses the threshold logical low (V_{IL}). The response pin is then set to V_{OL} (zero voltage).

4. The timer determines the time it takes for the response pin to charge to the logical opposite and resets to zero each time the stimulus pin changes to logical high. The change in capacitance can then be determined from the timer value before each reset occurring at the end of a cycle.

5. The process is repeated.

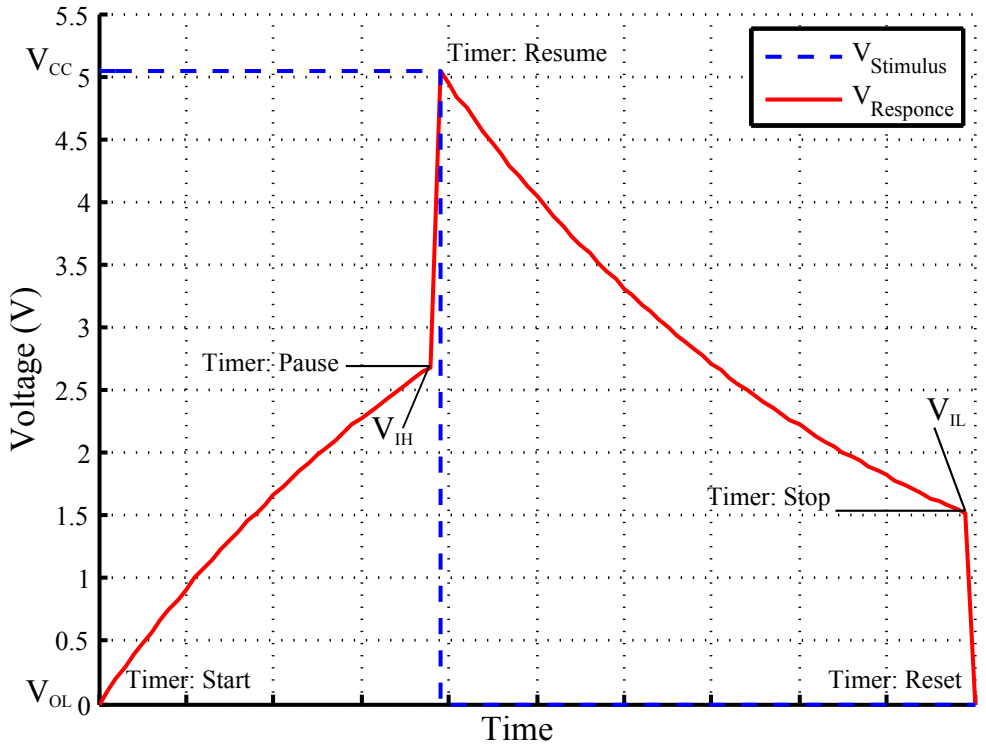

Figure 3.6: One cycle of the capacitive sensor's charge/discharge plot. The plot has a V_{CC} of $5.04V$ with V_{IH} and V_{IL} measured as $2.64V$ and $1.51V$, respectively.

The above described sequence can be seen in the capacitive sensor's charge/discharge plot in Figure 3.6. The value of the timer is directly proportional to τ, the RC time-constant in Equation 3.1. Since the resistor value (R) stays constant, the delay depends solely on the capacitance (C).

$$\tau = R \times C. \tag{3.1}$$

A human body entering the proximity of the sensor, changes the electrical properties between the sensor electrode and ground, which increases the total capacitance resulting in a higher RC time-constant. This will increase the capacitor's charge/discharge time. It is therefore possible to determine if a seat is occupied by interpreting the timer value. The microcontroller monitors the timer and regulates the oscillating frequency at which the voltages changes between the stimulus and response pins.

A multiple occupancy detection system requires multiple sensors since each sensor detects a single occupant. The sensors are installed on the sitting area of the seat as seen in Figure 3.7. One sensor is installed on each seat of the minibus taxi, except for the bigger rear seat where an additional sensor is placed. The sensing system is not designed to detect overloading, but to determine when a seat is occupied. The use of a capacitive sensing technique enables the sensors to distinguish between a human body and a non-human object (luggage for example).

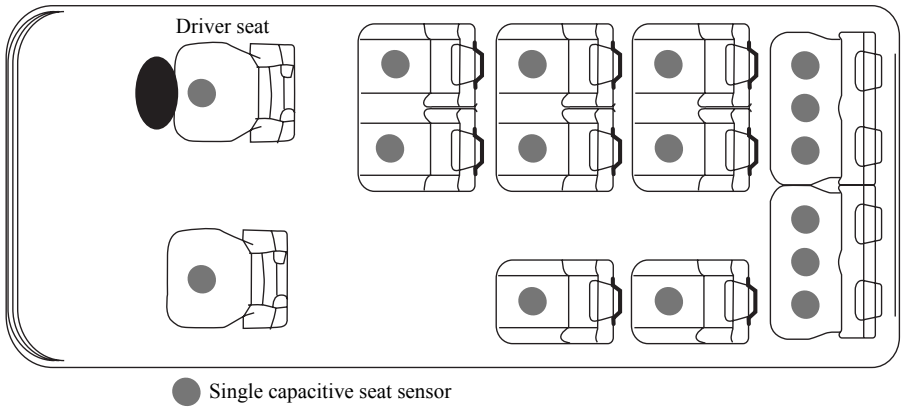

Figure 3.7: Top view of 14 seater Quantum taxi with occupancy sensors.

3.1.3 Occupant detection

In the previous section the design of the occupancy detection system was discussed. It was said that it is possible to determine if a seat is occupied by interpreting the timer value. In this section the detection of an occupant is discussed, by interpreting the timer value, which increases with an occupant on the seat.

From collected data, it was seen that the capacitance on the electrode contains a lot of noise. This is expected, since the sensing system is not contained to only detect the capacitance above the electrode (ideal model), but detects the capacitance in the proximity of the electrode. A filtering system is therefore implemented to remove these high frequency capacitance variations, which influences the output timer value.

The timer value of every charge/discharge cycle is filtered, using a low pass filter (LPF). An exponential moving average (EMA) is chosen as the LPF since it results in shorter effective lag than a simple moving average [86]. The EMA is a type of infinite impulse response filter that applies weighting factors which decrease exponentially. An empirically determined sampling rate of 50Hz is implemented for the occupancy sensor. Other sampling frequencies were tested, but this frequency resulted in good performance, and accurate results. The LPF takes the weighted average of the readings over the last 3 seconds. The 3 second weighted average was chosen since this filtering window filters out small manoeuvres performed by the occupant, when moving on the seat, and other external interferences on the vehicle.

When the filtered timer value exceeds the occupied threshold, the seat is seen as occupied. Timer values for the unoccupied state ranges between 0 and 50 cycles, and increases over 700 cycles when an occupant is present on the seat. An occupied threshold at 350 cycles is therefore chosen, since it accommodates for possible false readings.

A scenario that frequently occurs is when the minibus taxi stops to pick up or drop off passengers and the passengers move over the seats to make room for new passengers. A detection delay is therefore implemented that accommodates for the occupants moving over a seat, sitting temporarily on the sensor, but not actually occupying it. After the timer value indicated that the seat is occupied, the detection delay waits for 5 seconds,

and then changes the seat status. This applies for a change in state from occupied to unoccupied, and vice versa. This delay was determined empirically from numerous tests.

3.1.4 Theoretical representation and approximations

In this section a theoretical model, and simplified mathematical representation, of the capacitive sensor is developed to determine the relationship between the capacitance of an unoccupied and occupied seat. The analysis of the minibus taxi and capacitive sensors has indicated that a large number of factors can influence the sensors' capacitance. In order to determine a theoretical model of the capacitive sensor in a vehicle, some approximations are made.

The minibus chassis is chosen as the common electrical ground (GND) and reference point for the capacitive sensors. A change in capacitance between the electrode and the chassis is therefore determined with capacitive coupling assumed to be only between the electrode and ground. There are 14 or 15 passenger seats in a typical minibus taxi. For simplicity, the seats are assumed to have the same dimensions and material composition. The seat properties will be discussed later on in this section. The charge density distribution is assumed to be uniformly distributed on the electrode for the capacitive sensor to be approximated as a parallel plate capacitor (as discussed in section 3.1.1).

The simplified model of the sensor in the minibus taxi can be seen in Figure 3.8 with its corresponding circuit diagram in Figure 3.9. In Figure 3.8, S_1 represents a single capacitive sensor mounted in the seat where C_1 and C_2 are the parallel plate capacitance with respect to GND. Each of the seats will have such a sensor and thus a similar capacitive model. From Figure 3.9, V_S is the stimulus pin's output voltage, V_R is the response pin's input voltage, and R the resistor that stays constant. C_2 is the capacitance which changes when a human body enters the proximity of the sensor electrode.

The parallel plate capacitance (C) is given by

$$C = \frac{\epsilon_o \epsilon_r A}{d} \tag{3.2}$$

with:

- A plate area [m^2]
- d distance between plates [m]
- ϵ_o permittivity of free space $= 8.854 \times 10^{-12}$ F/m
- ϵ_r relative permittivity of the dielectric substrate between the plates [dimensionless].

Assuming that A and d stays constant, and since ϵ_o is a constant, only ϵ_r can change the capacitance.

With two parallel plates forming a capacitor, the electric field lines are not limited to the sensor, but curves outside the electrode causing the capacitance to be higher than what we would have calculated from the ideal expression Equation 3.2. This effect is

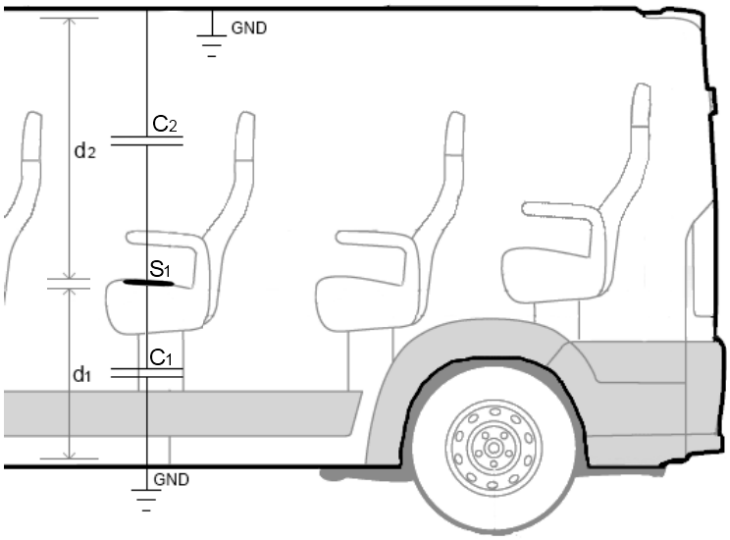

Figure 3.8: Simplified model of the capacitance between the sensor plate and minibus taxi. S_1 represents a single capacitive seat sensor and C_1 and C_2 the capacitance between the sensor and chassis (at common ground). C_1 stays constant where C_2 changes according to the presence and size of an occupant. d_1 and d_2 are the distance between the sensor and the chassis.

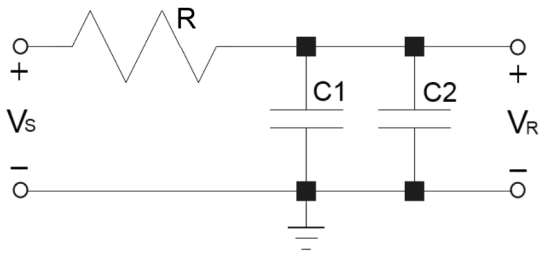

Figure 3.9: Circuit representation of the capacitive seat sensor. V_S is the voltage at the stimulus pin and V_R the voltage at the response pin. C_1 and C_2 are the capacitance between the seat and the chassis bellow and above the seat respectively. R is the high value resistor.

known as fringing. The capacitive sensor's electrode size (A) is therefore increased by 13% to accommodate the fringing effect [87] in the analysis in section 3.1.5.

Since a significant part of the dielectric substrate is composed of air, an effective dielectric constant (or effective relative permittivity) is derived by approximating the capacitive sensor as a microstrip transmission line. Microstrip transmission lines constitute of a conductive strip of width 'w' and a wider ground plane, separated by a dielectric substrate of thickness/height 'h'. Figure 3.10 gives the cross-section of a microstrip transmission line with the conductor (A) separated from the ground plane (D) by the dielectric substrate (C). The upper dielectric (B) is typically air.

The effective relative permittivity (ϵ_e) is somewhat less than the substrate's relative permittivity due to the part composed of air (with a relative permittivity of 1) and can

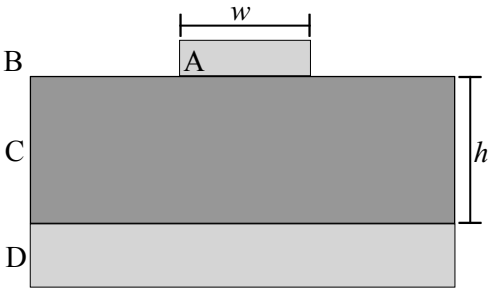

Figure 3.10: Representation of a microstrip transmission line. 'A' is the conductor separated from the ground plane 'D' by a dielectric substrate 'C'. 'B' is the upper dielectric, typically air. The dielectric substrate has a thickness of 'h' and the conductor a width of 'w'.

be approximated, according to [88], with the following expression:

when $\left(\frac{w}{h}\right) \geq 1$

$$\epsilon_e = \frac{\epsilon_r + 1}{2} + \frac{\epsilon_r - 1}{2}\left(1 + 12\left(\frac{h}{w}\right)\right)^{\frac{-1}{2}} \tag{3.3a}$$

when $\left(\frac{w}{h}\right) < 1$

$$\epsilon_e = \frac{\epsilon_r + 1}{2} + \frac{\epsilon_r - 1}{2}\left[\left(1 + 12\left(\frac{h}{w}\right)\right)^{\frac{-1}{2}} + 0.04\left(1 - \left(\frac{w}{h}\right)\right)^2\right]. \tag{3.3b}$$

As explained in section 3.1.2, the time constant depends solely on C_{TOTAL} where the total capacitance of two parallel capacitors in a circuit is given by

$$C_{TOTAL} = C_1 + C_2. \tag{3.4}$$

The capacitance under the seat (C_1) stays constant, contrary to the capacitance above the seat (C_2) which can be in either one of states: occupied (OCC) or unoccupied (UNOCC). The total capacitance on the electrode when no human body is in proximity of the sensor, i.e. the unoccupied state, is calculated as

$$\begin{aligned} C_{TOTAL(UNOCC)} &= \frac{\epsilon_o \epsilon_{e1} A}{d_1} + \frac{\epsilon_o \epsilon_{e2_{UNOCC}} A}{d_2} \\ &= \epsilon_o A \left(\frac{d_1 \epsilon_{e2_{UNOCC}} + d_2 \epsilon_{e1}}{d_1 d_2}\right) \end{aligned} \tag{3.5}$$

where $\epsilon_{e2_{UNOCC}}$ and ϵ_{e1} is the effective dielectric constant of respectively the dielectric substrate above and below the sensor electrode. The total capacitance on the electrode with a human body in proximity of the sensor, i.e. the occupied state, is calculated similarly:

$$\begin{aligned} C_{TOTAL(OCC)} &= \frac{\epsilon_o \epsilon_{e1} A}{d_1} + \frac{\epsilon_o \epsilon_{e2_{OCC}} A}{d_2} \\ &= \epsilon_o A \left(\frac{d_1 \epsilon_{e2_{OCC}} + d_2 \epsilon_{e1}}{d_1 d_2}\right) \end{aligned} \tag{3.6}$$

where $\epsilon_{e2_{OCC}}$ is the effective dielectric constant of the substrate above the sensor electrode when an occupant is present.

We have therefore calculated the expected capacitance on the sensor of an unoccupied and occupied seat. The only difference between the capacitance is from a change in ϵ_{e2}.

3.1.5 Analysis

The main composition of the vehicle's seat material is polyethylene foam [89], with a relative permittivity of 2.26 [90]. The relative permittivity of the vehicle's seat is therefore approximated as 2.26. From Equation 3.3a the effective relative permittivity (ϵ_{e1}) is calculated as 1.88, since the capacitive sensor electrode has a diameter w of 0.22m and dielectric substrate height h of 0.10m, which therefore results in a relationship where $\frac{w}{h} > 1$. The reason for this low substrate height is because of the metal found in the seat which effectively reduces the distance between the sensor electrode and ground. For the dielectric substrate above the electrode: the relative permittivity ($\epsilon_{r2_{UNOCC}}$) is estimated as 1, which is the relative permittivity of air, since almost all of it is air.

An occupant on the seat will increase the relative permittivity of the dielectric substrate above the electrode ($\epsilon_{r2_{OCC}}$) substantially, since the human body consists 70.4% of water [91], which has a relative permittivity of 74.1 [92]. The human body is therefore approximated as having the same dielectric properties of water. An effective relative permittivity is calculated from Equation 3.3b as 42.91, with w and h as 0.22m and 1.27m respectively resulting in a w/h relationship where $\frac{w}{h} < 1$.

The theoretical model is concluded by calculating the approximated capacitance on the sensor electrode. The unoccupied capacitance is calculated from Equation 3.5 to be 8.41pF and the capacitance on the electrode when an occupant is present is calculated from Equation 3.6 to be 22.59pF. The dimensions used during calculations are from actual measurements in a Quantum minibus taxi, with d_1 measured as 0.1m and d_2 as 1.27m. The area of the electrode is calculated as, $A = \pi(0.11 \times 1.13)^2$, which is increased by 13% because of the fringing effect. The following table is a summary of calculated theoretical capacitance, and includes the values of the two capacitances in parallel (C_1 and C_2) from the simplified circuit diagram in Figure 3.9.

Table 3.1: Calculated theoretical capacitance below (C_1) and above (C_2) the sensor electrode – the capacitances are in parallel as seen in Figure 3.9.

	Unoccupied capacitance (pF)	Occupied capacitance (pF)	Equations
C_1	8.07	8.07	3.2 and 3.3a
C_2	0.34	14.52	3.2 and 3.3b
C_{TOTAL}	8.41	22.59	3.5 and 3.6

By comparing the capacitance of the unoccupied state with the capacitance of the occupied state, there can be seen that the occupied state has a significantly larger capacitance. The relationship between occupied/unoccupied is calculated as 2.7, thus more than double. From the theoretical calculations it is therefore determined that an occupant can clearly be detected on the capacitive sensor electrode.

3.1.6 Conclusion

The analysis in this section shows that the capacitive sensing system can clearly detect an occupant on the minibus taxi's seat, and that this solution is ideal for the detection of multiple occupants in a minibus taxi.

In section 3.1.1, three different capacitive sensing techniques were discussed: shunt mode, transmit mode and loading mode. The shunt mode capacitive sensing technique is not a practical solution since multiple electrodes have to be added for the detection of a single occupant. Transmit mode capacitive sensing is not viable since the body is required to be connected to the electrode. The loading mode sensing technique was adopted since only a single electrode is required for the detection of an occupant.

In section 3.1.2, the implementation and design of the capacitive sensor was discussed, showing the circuit design with recommended values for the components. The sensor system measures the capacitance on an electrode from a charge-discharge cycle. The presence of an occupant can then be determined by studying a timer value which increases with the presence of an occupant on the electrode. The sensor layout in the taxi is also shown.

In section 3.1.3, the timer value from section 3.1.2 is filtered using an exponential moving average filter, and interpreted to determine if a seat status is occupied or unoccupied. The system discussed in this section accommodates for occupants moving over a seat but not actually occupying it.

A simplified mathematical model, of the designed capacitive sensor, was developed in section 3.1.4. In order to develop the mathematical model, some approximations were made. The section concluded with a developed simplified mathematical model that calculates the capacitance on the sensor electrode for an occupied and an unoccupied state.

In section 3.1.5, properties and dimensions of a seat in a Quantum minibus taxi was entered into the simplified mathematical model, and the expected capacitance calculated. There was found that the occupied capacitance is 2.7 times the unoccupied capacitance. The theoretical results show that the presence of an occupant on the seat can therefore clearly be detected by the designed capacitive sensor.

3.2 Reckless driving detection system

The implementation of accelerometers for the detection and classification of driving events is not a new concept as seen in Chapter 2. This section will discuss the novel techniques

used to identify reckless driving manoeuvres in augmenting acceleration data with vehicle speed, and occupancy information.

In section 3.2.1, the difference between minibus taxis' driving on urban and highway roads are discussed. Reckless driving events are also defined, and classified into urban events and highway events. Studying the difference between urban and highway events is important for the development of a reliable reckless driving detection system. In section 3.2.2, the detailed filter design is discussed. The filtering system prepares the unprocessed acceleration data, from the accelerometer, for the comparison with a reckless driving acceleration threshold. Crossing the threshold relates to a reckless driving manoeuvre. Two thresholds are suggested: a lateral threshold, which is dependent on speed, and a longitudinal threshold, which is static. Both of these thresholds are based on principles used for the design of roads. The reckless driving acceleration threshold, is discussed in section 3.2.3. In section 3.2.4, a compensation factor is developed to take occupancy count into consideration, which is combined with the threshold designed from road principles. After the filtered acceleration is compared with the developed threshold, section 3.2.5 introduces a value system that monitors the severity and the number of occurrences of reckless manoeuvres performed by a driver. In section 3.2.6, an analysis of the detection system follows, where the sampling rates for the accelerometer and the filtering system is determined. The reckless driving detection system is concluded in section 3.2.7.

3.2.1 Highway and urban driving

Before a reckless driving detection system can be developed, the differences between urban and highway driving manoeuvres are investigated. Some significant differences were observed.

Minibus taxis on long distance (highway) and short distance (urban) roads were studied by collecting acceleration data, from an accelerometer, and speed data, from a GPS. Acceleration data give us the duration and magnitude of the driving manoeuvre performed by the driver. Driving manoeuvres are classified into two categories: urban events, and highway events. An urban event is a manoeuvre performed by the driver that includes a pull-over, turn or braking action, where highway events include, circular road curve following, swerving and braking. The main differences between urban and highway events are listed in Table 3.2.

The typical speed limit on urban roads is 60 km/h, where highways have a maximum legal speed limit, for minibus taxis, of 100km/h. Speeding in urban areas is common, but does not come close to the excessive speeds reached on highways. Speeds of over 140km/h were recorded by tracked minibus taxis, which is 40km/h over the legal speed limit. Accidents occur frequently on both urban roads and highways, but highways' accidents shows a much higher fatality rate than urban roads [93]. Longitudinal and lateral events occur more frequently on urban roads than on highways, since minibus taxis regularly stop, or pull over to the side of the road to pick up passengers. Long

Table 3.2: Differences between minibus taxi drivers' driving on urban and highway roads.

Property	Urban roads	Highway roads
Typical legal travelling speeds	below 70km/h	below 100km/h
Maximum detected speed	below 80km/h	above 140km/h
Frequency of longitudinal event occurrences	high	low
Frequency of lateral event occurrences	high	medium
Typical duration of longitudinal event	short (13 seconds)	long (19 seconds)
Typical duration of lateral event	short (9 seconds)	long (17 seconds)
Accidents	injuries and fatal accidents do occur	high fatality rate
Types of manoeuvres/events	turns, braking, pull-over	circular road curve following, swerving, braking

distance taxis are loaded early in a long distance journey and they don't stop often. From the collected acceleration data, it was found that the average duration of longitudinal events is significantly shorter for urban events than highway events. The same was found for lateral acceleration events.

These differences show that the developed reckless driving detection system must incorporate both urban and highway road events. In order to accommodate these differences, a filtering and reckless event detection system is designed accommodating both urban and highway events.

3.2.2 Filter design

In this section, a filtering system is developed, that receives unprocessed (raw) lateral and longitudinal acceleration data from a 3-axis accelerometer, and prepares the data for the detection of reckless driving events.

Raw acceleration data is filtered with a low pass filter (LPF) to remove high frequency noise picked up from the vehicle and sensor noise. An exponential moving average (EMA) is chosen as the LPF. The filter output is given by

$$y_f[n] = \gamma x[n] + (1-\gamma)y[n-1] \tag{3.7}$$

where $\gamma = \frac{2}{N+1}$ and $y_f[n]$ is the output of the LPF and therefore the EMA value. The current sample is represented by $x[n]$ and N is the number of samples.

The derivative of the filtered acceleration data is then taken with respect to time to determine the rate of change of acceleration, i.e. the jerk, which is given by

$$\frac{dy_f(t)}{dt}_{t=nT_s} = y_{fd}[n] = \frac{y_f[n] - y_f[n-nT_s]}{T_s} \tag{3.8}$$

where T_s is the sampling period of the differentiator. The window width of the EMA is defined as $W_n = nT_s$. The transfer function of Equation 3.8 is given by

$$H_D(z) = \frac{Y_{fd}(z)}{Y_f(z)} = \frac{1-z^{-W_n}}{T_s} = f_s(1-z^{-W_n}). \tag{3.9}$$

Substituting Equation 3.7 into Equation 3.9 gives the complete jerk equation, namely

$$y_{fd}[n] = (1-\gamma)y_{fd}[n-1] + \gamma f_s(x[n] - x[n-W_n]). \tag{3.10}$$

Since jerk is the derivative of acceleration, it gives an indication of changes in acceleration. High acceleration peaks over a small Δt, results in high jerk values. By interpretation of the jerk, it is possible to determine sharp driving actions and therefore reckless driving manoeuvres. Gradually increasing acceleration, or constant high acceleration, will not result in high jerk values, although it may be dangerous. Jerk can therefore not be used alone as an indication of reckless driving.

This problem is overcome by summing the jerk samples ($y_{fds}[n]$) over a moving window. High concentrations of changes in acceleration are identified, which indicates a lateral or longitudinal driving event and is determined by the following equation

$$y_{fds}[n] = \sum_{k=n}^{W_n} |y_{fd}[k]| \,. \tag{3.11}$$

The summation of the acceleration data, essentially performs a Riemann integration over the jerk, back to acceleration, removing the unwanted DC-offset. The differentiation and summation system therefore shows characteristics of a high pass filtering (HPF) system, since the low frequency DC-offsets, including gravity, are removed.

A filtering system has therefore been developed that removes remove high frequency noise as well as unwanted DC-offsets from the acceleration data.

3.2.3 Reckless driving acceleration threshold from road design principles

Roads are designed to optimize efficiency and safety, whilst minimizing cost and environmental damage. Worn out tyres, heavy rainfall and light rain after a long dry spell significantly reduce the friction between the road and a vehicle's tyres [94]. This applies particularly to areas where the road surface is polluted by rubber and oil spills, as is the case in urban areas and the immediately surrounding rural areas. In road design, the friction relationship between a vehicle's tyres and the road surface is represented by a friction coefficient. For the purposes of road design, it is desirable to design for a friction coefficient lower than the value at which skidding is expected, since any of these determined factors are likely to present on any given road.

In this section, a correlation between the friction coefficient, used for the design of roads, and in-vehicle inertial acceleration is determined. The correlation between the friction coefficient and acceleration provides us with a conservative reckless acceleration threshold. Two different frication coefficients exist. The one is for lateral manoeuvres, which is discussed in section 3.2.3.1, and the other for longitudinal manoeuvres, discussed in section 3.2.3.2.

3.2.3.1 Lateral threshold

A key determinant of the safeness of a curvature in the road is the curve radius. A vehicle moving around a circular curve experiences a radial force, usually referred to as the

centrifugal force [26]. This outward radial force is opposed by the centripetal acceleration acting towards the centre of the curvature. The amount of centrifugal force the vehicle can withstand before slipping outwards depends on the side friction between the tyres and the road and the vehicle's weight along the inclined surface. Roads are designed with an incline to aid the centripetal acceleration in balancing out the centrifugal force. This inclination of the roadway is known as superelevation [95]. The forces acting on the vehicle are illustrated in Figure 3.11.

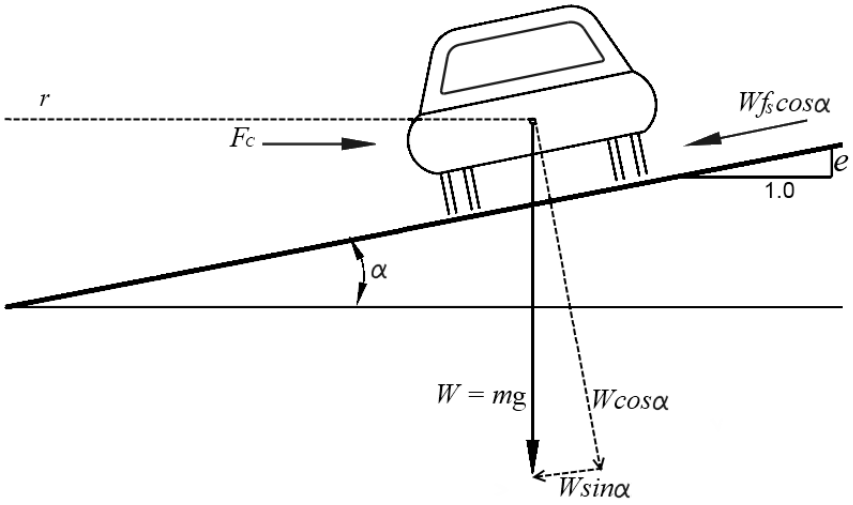

Figure 3.11: Forces acting on a vehicle travelling on a horizontal curve section of a road. Image adapted from [26]

The inclination of the road is denoted with α, and the component of weight (W) along the inclined surface is $W \sin \alpha$. The force of friction down the inclined surface is $W f_s \cos \alpha$, where f_s is the coefficient of side friction.

The centrifugal force, F_c is given by [26] as

$$F_c = \frac{W a_c}{g} = \frac{W u^2}{gr} \tag{3.12}$$

since the equation for centripetal acceleration is

$$a_c = \frac{u^2}{r} \tag{3.13}$$

with

a_c	acceleration for curvilinear motion
u	speed (m/s)
r	radius of the curve
W	weight of the vehicle
g	gravity (9.8m/s^2)

From Equation 3.12 it can be seen that increasing the curve radius (r), the amount of centrifugal force experienced by the vehicle decreases; however, a minimum curve radius is desired to minimize the cost and environmental damage.

An expression of the minimum curve radius has therefore been developed by civil engineers for designing roadways. When the vehicle in Figure 3.11 is in equilibrium with respect to the incline (vehicle moving forward, but neither up nor down the incline); the horizontal force component, is given by

$$F_c \cos\alpha = W \sin\alpha + W f_s \cos\alpha. \tag{3.14}$$

Substituting Equation 3.12 into Equation 3.14, gives

$$\begin{aligned} \frac{Wu^2}{gr}\cos\alpha &= W\sin\alpha + W f_s \cos\alpha \\ \frac{u^2}{gr} &= \tan\alpha + f_s \\ r &= \frac{u^2}{g(\tan\alpha + f_s)}. \end{aligned} \tag{3.15}$$

Superelevation is described in terms of the rate of superelevation (e) which is the rise in the roadway surface elevation as you move from the inside to the outside edge of the road; i.e. $\tan\alpha$, which is the tangent of the angle of inclination of the roadway. Equation 3.15 can therefore be written as

$$r = \frac{u^2}{g(e + f_s)}. \tag{3.16}$$

Equation 3.16 gives the minimum curve radius for road design. In order to prevent vehicles from slipping outwards due to centripetal acceleration exceeding the design parameters, we derive a threshold from this minimum curve radius.

A conservative approach to calculating the minimum radius of a curvature, is to take the rate of superelevation as zero (no incline), which results in

$$r = \frac{u^2}{g f_s}, \tag{3.17}$$

and rearranging Equation 3.17 gives

$$g f_s = \frac{u^2}{r}. \tag{3.18}$$

In order to find the maximum centrifugal acceleration (conservative approach) that a vehicle can experience before slipping, we combine Equation 3.18 with Equation 3.13, which results in

$$a_c = g f_s. \tag{3.19}$$

The maximum centrifugal acceleration is therefore represented in terms of gravity and the side friction coefficient. According to Geometric Design Guidelines in [95], the coefficient of side-friction is

$$f_s = 0.21 - 0.001U \tag{3.20}$$

where U is the vehicle speed in km/h. Combining Equation 3.20 and 3.19 gives

$$\frac{a_c}{g} = f_s = 0.21 - 0.001U. \tag{3.21}$$

Since g-force (G) is a_c/g [96], Equation 3.21 can therefore be written as

$$G_{lat} = 0.21 - 0.001U \tag{3.22}$$

which gives the maximum lateral g-force threshold (G_{lat}) around a curve.

A lateral reckless acceleration threshold, that is dependent on the vehicle's speed, has therefore been designed. The threshold uses in-vehicle inertial measurements and road curvature design to give an indication of potential reckless events.

3.2.3.2 Longitudinal threshold

In this section, a longitudinal threshold, for the detection of reckless events, is designed.

A nominal deceleration rate of 3.5m/s^2 is recommend by AASHTO (American Association of State Highway and Transportation Officials) [97], which relates to 0.35G, although most drivers stop at a rate higher than 4.5m/s^2 when confronted with the need to stop for an unexpected object in the roadway.

This is a conservative and comfortable longitudinal deceleration rate for most drivers and is within a driver's capability to stay within the road lane and maintain steering control during the braking manoeuvre on wet surfaces. This deceleration rate is therefore implemented as the longitudinal threshold for reckless driving events.

In section 3.2.3.1 a dynamic lateral threshold, which reduces with an increase in speed, was designed, where the longitudinal threshold designed in this section is static at 0.35G. The two developed thresholds follow a conservative design. A threshold, that is occupancy dependant, is introduced in the next section as an addition to these two thresholds.

3.2.4 Occupancy dependant threshold

The number of passenger in a minibus taxi affects the weight and dynamics of the vehicle. We therefore propose an additional, empirically determined threshold, which is based on the occupancy count, and combined with the acceleration threshold from road design principles.

The weight of a 14-seater Quantum minibus taxi is 1860kg and the gross laden mass is 3150kg. By taking the average weight of a person in Africa as 60.7kg [98], and since a legal maximum of 15 passengers are allowed in the taxi, we can calculate the total additional

mass as 910.5kg which is 29% of the vehicle's laden mass. The momentum of the vehicle increases with the additional weight in the minibus taxi. A dynamic occupancy dependant threshold is therefore implemented, in which the threshold decreases with an increased number of occupants in the vehicle. The threshold decreases linearly, with a total decrease of 0.035G, which is 10% of the maximum longitudinal g-force, when 16 occupants are in the minibus taxi. The resulting threshold, which is occupancy dependant, is therefore given by the following equation

$$G_{occ} = -0.035/16P = -0.0021875P \tag{3.23}$$

where P is the total number of passengers in the taxi.

This threshold is summed with the lateral and linear acceleration thresholds from road design principles. The complete lateral acceleration threshold is therefore

$$G_{lat} = 0.21 - 0.001U - 0.0021875P \tag{3.24}$$

and the longitudenal acceleration threshold is

$$G_{lon} = 0.35 - 0.0021875P. \tag{3.25}$$

An occupancy compensation factor has therefore been developed, which is combined with the threshold, designed from road principles, in section 3.2.3. In the next section, the developed threshold (Equation 3.24 and 3.25) is compared to the filtered output, from section 3.2.2, which classifies the reckless driving events.

3.2.5 Value system to classify reckless manoeuvres

In this section, a value system is suggested to determine the severity and the number of occurrences of reckless manoeuvres. Filtered acceleration data, from section 3.2.3, is compared to the reckless acceleration threshold, developed in section 3.2.4. The acceleration value above the threshold is calculated when the acceleration exceeds the threshold, and the severity of a reckless manoeuvre is determined from this value. The difference between the current acceleration and the current threshold is calculated and compared with a reckless level system summarised in Table 3.3. From the table we can see that higher acceleration values lead to higher reckless levels. For every reckless event, the highest acceleration difference in that event, is compared to the table.

Acceleration readings over the threshold that have a difference lower than 0.03G, have a given level of one. The given levels add up for every reading over the threshold with the different levels seen in Table 3.3. For every hour of driving where no reckless events occurred, a value of one is deducted from the total level sum. The sum of the levels added up gives an indication of how reckless the drivers' driving was. Reckless events with an acceleration difference over 0.8G depict that the vehicle was in an accident. When the sum goes over a certain value (e.g. 10) the involved authorities could be notified.

Table 3.3: Summary of the value system.

Acceleration over threshold (milli-G)	Reckless level
0 - 34	1
35 - 69	2
70 - 104	3
105 - 139	4
140 - 174	5
175 - 209	6
210 - 799	7
> 800	10

An example follows: for a minibus taxi, travelling at 50km/h, with a total of 10 passengers (11 including the driver), the longitudinal and lateral acceleration threshold is calculated as

$$\begin{aligned} G_{lat} &= 0.21 - 0.001 \times 50 - 0.0021875 \times 11 \\ &= 0.136 \\ G_{lon} &= 0.35 - 0.0021875 \times 11 \\ &= 0.326. \end{aligned}$$

If the driver goes around a bend experiencing a g-force value of 0.2G, the event is registered as a level 2 lateral reckless event. If the driver stops suddenly, and experiences a g-force value of 0.3G, the event is not registered as a reckless event, and therefore ignored.

The developed level system therefore processes the acceleration over the threshold, and gives an indication of the reckless scale of a manoeuvre, enabling monitoring authorities to make informed decisions about the drivers' driving.

3.2.6 Analysis of the reckless driving detection system

In this section the theoretical design is analysed with discussions of what is to be expected in the results. First, the sampling rate to be used for the accelerometer is discussed, followed by the low pass filter sampling rate. The interval over which the jerk and summation takes place is then evaluated.

3.2.6.1 Sampling rate

The lowest sampling rate for the accelerometer is desired to maximise power efficiency and performance, and minimise the number of samples to transfer and store.

The accelerometer and LPF sampling frequency was determined empirically as 20Hz. Other sampling frequencies for the accelerometer were tested, but this frequency resulted in good performance, producing acceleration data for all driving manoeuvres.

Since the accelerometer samples at 20Hz, the EMA takes the weighted averages over the last second. Other sampling times were evaluated, but this sampling time proved to work well, since engine noise and other high frequencies were filtered out without affecting any relevant data.

3.2.6.2 Differentiation and summation analysis

In this section, the duration of events is investigated in order to determine the optimal interval over which the low pass filtered acceleration must be differentiated and summed.

From collected vehicle acceleration data, it was found that the duration from the beginning to the peak of an acceleration event, has the same duration as from the peak to the end of that event. An example of this can be seen in Figures 3.12 and 3.13 on page 46. An assumption is therefore made, that the acceleration events tend to be symmetrical. The optimal interval, over which the data is differentiated to find the highest jerk values, is from the lowest acceleration value to the highest, i.e. from the beginning of an event to the peak. This interval therefore relates to half of the total event duration.

A difference in the duration between urban and highway events is expected, as explained in section 3.2.1. The durations of longitudinal and lateral events are also expected to differ. To determine the event durations, empirical data from longitudinal and lateral acceleration in urban and highway scenarios were analysed, and the duration of significant events determined. Very small acceleration levels were observed for manoeuvres that have low potential of risk, and regarded as insignificant. The average event durations from the collected data of multiple events from different minibus taxis and roads were determined. The results of the duration for the different events can be seen in Table 3.4. To capture

Table 3.4: Summary of the duration of events for urban and highway roads. Results are in seconds.

	Longitudinal acceleration	Lateral acceleration
Urban roads	12.88	8.82
Highway roads	19.39	17.03

the durations of an event, the window size used in the EMA (section 3.2.2) needs to match the event durations. Since the acceleration curve is symmetrical, the peak acceleration is at half of the event's duration. An average event duration of 14.53 seconds is calculated from Table 3.4 with 7.27 seconds as the half of the duration. This differentiation duration was tested on longitudinal and lateral acceleration in urban and highway scenarios, but it was found that the 7 second differentiation duration did not detect all events in the urban scenario. A 5 second differentiation duration showed optimal results for both urban and highway scenarios. Since the window size for the differentiation and summation is the same (section 3.2.2), the summation's durations is also taken as 5 seconds.

Figure 3.12 is an example of how the duration of longitudinal urban events is determined. The values above the zero y-axis are longitudinal forward acceleration and are not taken into account, since this type of acceleration does not directly lead to accidents. Acceleration bellow the zero y-axis is deceleration and represents braking events or sudden stops (e.g. accident). The acceleration plot in Figure 3.13 shows the duration of three

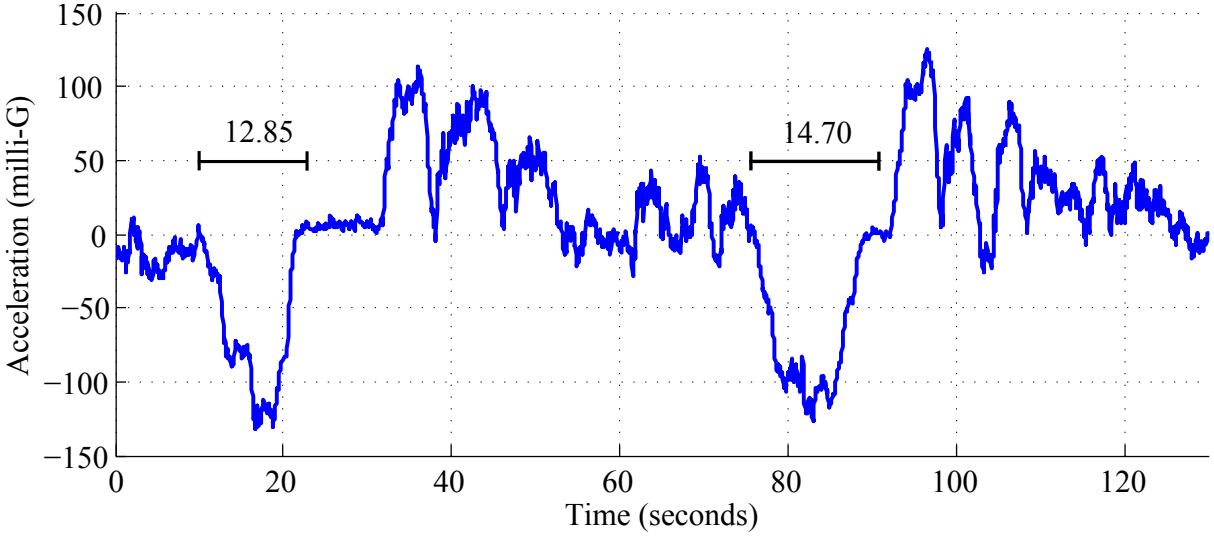

Figure 3.12: Longitudinal acceleration in an urban area showing two braking events. Values below the zero y-axis are braking events or sudden stops and values above are forward acceleration.

highway longitudinal events. The values above the zero y-axis are right turns and values below are left turns.

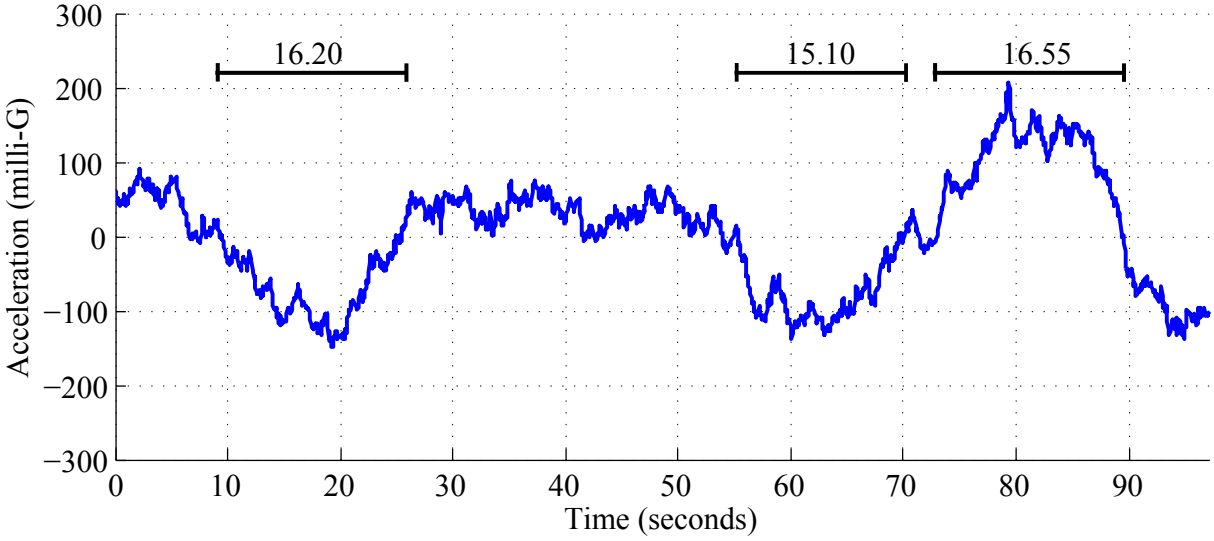

Figure 3.13: Lateral acceleration on a highway showing two left turns and a right turn. Values above the zero y-axis are right turns and values below are left turns.

In this section, the differentiation and summation durations were analysed and an optimal 5 second window established.

3.2.7 Conclusion

The reckless driving detection system is concluded in this section, giving an overview and commenting on some key concepts of each section.

In section 3.2.1, a number of differences between urban and highway roads were observed. The filtering system, developed in section 3.2.2, had therefore to be designed to incorporate these differences. The differentiation and summation filtering system behaves like a high pass filter (HPF), since it removes the unwanted DC-offset, and serves two functions:

- If the accelerometer is not installed perfectly level in the vehicle a resulting DC-offset will be present due to gravity. The HPF removes this offset.
- When the vehicle encounters a slope, gravity will induce an acceleration reading on the x-axis and/or y-axis. This reading can be very high, depending on the gradient of the slope, and may trigger a false positive. The implementation of the HPF removes the effect of the gravitational field on the unwanted axis.

In section 3.2.3, a reckless diving acceleration threshold is designed, from principles used in road design. Two thresholds are developed: a lateral and longitudinal threshold. The lateral reckless acceleration threshold is dependent on the vehicle's speed, and was designed, using in-vehicle inertial measurements, to give an indication of potential reckless events. The longitudinal threshold is static at 0.35G, and is based on a nominal deceleration rate of 3.5m/s^2. Exceeding these parameters can therefore increase the risk of an accident. An occupancy dependent threshold was introduced in section 3.2.4, and a compensation factor developed. The compensation factor takes the number of occupants in the minibus taxi in to account, since each occupant increases the weight of the vehicle, which results in increased momentum. The compensation factor is added to the threshold designed from road principles. An accident is therefore not guaranteed when exceeding the threshold, but relates to a high potential for loss of control over the vehicle. These parameters are incorporated into the development of an acceleration threshold to increase the safety of the driver, passengers, pedestrians and other vehicles on the road.

A value system was introduced in section 3.2.5, which calculates the acceleration over the threshold (when a reckless event occurs), and compares with a level table. The level table therefore gives a quick indication of how reckless the event was.

In the analysis of the reckless driving detection system (section 3.2.6), an optimal sampling rate for the filtering system was determined. The accelerometer and the EMA samples at 20Hz. An optimal 5 second sampling window for the differentiation and summation of the EMA filtered acceleration was established.

A reckless driving detection system has therefore been developed, that accepts raw noisy acceleration data, filters it, and compares it to a threshold that is based occupancy information, in-vehicle inertial measurements, and the friction coefficient between the vehicle and the road.

3.3 Hardware and software setup

The sensing and reporting system, which was designed in the two parts, is implemented as a prototype, with the hardware and software setup discussed in this section. An overview of the system was disused in the introduction of this chapter (page 24), and the network diagram of the sensing and reporting system was shown in Figure 3.1 on page 25. Figure 3.14 shows an image of the developed prototype (left) and a capacitive sensor (right). The prototype can be connected to the minibus taxi's cigarette lighter receptacle, but a

Figure 3.14: This figure shows the developed prototype (left) and the capacitive occupancy detection sensor (right).

12V 7Ah Sealed Lead Acid rechargeable battery was used for practicality.

Figure 3.15 shows the main software functions for the prototype. A detailed discussion of the software setup can be found in Appendix A. The software is written into two programs as seen in the figure: an end device microcontroller program, and a Gateway unit microcontroller program.

Arduino was chosen as the microcontroller platform for the prototype, and the Arduino code written in the C programming language. Arduino is an open-source electronics

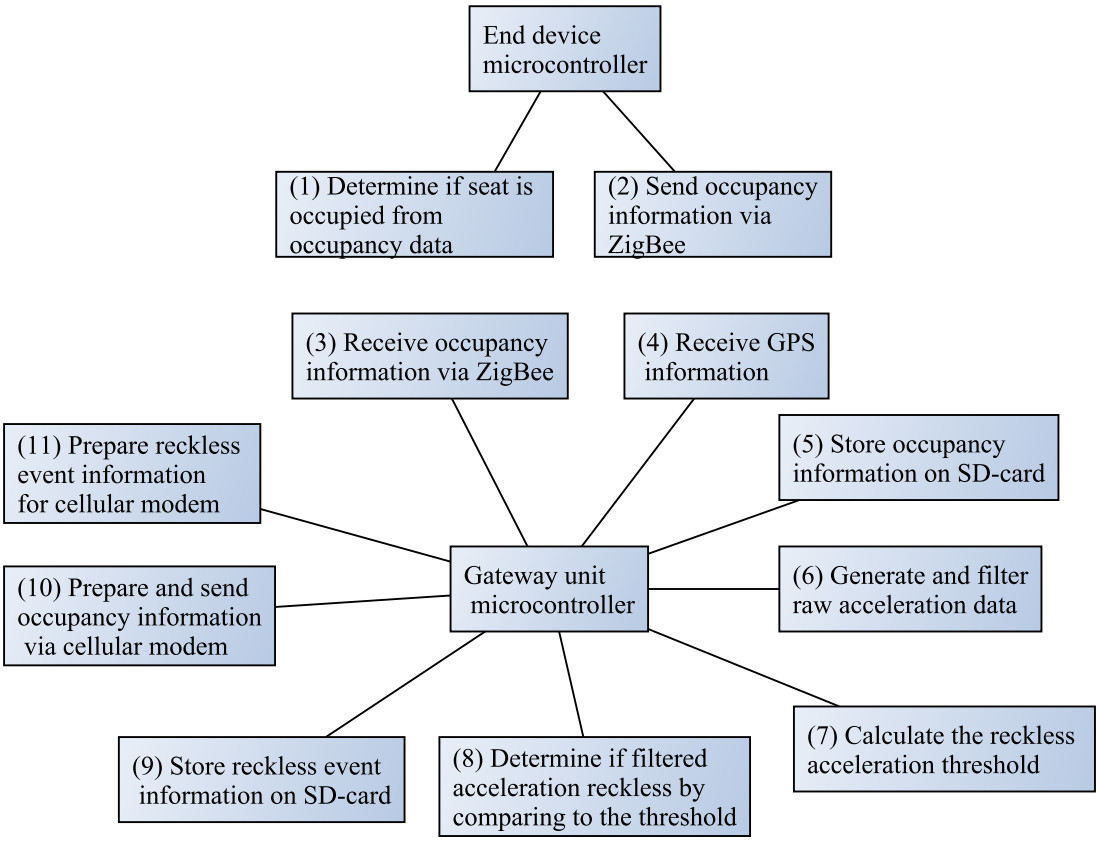

Figure 3.15: Software functions for the prototype. The numbers indicate the sequence in which the flow diagrams are discussed in Appendix A.

prototyping platform based on flexible hardware and software [99]. The board was chosen since it is inexpensive, and provides all the circuitry necessary for the other electronic components in the prototype to be connected. Arduinos can be expanded with *shields*. Arduino shields are boards that can be plugged on top of the Arduino, extending its capabilities. An Arduino Mega2560 microcontroller board, which is based on the ATmega2560, is used as the Gateway unit microcontroller. The Arduino Mega2560 is ideal for the Gateway unit, since it has 4 serial ports, 54 digital input/output pins, and 16 analog inputs. The serial port (also known as a UART) is used for communication between the Arduino board and a computer or other devices (with serial communications capability).

For the occupancy detection microcontroller (end device microcontroller), the Arduino Uno, based on the ATmega328, is chosen. The electrodes are connected via copper wires to the digital input/output pins of the Arduino Uno. The Arduino Uno has 14 digital input/output pins and 1 serial port. The Arduino Uno costs less ($30) than the Arduino Mega2560 ($59), and was chosen since only the digital input/output pins and a single serial port is required. Two of the 14 digital input/output pins are used for the serial port communications: pins 0 (RX) and 1 (TX). 12 digital input/output pins are therefore available for the sensor electrodes, and 9 sensors can be connected to one Arduino Uno, since 3 pins are used as stimulus pins (see section 3.1.2).

The sensors' electrodes (placed on the minibus taxi seat) are fabricated from thin household aluminium foil discs, with a diameter of 22cm, and copper wires attached. A thin piece of paper is attached on both sides of the sensor for insulation of the conducting aluminium disc. Two 10MΩ resistors are connected in series to create a 20MΩ resistor. The electrode configuration is connected to the end device microcontroller as described in section 3.1.2. The processed data on the end device microcontroller (Arduino Uno) is then sent via ZigBee network to the Gateway microcontroller (Arduino Mega2560).

Figure 3.1 on page 25, illustrates that the end device microcontroller is connected to the Gateway unit via a wireless ZigBee network. The Arduinos are fitted with XBee ZB modules, which provide them with wireless ZigBee connectivity. XBee ZB modules have a 40m range, which is more than enough for the minibus taxi environment. The XBee ZB module is connected to the Arduino trough a serial port.

Multiple devices are connected to the Arduino Mega2560, which include the following: GPS modem, cellular modem (GSM modem), XBee ZB shield, SD-card read/write device, accelerometer, and some LED's and a buzzer for the warning system.

A GPS shield, with an active antenna, is attached to the Arduino and provides the prototype with satellite navigation information. The active GPS antenna has a magnetic strip which enables the GPS antenna to be attached to the side of the minibus taxi for accurate satellite reception. The GPS communicates with the Arduino Mega2560 through one of its serial ports. The GPS shield is provided with a micro SD-card socket for SD-card storage functionality. The SD-card provides the system with black box capability. Every seat-occupancy event, and reckless driving event is logged on this storage device. The information and text stored on the SD-card are separated by commas for easy comma separated extraction.

The requirements for a 3-axis accelerometer is that the device must be able to detect g-force values up to 1.5G, have low voltage operation, interface with Arduino, and must have a low cost. Freescale Semiconductor's MMA7361L 3-axis accelerometer met this criteria [100]. The accelerometer allows a selection between two sensitivities. The highest sensitivity was chosen, which reduces the maximum detection g-force value from 6.0G to 1.5G.

The acceleration values produces by the accelerometer is filtered with a software function. It is then compared to an accident threshold (0.8G), and a lateral (x-axis) and longitudinal (y-axis) threshold. The difference between the threshold and the acceleration value is calculated and compared to the reckless driving table (Table 3.3 on page 44) that assigns the reckless level value. From studied data, the results show that new reckless events do not occur after each other in less than 10 seconds. The prototype is therefore implemented with a function that calculates the maximum reckless level in a 10 seconds interval after the first threshold crossing in that event. This prevents the system from reading a single event as multiple reckless events. If an event has a very long duration and is still above the threshold after 10 seconds, the event is stored as two reckless events. The highest level value is determined in the 10 seconds by comparing each new level value

with the current highest, storing the highest between the two values.

The Sierra Wireless AirLink GL6100 is used as the wireless modem that allows information to be uploaded onto the online platform through the wireless network. It uses an external SIM (Subscriber Identity Module) and offers quad band 850/900/1800/1900 MHz GPRS Class 10 capabilities. The modem communicates with the Gateway unit microcontroller using a RS232 interface.

Chapter 4

Experimental Investigation and Results

In this section the sensing and reporting system that was designed in chapter 3 is evaluated. The occupancy detection system is evaluated first (section 4.1) to determine if the designed system can successfully detect occupants in a minibus taxi. In section 4.2, the reckless driving detection system design is evaluated to determine if the proposed filtering and detection system is realisable, and that different reckless driving manoeuvres can be detected.

4.1 Capacitive sensing for occupancy detection

In this section the capacitive occupancy detection system is evaluated and the results discussed. The occupancy detection prototype (ODP) (see section 3.3) was implemented in a Toyota Quantum minibus taxi. All the simulations and tests discussed in this section were performed in a minibus taxi to get the most accurate simulation of the real-world scenarios. Three electrodes were connected to the ODP for the detection of three occupants. Small, medium and large sized occupants were used to ensure size coverage. Figure 4.1 shows the test setup of the prototype in the Quantum minibus taxi when the results were generated.

In section 4.1.1, charge and discharge time of the sensor electrode is measured, and the capacitance calculated from it. The capacitance is then compared to the expected theoretical capacitance calculated in section 3.1.4. In section 4.1.2, the capacitive sensing system is tested in different scenarios to determine if the designed system is realisable for the heterogeneous minibus taxi environment. The seat-sensor layout is shown in Figure 4.2, and is used in both sections.

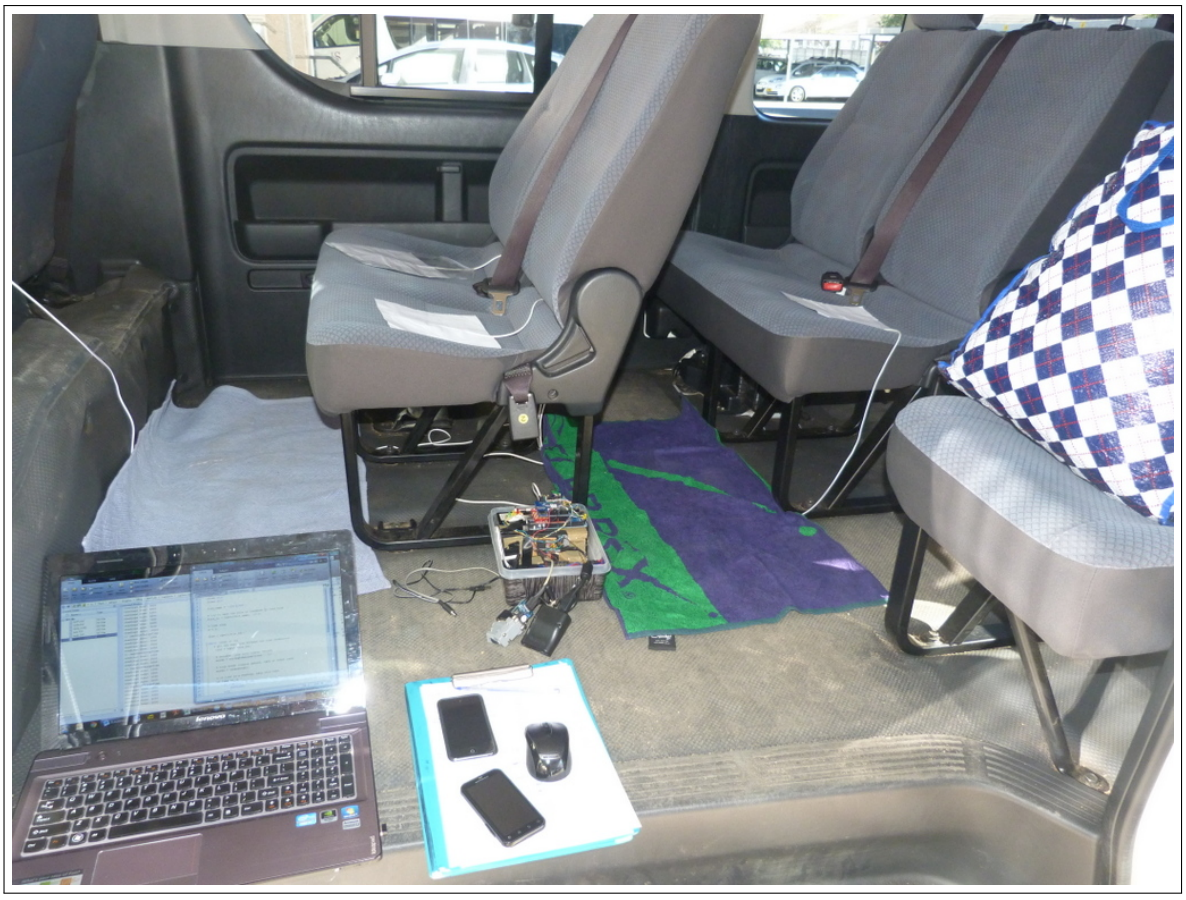

Figure 4.1: Test setup of the prototype in the Quantum minibus taxi, used in section 4.1.1 and 4.1.2.

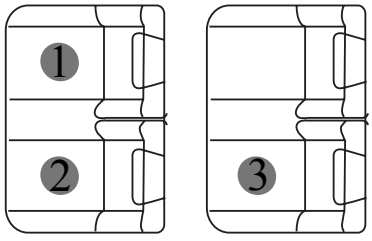

Figure 4.2: Seat-sensor layout for seat 1, 2 and 3, used in section 4.1.1 and 4.1.2.

4.1.1 Measurements

In this section the capacitance on the sensor electrode, for an unoccupied and occupied seat, is measured and compared to the expected capacitance calculated with the developed mathematical model in section 3.1.4.

The capacitance of the sensor electrode is determined by measuring the charge and discharge time of the electrode. The ODP has three sensor electrodes connected, and logs the charge and discharge times at a sampling rate of 50Hz on a SD-card. The data is stored without any filtering applied. Charge and discharge data is then extracted from the SD card, and plotted in MATLAB, to determine the start and end point of the

occupied or unoccupied states. Eight tests were run on the three sensors (Figure 4.2) in the minibus taxi to determine the charge and discharge times for all possible seat-occupant combinations.

An example of how the charge and discharge capacitance is determined follows. Sensor 1 and sensor 2 is occupied and sensor 3 is unoccupied as seen in Figure 4.3. Sensor 1, 2, and 3 is the top plot, middle and bottom plots respectively. The red dashed line is the discharge time and the solid blue line the charge time. An average of the sample

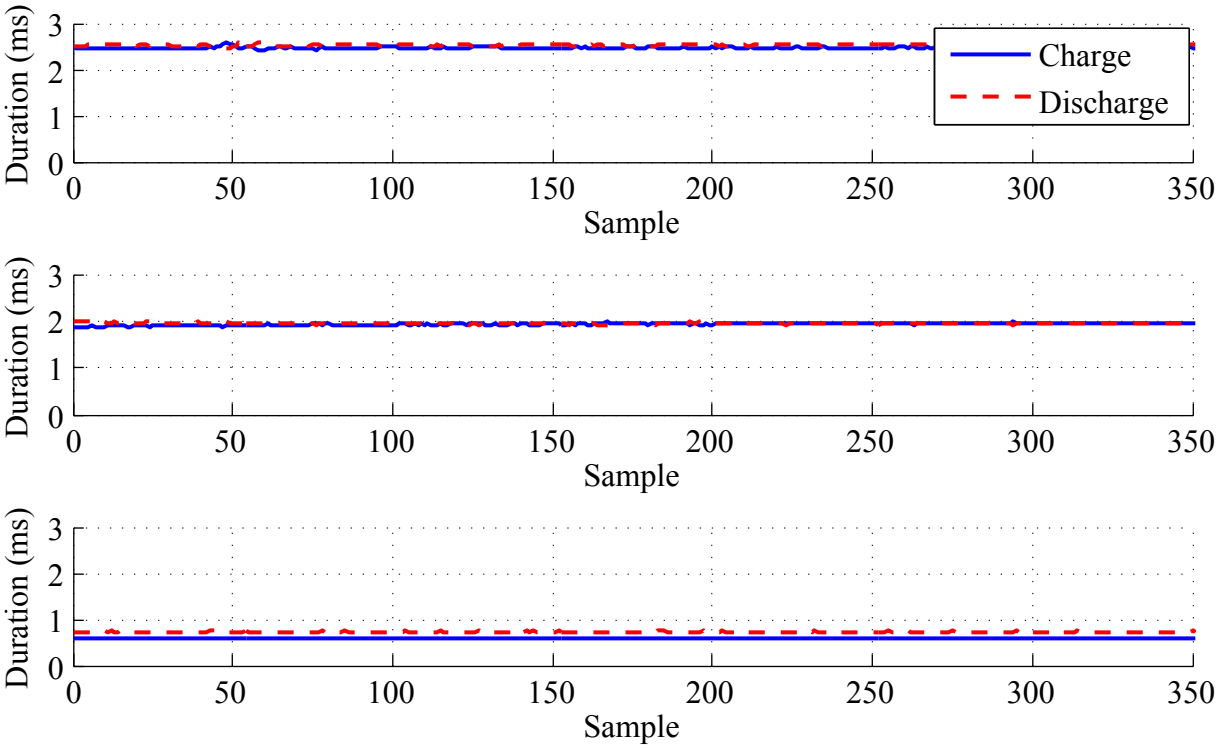

Figure 4.3: Charge and discharge plot, in microseconds, for occupied sensor 1 (top), occupied sensor 2 (middle), and unoccupied sensor 3 (bottom).

readings for sensor 1 is taken to determine the capacitance for the occupied state. The average charge time (t_C) is calculated as 2.47ms and the discharge time (t_D) as 2.53ms. The capacitance can then be determined from Equation 4.1 using the charge time and from Equation 4.2 using the discharge time

$$C_C = \frac{-t_C}{R \ln\left(1 - \frac{V_{R_C}}{V_S}\right)} \tag{4.1}$$

$$C_D = \frac{-t_D}{R \ln\left(\frac{V_{R_D}}{V_S}\right)} \tag{4.2}$$

with $R = 20M\Omega$, $V_S = 4.6V$, $V_{R_C} = 3.06V$ and $V_{R_D} = 1.53V$. These parameters were determined from the hardware design (section 3.3), measurements of the prototype components, and the microcontroller's electronic specifications [101]. For the ideal system,

the charge and discharge time capacitance is identical. The charge time capacitance is calculated from Equation 4.1 as 113pF and the discharge capacitance from Equation 4.2 as 115pF. Averaging the charge and discharge times from sensor 2's plot gives 1.94ms and 1.95ms respectively for the occupied state. These values lead to a charge time capacitance of 89pF and discharge time capacitance of 88pF. The unoccupied charge and discharge time on sensor 3 is determined as 0.60ms and 0.74ms respectively, which leads accordingly to a charge and discharge capacitance of 27pF and 33pF. This example's seat status combination can be seen in Table 4.1, and its charge and discharge time in Table 4.2, as test nr. 4.

The seat-status combinations for the eight tests are summarised in Table 4.1, and Table 4.2 shows the average charge and discharge time for each of the combinations.

Table 4.1: Seat-status combinations for the measurement tests.

Test	Seat 1	Seat 2	Seat 3
1	Unoccupied	Unoccupied	Unoccupied
2	Occupied	Unoccupied	Unoccupied
3	Unoccupied	Occupied	Unoccupied
4	Occupied	Occupied	Unoccupied
5	Unoccupied	Unoccupied	Occupied
6	Occupied	Unoccupied	Occupied
7	Unoccupied	Occupied	Occupied
8	Occupied	Occupied	Occupied

Table 4.2: The sensor electrode's charge and discharge time for each test. Values are in microseconds.

	Sensor 1 (ms)		Sensor 2 (ms)		Sensor 3 (ms)	
Test	Charge	Discharge	Charge	Discharge	Charge	Discharge
1	0.61	0.78	0.60	0.75	0.53	0.67
2	2.51	2.40	0.67	0.84	0.56	0.71
3	0.68	0.86	1.90	1.78	0.58	0.72
4	2.47	2.53	1.94	1.95	0.60	0.74
5	0.64	0.80	0.62	0.78	1.59	1.67
6	2.36	2.32	0.68	0.87	1.59	1.71
7	0.69	0.92	1.93	1.87	1.61	1.77
8	2.30	2.41	1.88	1.91	1.64	1.82

The capacitance on the sensors, for all the combinations, are calculated using Equation 4.1 and 4.2 as discussed in the example. The average of the charge and discharge capacitance is then taken. The results can be seen in Table 4.3. These tests are performed since they provide a good indication of the measured capacitance on the sensors. The theoretically calculated capacitance (from section 3.1.5) was calculated as 8pF and 23pF

Table 4.3: Occupied and unoccupied capacitance on the electrode. Values are in picofarad.

	Seat 1 (pF)	Seat 2 (pF)	Seat 3 (pF)
1	32	31	27
2	112	34	29
3	35	84	30
4	114	88	30
5	33	32	74
6	106	35	75
7	37	86	77
8	107	86	79

for the unoccupied and occupied state respectively. Figure 4.4 shows the normalised occupied and unoccupied capacitance on the electrode for the eight tests, and includes the theoretical results.

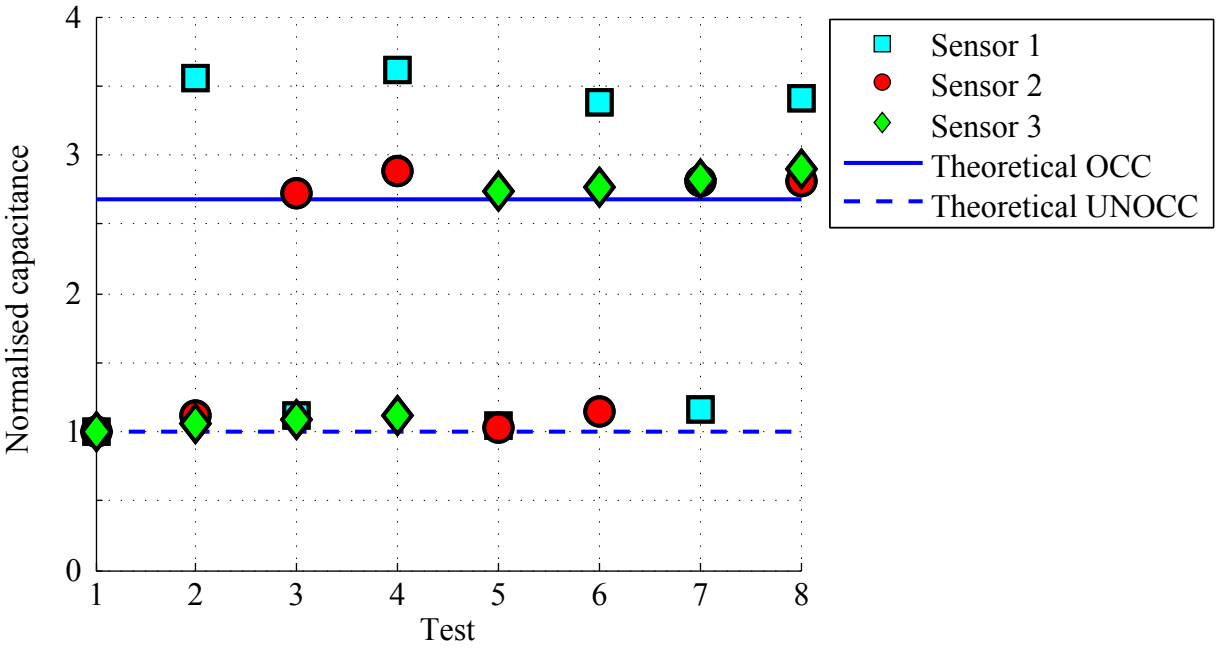

Figure 4.4: Results from the eight tests comparing the measured capacitance on the sensor electrode to the expected theoretical capacitance for an occupied and unoccupied electrode. The normalised occupied and unoccupied capacitance is shown. Test 1's capacitance readings (all three seats are unoccupied) are used to normalise the measured capacitance results.

Test 1 is regarded as the baseline, or reference point, for the unoccupied capacitance, since all three sensors are unoccupied. It is therefore used to normalise the capacitance values for the other tests. In the unoccupied state, sensors 1 to 3 exhibit capacitances of 32pF, 31pF and 27pF respectively. Sensor 1 has the highest capacitance and sensor 3 the lowest capacitance. The variation could be because of a difference in the sensitivity of the sensor electrodes, or additional electrical coupling inside vehicle. Sensor 1's sensitivity is similar to sensor 2's sensitivity, which are next to each other.

In Test 2, sensor 1 is occupied and sensor 2 and 3 unoccupied. A slight capacitance increase on the two unoccupied sensors is observed. Sensor 2 increased with 3pF and sensor 3 with 2pF. Although this slight increase is insignificant, we can see that the addition of capacitance on a single sensor influences all the sensors. The capacitance for the occupied state on sensor 1 shows a significant increase of 80pF, which is 2.5 times the unoccupied state. Test 2 is regarded as the reference point for sensor 1's occupied capacitance.

For Test 3, sensor 2 is occupied, with sensor 1 and 3 unoccupied. The results are similar to Test 2. Sensor 1 and 2 in the unoccupied state both increases with 3pF. The capacitance on the occupied sensor 2 is 84pF, which is an increase of 53pF. The occupied sensor's capacitance is therefore more than double the unoccupied state, but is less that the increase of sensor 1's occupied capacitance. Test 3's occupied state is the reference point for sensor 2's occupied capacitance.

Test 4 was explained in the example in the beginning of this section. Sensor 3 has the same capacitance as in the previous tests. The capacitance on sensor 1 is 114pF, which is 2pF more than in Test 2. Similar results follow for sensor 2, with an increase of 4pF from Test 3. This corresponds with the capacitance increase on the sensors in the unoccupied state.

In Test 5, sensor 3 is occupied and sensor 1 and 2 is unoccupied. This test is regarded as the reference point for sensor 3's occupied state which has a capacitance of 74pF. The increase from the unoccupied reference is 47pF, which is substantially less that the increase of sensor 1's occupied state, but is still more than double the unoccupied state. The capacitance of sensor 1 and 2 in the unoccupied state is similar to previous results.

For the remaining tests, sensor 3 stays occupied. An increase in the capacitance of the other two sensors is therefore expected. The maximum capacitance increase on sensor 2, for the remaining tests, is 4pF. In Test 6 and Test 8, sensor 1 shows an unexpected decrease of 6pF and 5pF respectively in the occupied state. This decrease in capacitance is related to occupant 1 occupying a slightly different position on the sensor from the previous tests.

The experimental results demonstrate that sensor 1 has the highest capacitance readings, with an average of 110pF for the occupied state. Sensor 2 has an average of 86pF, and sensor 3 an average capacitance of 76pF. As previously mentioned, occupant 2 has a small body mass, occupant 1 slightly bigger and occupant 3 the largest body mass. Sensor 1 and sensor 2 behave as expected, with an increase in capacitance with the increased body mass. The unexpected lower capacitance on sensor 3 shows that the sensor is less sensitive than the other two sensors, most likely due to its location in the vehicle.

The experimental results are compared with the expected theoretically calculated capacitance. The measured capacitance is higher than the expected theoretical capacitance. The unoccupied theoretical capacitance has a value of 8pF, compared to the lowest measured capacitance of 27pF. For the occupied state, the expected capacitance is also lower than the measured capacitance. The theoretical capacitance has a value of 23pF, com-

pared to the lowest measured capacitance of 75pF. The difference between the theoretical and the measured capacitance is as a result of the approximations made in the theoretical calculations and external factors (electrical coupling between the sensor and metal objects in the seat) affecting the sensor properties. Although the results differ, the aim of these tests is to determine if the capacitive occupancy detection system is a viable option for the detection of occupants in a minibus taxi. In Figure 4.4, the normalised results show that both the theoretical and measured capacitance increases significantly from the unoccupied to the occupied state. For the theoretical calculations, the relationship between the occupied and unoccupied capacitance (C_{OCC}/C_{UNOCC}) is 2.7, and the relationship for the measured capacitance, is 2.8, taking the average ratio from all the tests.

The measurements and ratios therefore prove that the occupancy detection system is a viable option for the detection of occupants in a minibus taxi, since the occupied capacitance is more than double the unoccupied capacitance.

4.1.2 Occupancy detection system in different scenarios

The ODP's SD-card storage function is set up to log the sensor readings at a sampling rate of 50Hz for each of the three electrodes. The data is low pass filtered before it is stored on the SD card and is used for the occupancy detection system results throughout the following sections. A LED system is added to indicate the detected presence of an occupant on a seat. For every change in seat status, the microcontroller stores the seat number and previous state on the SD card.

Seven different scenarios are investigated with multiple tests for each scenario. The tests include all the different combinations of how passengers can occupy the minibus taxi seats. Before each test the sensors are kept unoccupied to establish a base-line or reference value, and an occupant occupies a seat for at least 15 seconds before leaving the seat. These scenarios are used to further determine if the capacitive occupancy sensor system is a viable option for the detection of multiple occupants in a minibus taxi. The system must be robust, in other words, it must be able to endure constant changes of occupants on the seats, foreign objects (e.g. bags and electronic devices) and possible water spills. The effect of an occupant sitting partially on the sensor is also investigated. Sensor 1 has a medium sized occupant, sensor 2 a smaller sized occupant, and sensor 3 a large occupant, throughout the different scenario tests.

An example of the results can be seen in Figure 4.5, where the top plot shows the readings of sensor 1, the middle plot sensor 2 and the bottom plot sensor 3.

The red dashed line is the occupancy threshold of 350 cycles and the blue line, the sensor readings. The detected occupied state is indicated by the shaded area. This applies to all of the figures in this section. The seat-sensor layout was shown in Figure 4.2 on page 53.

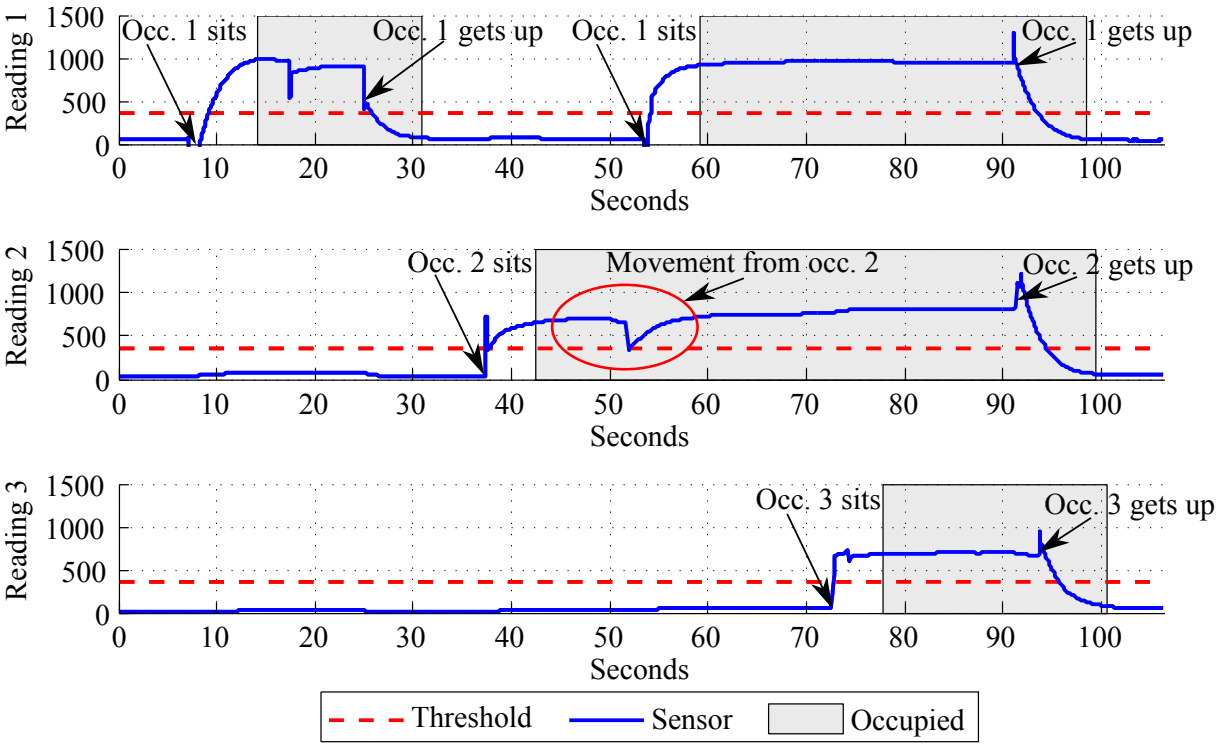

Figure 4.5: Plot of occupancy readings showing the first scenario where occupants sit normally on the sensors. Sensor 1 is the top plot, sensor 2 the middle plot, and sensor 3 the bottom plot.

4.1.2.1 Scenario one: normal occupancy

Figure 4.5 shows the results of the first scenario where three occupants cover the seat sensors completely when they sit. All three seats are unoccupied for the first 7 seconds, after which seat 1 receives an occupant. Sensor 2 receives an occupant at 37 seconds, and sensor 3 at 73 seconds. Before sensor 1's readings increase, the readings decrease sharply for 1 second. The sudden dip is not always present, but relates to a disturbance of the sensor the moment the occupant takes a seat. At 9 seconds, sensor 1's reading crosses the threshold, but the reported occupied status does not change immediately, since the system has been designed to account for passengers temporarily moving over the seat, and not actually occupying the seat. The readings have to stay above the threshold for 5 seconds or longer before a change in the reported occupied status takes place (see section 3.1.3). The change in the reported occupied state takes place at 14 seconds and stays occupied before changing to unoccupied at 30 seconds. It can be noted that the seat status does not change to unoccupied immediately at 25 seconds, because of the 5 seconds waiting period. The small fall in the sensor reading at 17 seconds is a result of the occupant moving on the seat.

The results show that the presence of an occupant on one sensor does not have an effect on the occupied state reported by other sensors. This is confirmed in Figure 4.5 between 10 and 25 seconds, where sensor 1 has an occupant present without significantly effecting sensors 2 or 3, where a very small increase in sensor readings from 20 to 70

cycles on sensor 2 is noted. On sensor 2, an occupant takes a seat at 37 seconds, and the seat's reported status is changed to occupied at 42 seconds. The sensor readings reduce to below the threshold at 51 seconds (circled with red marker), which is a result of the occupant getting up from the seat, but immediately returning to the seated position on the sensor. The sensor system accommodates such movements, and the reported occupied state therefore did not change. A sudden decrease in a sensor's readings corresponds to an occupant leaving the seat, which can be seen in the figure at 25 and 92 seconds for sensor 1, at 93 seconds for sensor 2, and at 95 seconds for sensor 3.

The effects of multiple occupied sensors on each other and on other unoccupied sensors are also investigated. Sensor 1 and 2 are occupied between 60 and 70 seconds, without effecting sensor 3. In the last test all three sensors are occupied simultaneously, with the results as expected, but a spike is noted at the end of the readings. The spike is related to the disturbance of the sensor when the occupant leaves the seat. These results demonstrate that the sensor system is able to successfully detect multiple occupants in a minibus taxi.

4.1.2.2 Scenario two: occupant partially on a sensor

Figure 4.6 shows the results of the second scenario, where three occupants cover the seat sensor partially when they sit. The first occupant covers 75% of the sensor electrode.

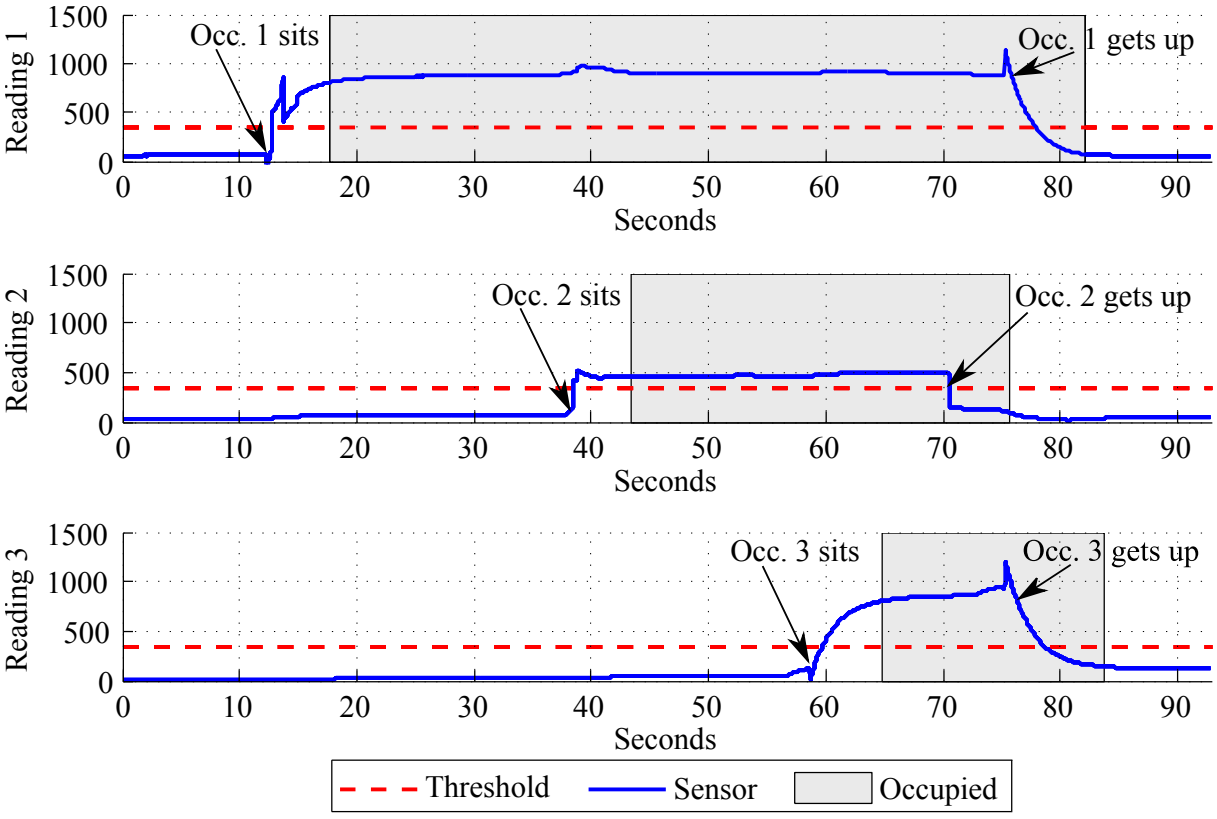

Figure 4.6: Three sensor readings: sit partially on sensor. Occupant 75% on sensor 1 (readings 1), occupant 50% on sensor 2 (readings 2), and occupant 100% on sensor 3 (readings 3).

The results of the sensor, in Reading 1, show an increase in the sensor readings at 13 seconds with remarkably high readings. By comparing the occupied readings with scenario one's results, we notice that the values are similar for a 100% and 75% covered seat sensor. At 40 seconds, the second sensor is occupied by a 50% covered seat sensor. The occupied threshold was chosen carefully to accommodate the decreased readings, since the readings for this test are relatively low compared to sensor 3's readings where an occupant completely covers the electrode.

These results confirm that the system detects an occupant when an electrode is partially covered by the occupant.

4.1.2.3 Scenario three: occupant next to sensor

The third scenario investigates the effect on the sensor readings when an occupant does not sit on the electrode, but sits next to the sensor electrode. The expected outcome is that the sensor readings stay under the occupied threshold when an occupant is near the electrode and not on it. The results can be seen in Figure 4.7.

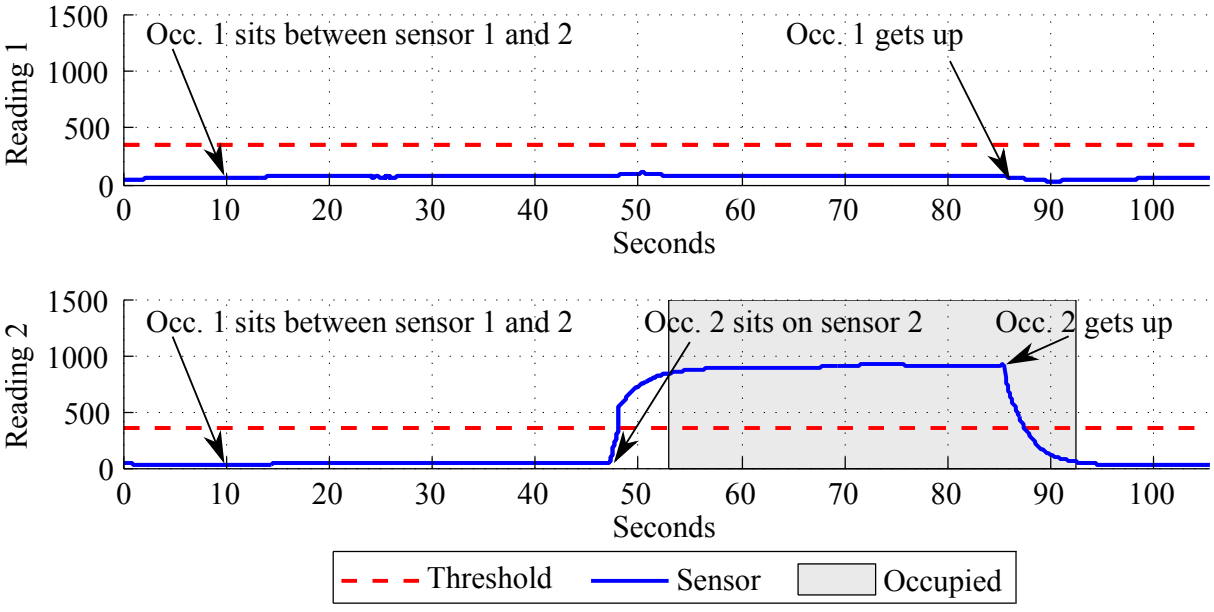

Figure 4.7: Occupancy readings from an occupant sitting next to a sensor. An occupant sits between sensor 1 (top plot) and 2 from 10 to 86 seconds. A second occupant sit on sensor 2 (bottom plot) at 48 seconds, while the first occupant remains seated between the two sensors.

No occupant is present up to 10 seconds after which an occupant takes a seat between sensor 1 and 2. From the figure there can be seen that the results do not show a significant increase in sensor readings. A second occupant takes a seat on sensor 2 at 48 seconds, while the first occupant remains seated between the two sensors, and a typical increase in the readings is seen on sensor 2 without effecting sensor 1. Sensor 3 showed similar results.

These results confirm that the system does not detect an occupant that is near the sensor and does not sit on it.

4.1.2.4 Scenario four: occupant sits on a sensor while touching a metal object in the taxi

The results of the fourth scenario, where the seated occupants make contact with a metal object in the minibus taxi is shown in Figure 4.8. This scenario is investigated to eliminate

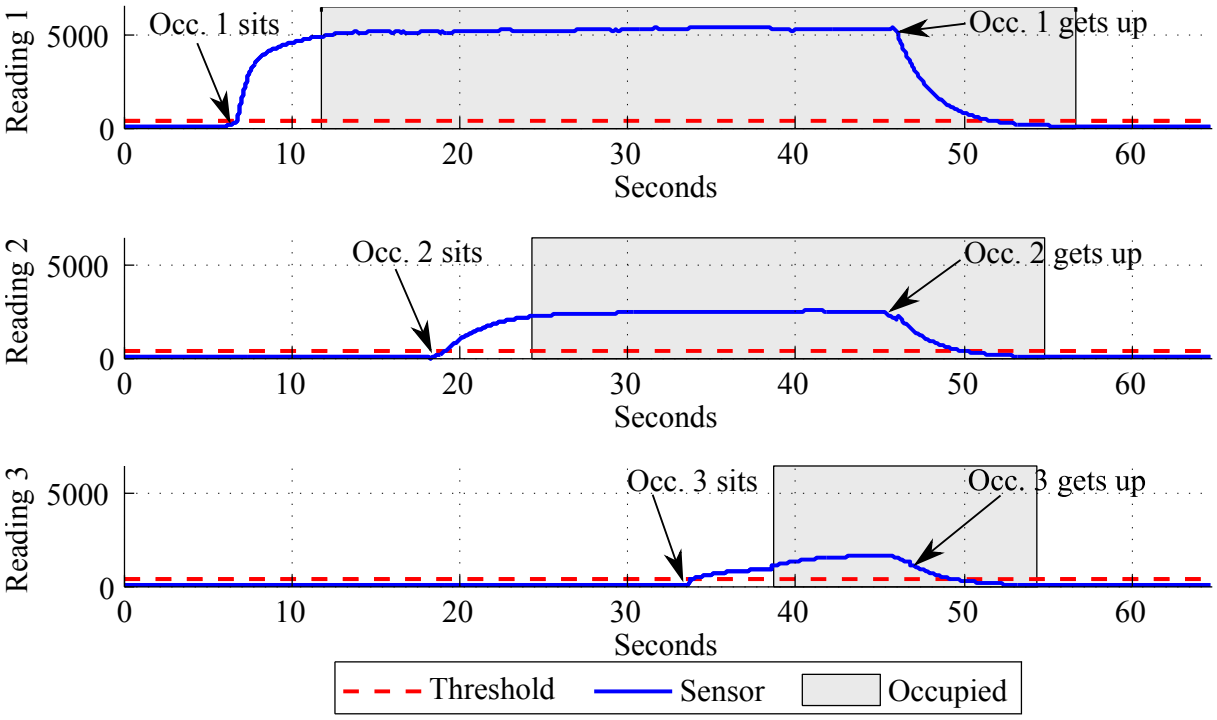

Figure 4.8: Three sensor readings: occupant sits on a sensor while touching a metal object in the taxi. Sensor 1 is the top plot, sensor 2 the middle plot, and sensor 3 the bottom plot.

a possible disturbance of the electrodes which might disrupt the system.

The occupant on sensor 1 touched a metal rod on the inside of the minibus taxi (at 8 seconds), and the occupant on sensor 2 the metal structured below the seat (at 20 seconds). Both of these tests resulted in a big increase in the sensors' readings. The occupant on sensor 3 touched a small metal rod connected to the headrest of the seat at 35 seconds. This also increased the sensor's readings. Larger metal objects lead to higher readings.

The significant increase in sensor readings is related to added capacitance on the sensor electrode which comes from touching a metal object. The added capacitance directly influences the charge/discharge time and therefore increases the readings. These tests therefore show that an occupant making contact with a metal object in the vehicle does not disrupt the system.

4.1.2.5 Scenario five: foreign object on seat (non-conducting)

It is common for passengers to bring luggage aboard on public transportation vehicles. Passengers tend to bring large bags onto the minibus taxi, especially for long distance journeys. The sensor system must therefore be able to distinguish between a human body and a foreign object. The following tests investigate the influence of a non-conducting object on the sensor electrode. A large bag filled with cotton and nylon material were placed on the electrode, with results to be seen in Figure 4.9. The bag can be seen in Figure 4.1 on page 53 (located on the right).

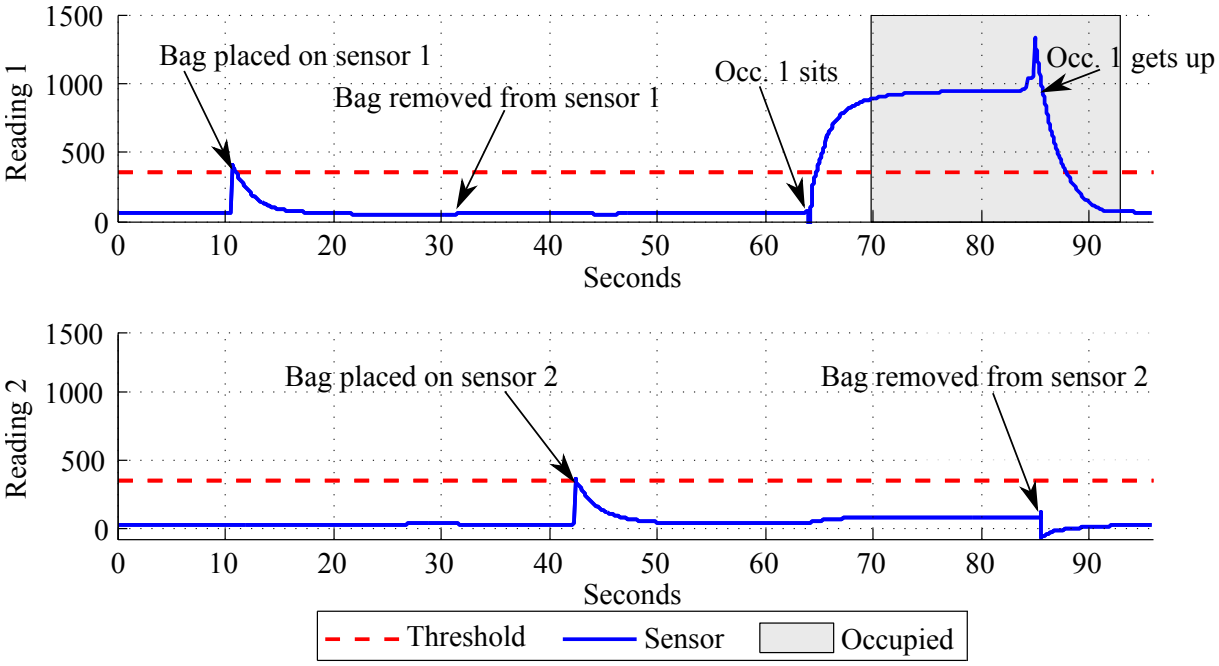

Figure 4.9: The effect of luggage on the sensors. Sensor 1 is the top plot, and sensor 2 the bottom plot.

The bag was placed on the first electrode at 11 seconds. A sudden small rise can be seen as result of disturbing the sensor, but does not lead to a status change. The bag stays on the electrode for 20 seconds when it is removed and placed on sensor 2 at 42 seconds. A similar spike in the readings can be seen, when the bag is placed on the electrode.

Seat 1 receives an occupant at 65 seconds, who occupies the seat for 20 seconds before removing the bag and leaving the seat.

The results demonstrate that the presence of a bag on the sensor electrode does not contribute to increased sensor readings.

4.1.2.6 Scenario six: foreign object on seat (electronic device)

The tests of the scenario in this section are similar to the previous scenario's test, except that non-conducting foreign object is substituted by an electronic device. A laptop was chosen as the electronic device. The results are in Figure 4.10.

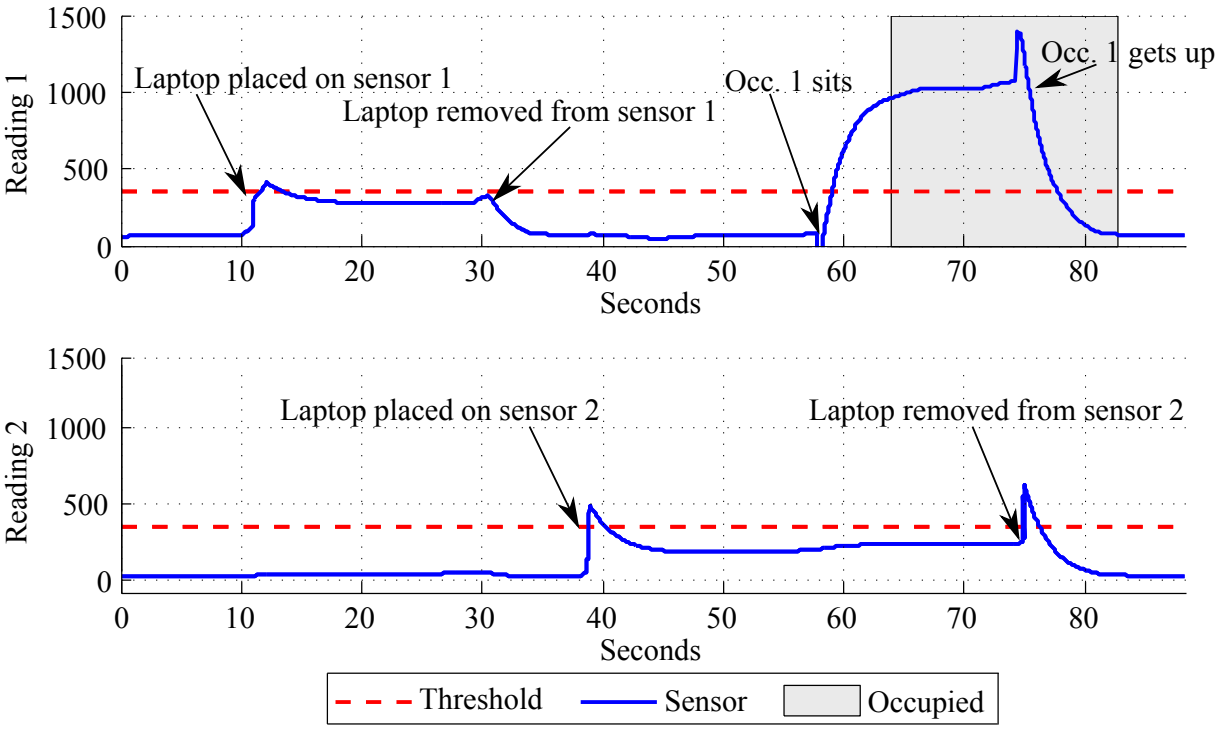

Figure 4.10: Two sensor readings: electronic device. Sensor 1 is the top plot, and sensor 2 the bottom plot.

The laptop is placed on sensor 1 at 11 seconds and removed at 30 seconds. A change in the sensor readings are observed with an average reading of 295 cycles. After that laptop has been removed, it was placed on sensor 2 for 37 seconds. The average readings on sensor 2 when the laptop is present are 254 cycles. The readings are therefore not high enough to change the seat's status. An occupant joined sensor 1 at 80 seconds and occupied the seat for 19 seconds before removing the laptop from seat 2 and leaving the seat.

The results demonstrate that an electronic device has an influence on the electrode, but the effect is low enough to not affect the reported occupied state.

4.1.2.7 Scenario seven: foreign object on seat (water on seat)

The last scenario is to determine if liquid spilled on a seat has any effect on the sensor system. Sensor 1's electrode is sealed with a plastic bag and soaked in water, and the rest of the sensor setup stays unchanged. The results of the test can be seen in Figure 4.11.

Seat 1 receives an occupant at 16 seconds with the reported status changed at 21 seconds to occupied. At 34 seconds the occupant readjusts on the seat. This readjustment leads to an increase in the sensor readings. The occupant then leaves the seat at 55 seconds, changing the seat status to unoccupied 5 seconds later. From these results we can see that water on the sensor electrode does not have any effect on the system.

The results of the different tests performed in sections, show that the occupancy detection system has a robust sensor setup, and can detect occupants in the minibus

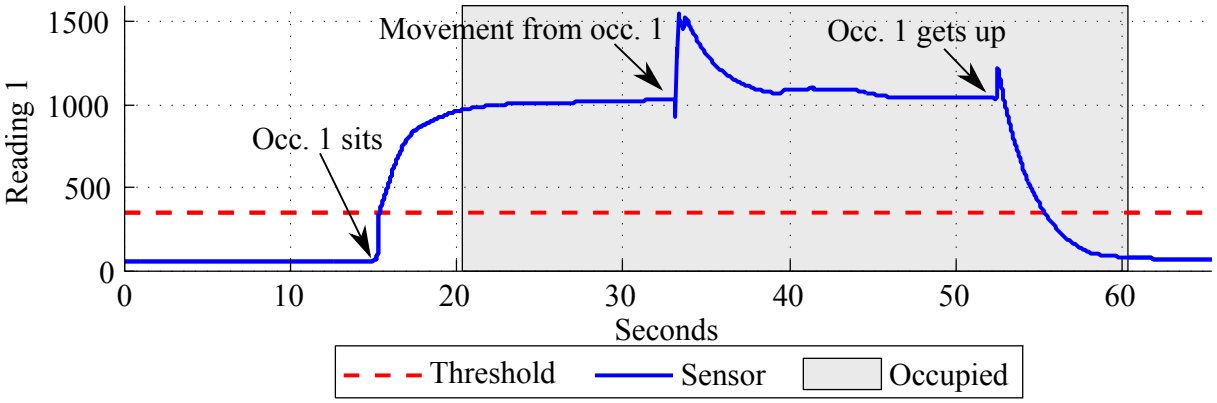

Figure 4.11: Water around sensor 1.

taxi's heterogeneous environment.

4.2 Reckless driving detection system

A reckless driving detection system was designed in section 3.2. For the designed system, lateral and longitudinal acceleration data is generated by a 3-axis accelerometer, speed data by a GPS unit and occupancy information from an occupancy detection sensor designed in section 3.1. The augmented data is used to design a lateral and longitudinal reckless acceleration threshold that is based on the principles of road design. If a driver performs a manoeuvre that leads to acceleration values exceeding the defined lateral or longitudinal threshold, a reckless event has occurred.

In this section, the reckless driving detection system is evaluated to determine if the assumptions made for the design holds true and if the system is a viable option for the detection of reckless driving events. More than 35 hours of road acceleration data was collected from 41 different minibus taxis. The collected road data consists from 25% on urban, and 75% on highway roads. The data was captured and stored on the prototype's SD-card.

In section 4.2.1, speed data collected from urban and highway roads are studied to confirm that minibus taxis travel at excessive speeds. A typical long distance taxi journey is used as an example. In section 4.2.2, the difference in duration between urban and highway events is investigated, to confirm the statement made in section 3.2.1, namely that highway events have longer event durations than urban events. In section 4.2.3, the designed filtering system, from section 3.2.2, is evaluated. The corresponding dynamic threshold, which is dependent on speed and occupancy information, is discussed in section 4.2.4. In section 4.2.5, different driving manoeuvres are investigated, by evaluating the filtered acceleration output data.

4.2.1 Minibus taxi speed results

A map of a typical long-distance minibus taxi journey in South Africa can be seen Figure 4.12. This journey is roughly 2400km (both directions). The speed samples of the trip are shown in Figure 4.13 and summarised in Table 4.4. It can be noticed that the speeds

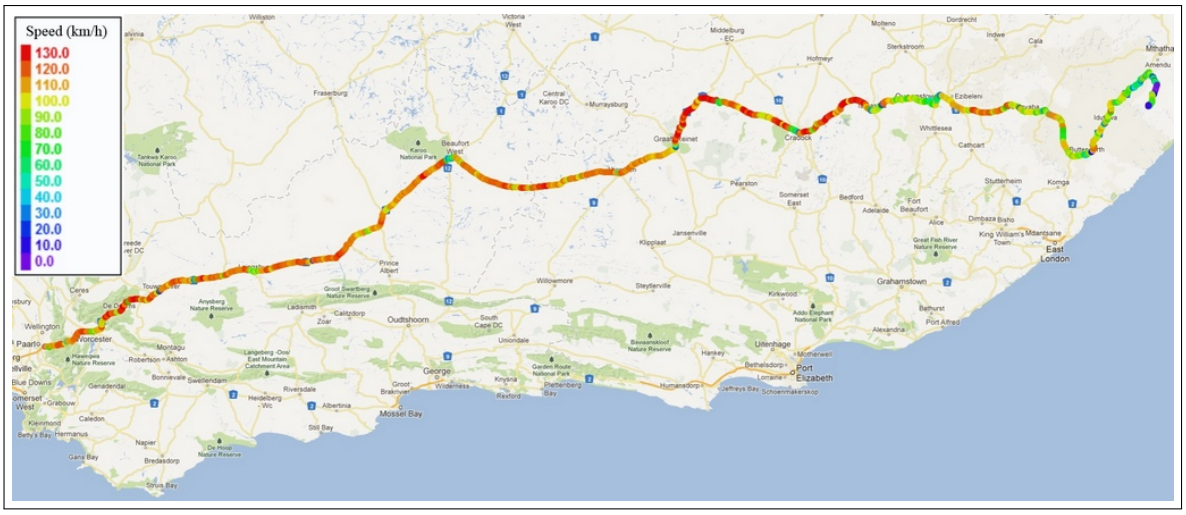

Figure 4.12: Route of a long-distance taxi with recorded speed in colour-coding.

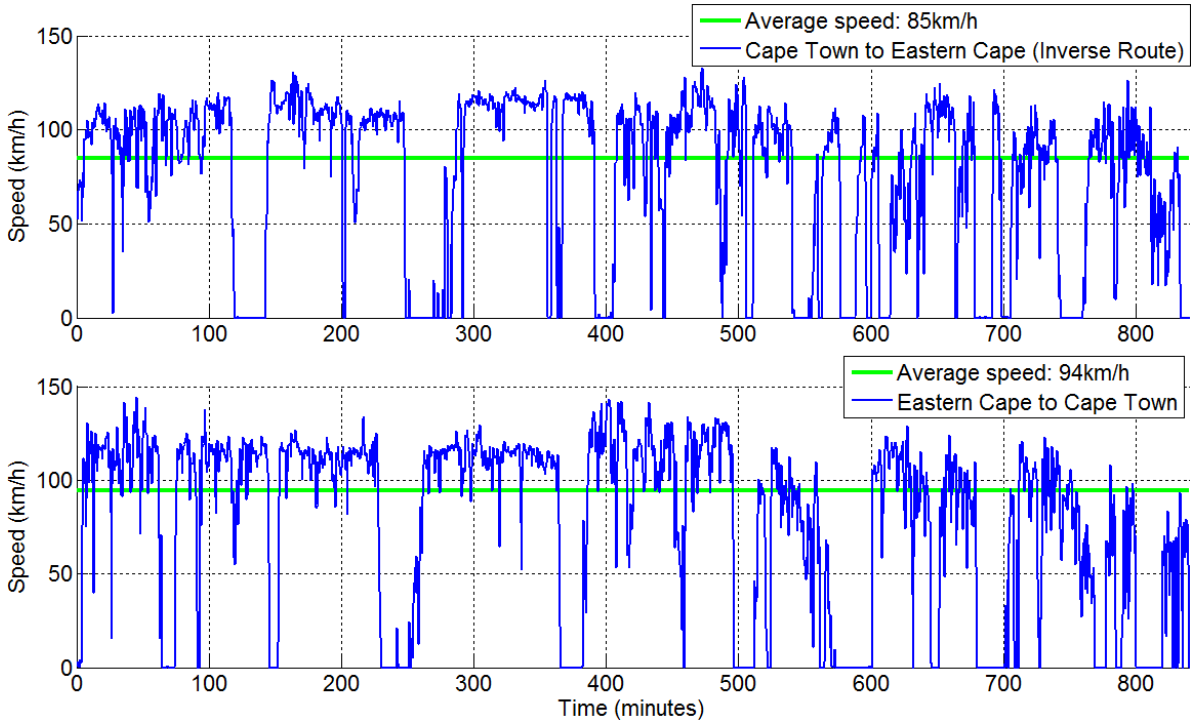

Figure 4.13: Speed plot from studied taxi journey in Figure 4.12.

of the return journey have increased by roughly 10%. The increased speed for the return journey is as a result of the minibus taxi departing late, after waiting for passengers, and then rushing to arrive in time for work on Monday morning. As previously stated,

Table 4.4: Speeds of a minibus taxi weekend journey (both directions).

Threshold	To the Eastern Cape	Return to Cape Town
> 100	48 %	59 %
>110	27 %	44 %
>120	3 %	13 %
>130	0 %	4 %
>140	0 %	1 %
Number of samples	1586	1424

the minibus taxi has to obey a legal speed limit of 100km/h, but 48% of the total speed samples to the Eastern Cape exceed this limit, and 59% for the return journey back to Cape Town. An average speed of 94km/h is maintained for the return journey, including stops. For the long-distance journey, minibus taxis typically depart at sunset on Friday night and return before sunrise on Monday morning. The trips therefore primarily take place at night.

From these results, it can clearly be seen that minibus taxi drivers, drive at excessive speeds.

4.2.2 Long-distance and urban events

It was stated in section 3.2.1 that urban events have shorter acceleration durations, for longitudinal and lateral manoeuvres, than highway events. The duration of longitudinal and lateral acceleration events for urban and highway scenarios are therefore investigated in this section. A data sample for lateral and longitudinal acceleration for urban and highway roads, from the 35 hours of collected data, were identified and each is discussed here.

The selected low pass filtered longitudinal acceleration sample is shown in Figure 4.14. From the figure it can be seen that the urban event lasts 9.3 seconds, with a maximum acceleration peak of 150 milli-G, compared to the highway event that lasts 22 seconds event though the event's maximum acceleration peak is 105 milli-G. A higher acceleration peak usually corresponds with an increase in the event's duration. The highway braking event, for this example, is therefore more gradual that the urban event. Between 30 and 50 seconds, on the highway plot, inconsistent acceleration can be noted, which is due to the gear-changes of the minibus taxi.

Figure 4.15 shows low pass filtered lateral acceleration for an urban and highway road segment. It can be seen that the urban event has a shorter duration than the two highway event for the lateral acceleration results which corresponds with previous results. The first highway turn event's duration is almost double the urban event. The highway acceleration events have higher peaks than the urban acceleration event. Higher acceleration for lateral manoeuvres is related to roads with a smaller curve radius or to an increased speed around the curve. Since highway roads are designed with larger curve radii than urban roads, it

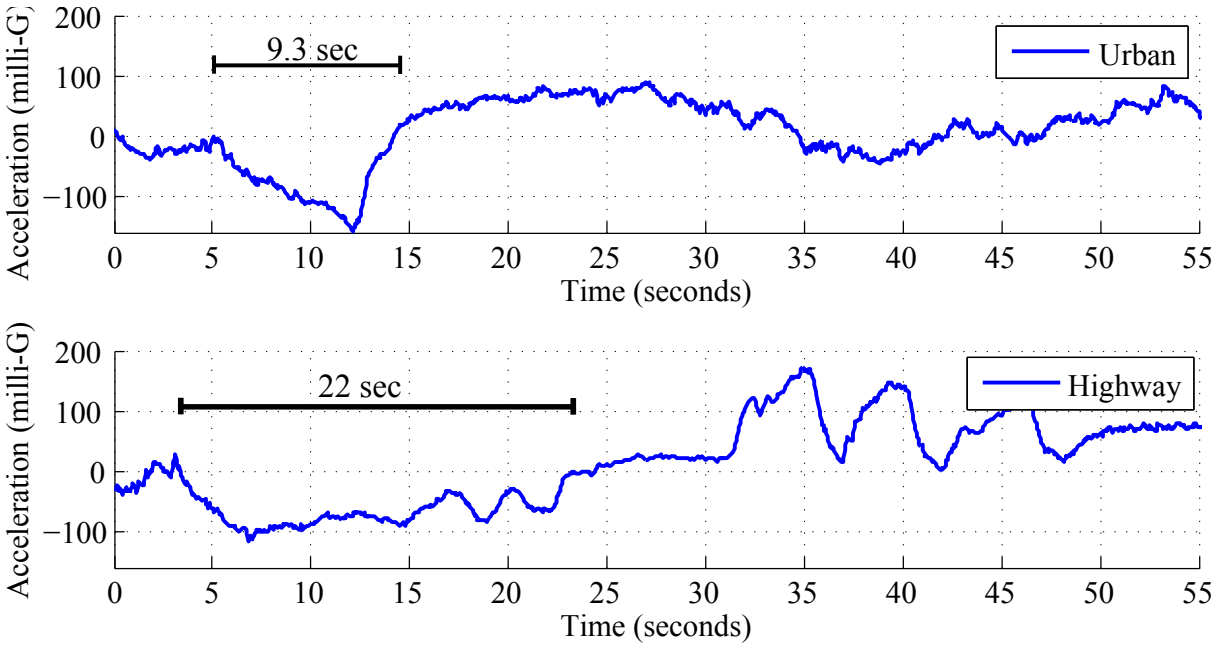

Figure 4.14: Comparison of urban and highway low pass filtered longitudinal acceleration data.

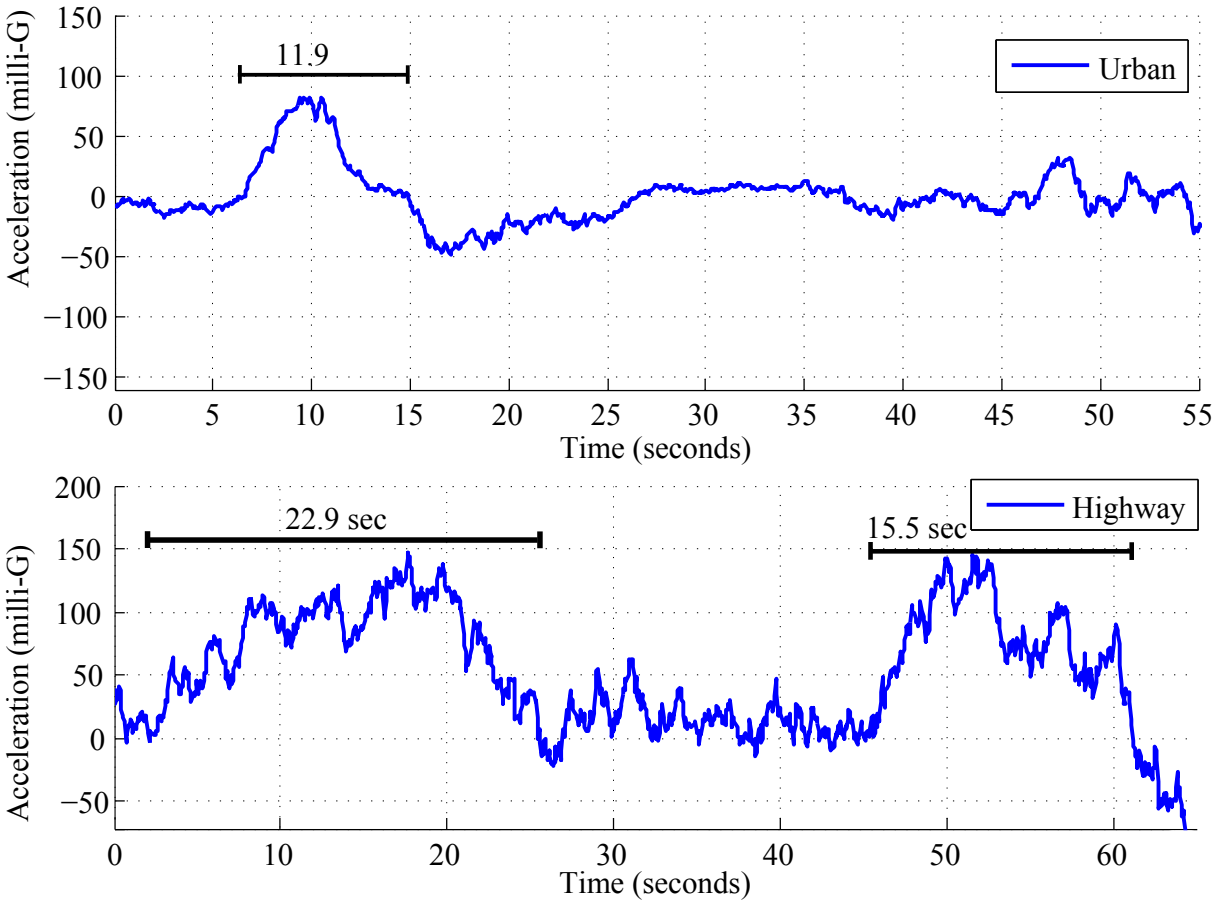

Figure 4.15: Comparison of urban and highway low pass filtered lateral acceleration data.

can safely be assumed that the minibus taxi was travelling at a higher speed around the curve than in the urban event, as expected.

From the 35 hours of collected road data, it was confirmed that urban events have shorter durations than highway events.

4.2.3 Filtering results

In this section, the proposed acceleration filtering system from section 3.2.2 is evaluated, based on collected road data.

One of the journeys undertaken includes a trip in a minibus taxi from Cape Town to the Eastern Cape (total distance: 580km, travelling time: 6 hours). A road section of the trip was identified where the most lateral g-force was exerted on the minibus taxi. The selected 6 km road section, which was also regarded the most erratic for the journey, is shown in Figure 4.16. The selected road section is a mountain pass notorious for its road accidents. Only two occupants were present in the taxi (a occupant in the front passenger

Figure 4.16: Road sample in a pass from a long distance journey where reckless driving was detected.

seat and the driver). The seat layout can be seen in Figure 4.17.

The raw acceleration values (unprocessed values) for this road section is low pass filtered using the LPF from section 3.2.2. The longitudinal and lateral acceleration output from the LPF is shown in Figure 4.18 on page 70 and compared with the unprocessed data. The blue plot is the unfiltered acceleration and the red plot the LPF acceleration. Left (nr. 2) and right (nr. 3) turns in Figure 4.16 relate to negative and positive values, respectively. From the figure it can be seen that the LPF filter removes the high frequency noise. We can see from the acceleration plot that the first turn induces in the highest acceleration and the last turn, at nr. 4, is the lowest. The road segment for an initial turn at 50 seconds on the acceleration plot, is not indicated in Figure 4.16. At this turn

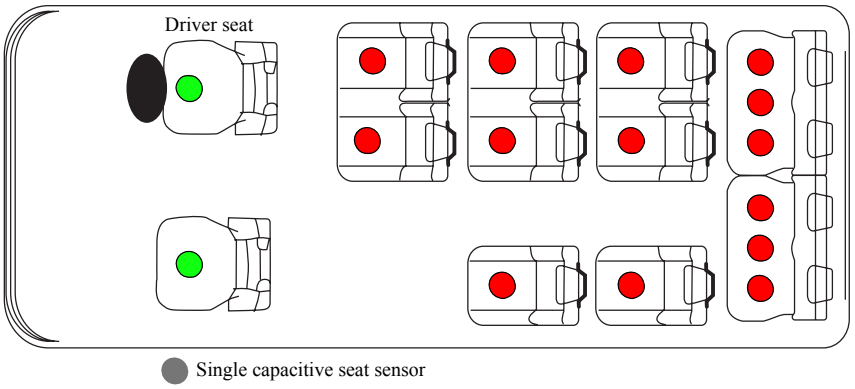

Figure 4.17: Minibus taxi seat-sensor layout.

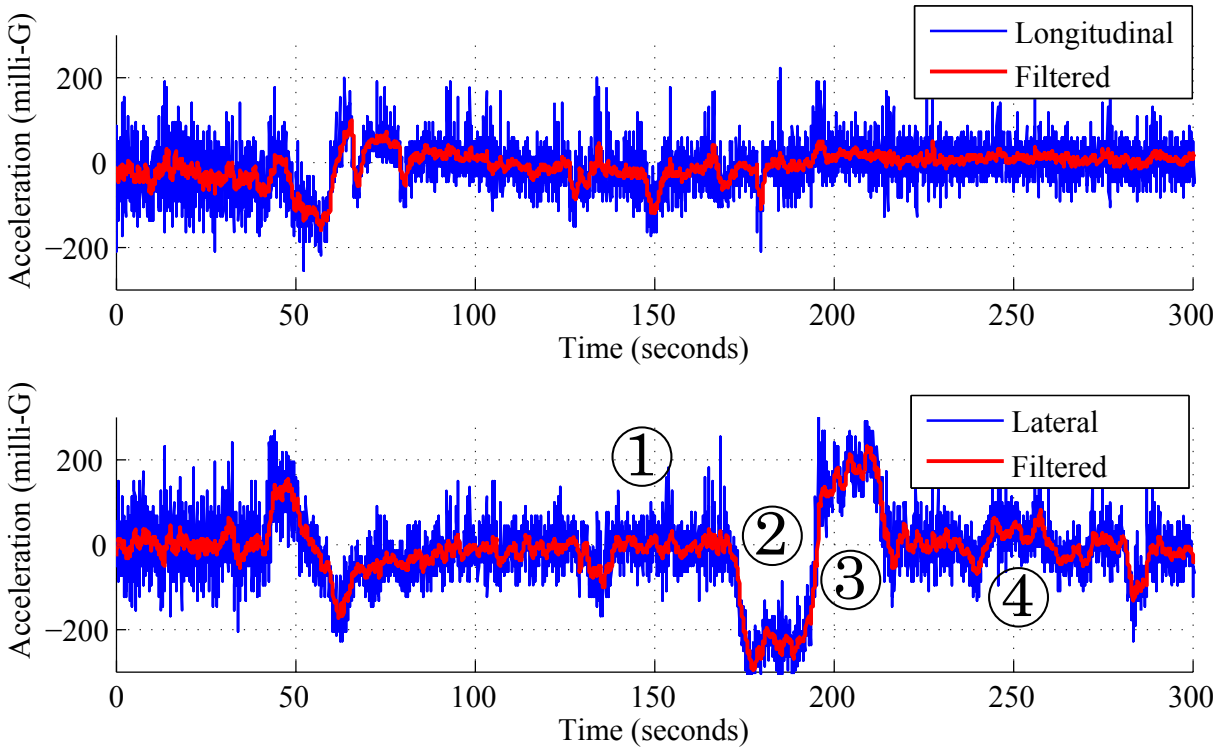

Figure 4.18: Raw acceleration data (blue) with the corresponding low pass filtered acceleration (red). The top Plot is the longitudinal acceleration and the bottom plot is the lateral acceleration. The numbers on the lateral plot correspond with the numbers in Figure 4.16.

the road bends to the right and then joins the highway at a junction, where the minibus taxi turns left.

After the data has been low pass filtered, the derivative of the filtered acceleration data was calculated to determine the jerk (see Equation 3.8), and the output can be seen in Figure 4.19. This plot shows the longitudinal and lateral jerk that correspond with changes in acceleration from the data in Figure 4.18.

Although the jerk is a good indication of reckless manoeuvres performed by the driver, it has two limitations. The first limitation is for roads with a high curvature radius, i.e. a long bend in the road. Vehicles travelling at a constant high speed around such a bend

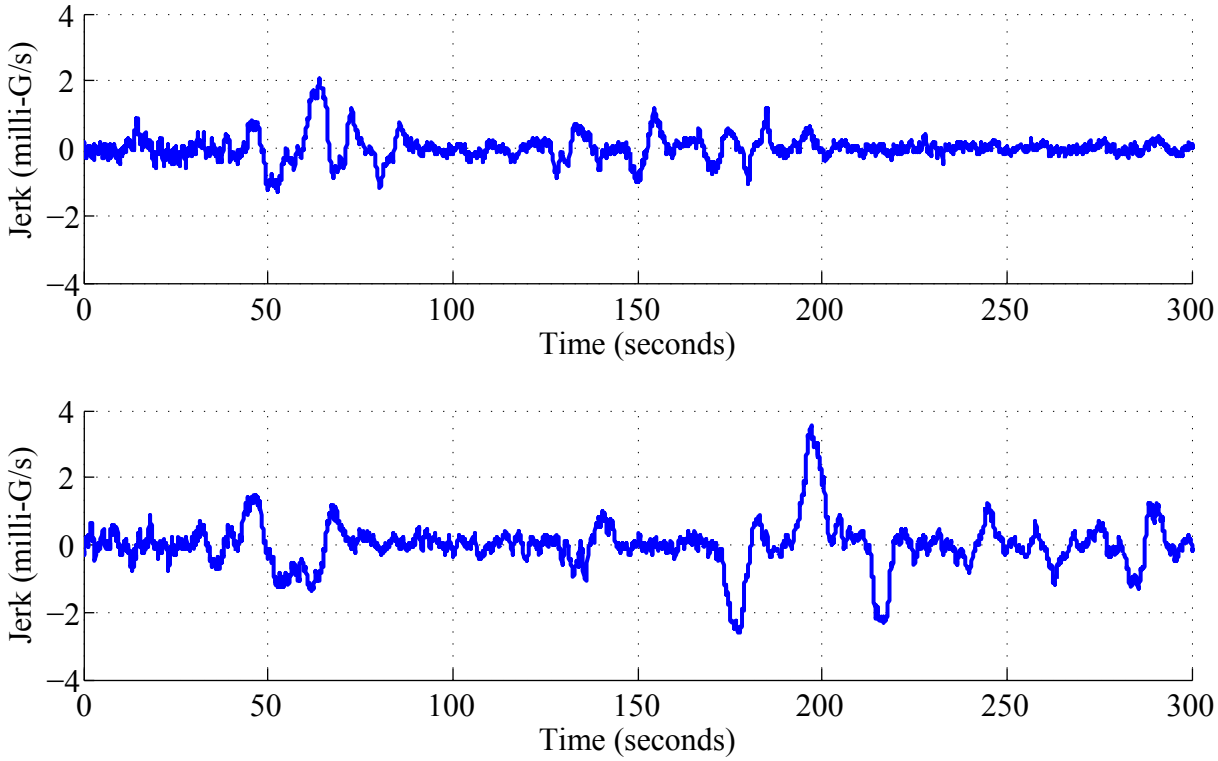

Figure 4.19: Plot of the calculated longitudinal (top) and lateral (bottom) jerk from the low pass filtered acceleration plot in Figure 4.18.

experience a constant high acceleration and the derivation lead to only a jerk peak in the beginning and the end of the turn, with only small changes in between. The second limitation, is for acceleration readings with sudden changes, but has low acceleration peaks. An example of such an occurrence is a disturbance of the sensor when tampered with. These limitations are overcome by summing the jerk values and therefore detecting high concentrations of jerk.

The summed values of the jerk, which essentially partially integrates the jerk back to acceleration, is illustrated in Figure 4.20. High concentrations of acceleration are observed at 50 seconds for both longitudinal and lateral, and at 200 seconds for lateral which corresponds with the LPF acceleration and jerk results. Comparing the peaks of the lateral jerk-summation plot at 200 seconds, with the LPF acceleration, we see that the values are similar. The maximum jerk-summation value is 276 milli-G and the absolute maximum LPF acceleration value is 283 milli-G. The jerk-summation therefore shows the same acceleration behaviour as the LPF acceleration. The filtered output clearly illustrates the high acceleration experienced through the turns.

From the filtering results it can be seen that the low pass filtering system removes the high frequency acceleration variations from the raw data, and the implemented jerk-summation system shows high concentrations of acceleration. The high concentrations of acceleration from the jerk-summation can be studied to determine if a reckless event has occurred.

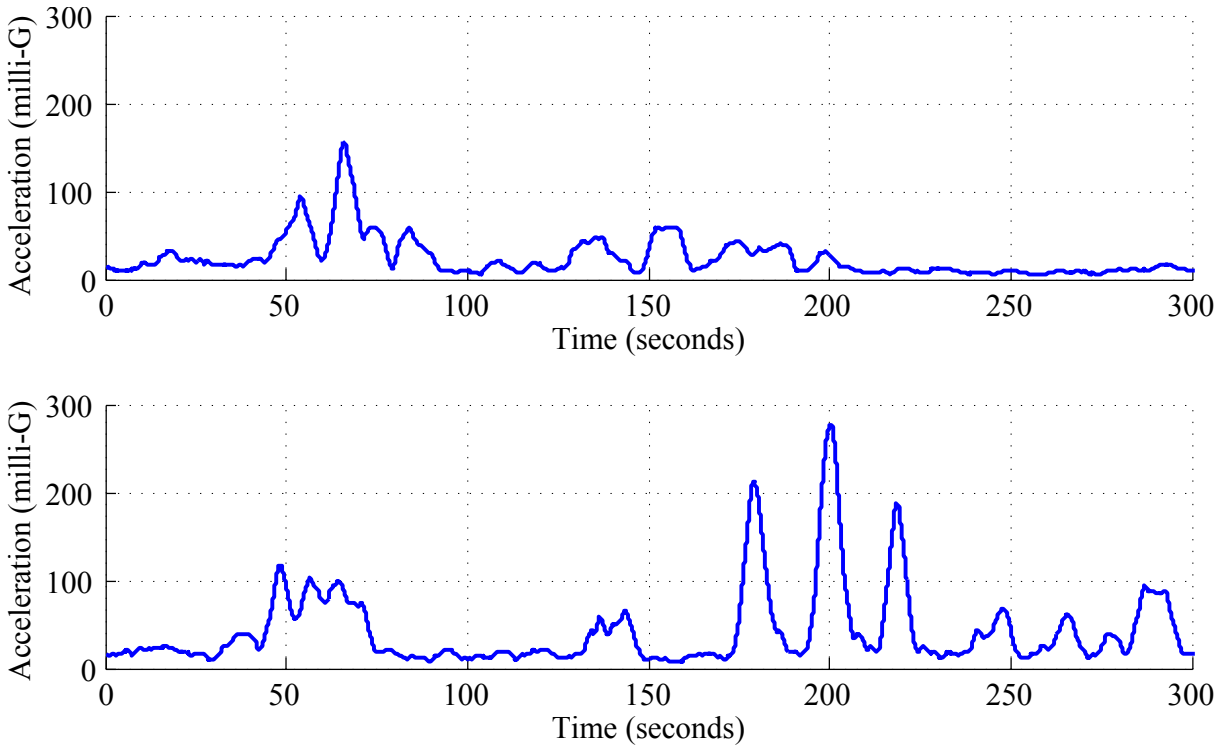

Figure 4.20: Longitudinal (top) and lateral (bottom) plot of the summed EMA-jerk values in Figure 4.19 showing high acceleration concentrations at 200 seconds.

4.2.4 Lateral and longitudinal threshold

In this section the developed reckless acceleration threshold, which is based on road design principles, is evaluated. The same road section as in the previous section is investigated (Figure 4.16 on page 69).

The minibus taxi's speed through the road section is shown in Figure 4.21. Also shown are thresholds calculated from section 3.2.3. An average speed of 91km/h is maintained, despite a speed limit of 50km/h. The minibus taxi was travelling at a speed of 89km/h turning into the hairpin bend at nr. 3 as seen in the Google Street View image in Figure 4.22. On the straight (nr. 1 in Figure 4.16), before the left turn, a top speed of 122km/h was reached, 22km/h above the absolute maximum legal limit for minibus taxis. The minibus taxi driver was therefore clearly speeding on this road segment, which can easily be detected since the maximum legal speed limit was crossed. Speeding in the mountain pass, as seen on the speed plot, won't unfortunately be picked up with only speed detection since the travelling speed is under the maximum legal limit. To determine if the legal speed limit has been exceeded, constant comparisons between the current travelling speed and a speed database, containing the speed limits for all roads in the country, is required, which is difficult and costly to implement.

The proposed dynamic threshold is therefore a realisable alternative solution. It takes the vehicle's current speed into account and reduces the threshold accordingly, therefore restricting the driver to stay within a safe travelling speed. The dip in speed when the

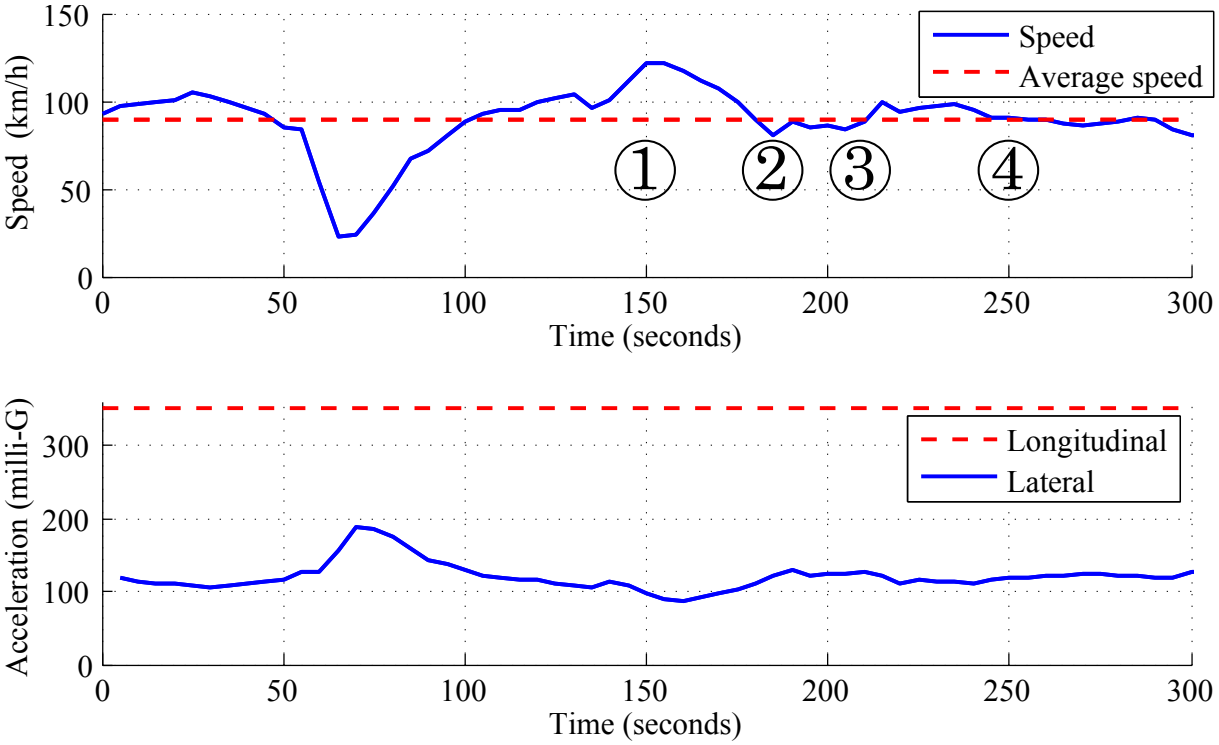

Figure 4.21: Speed and average speed of the minibus taxi (top) with the corresponding dynamic threshold and speed independent longitudinal threshold (bottom). The numbers on the speed plot correspond with the numbers in Figure 4.16.

Figure 4.22: Google Street View image showing over speeding at a hairpin bend. Speed limit is 50km/h, but the minibus taxi is travelling at 89km/h and therefore leading to high lateral acceleration values.

taxi slows down at the road junction is seen at 70 seconds on Figure 4.21 and as a result, the threshold raises, thereby allowing higher acceleration around the bend. The speed-independent longitudinal threshold is the red dashed line on the same plot.

The combined threshold and filtered acceleration plot is shown in Figure 4.23 for the lateral and longitudinal results of the discussed road segment. In this figure the final

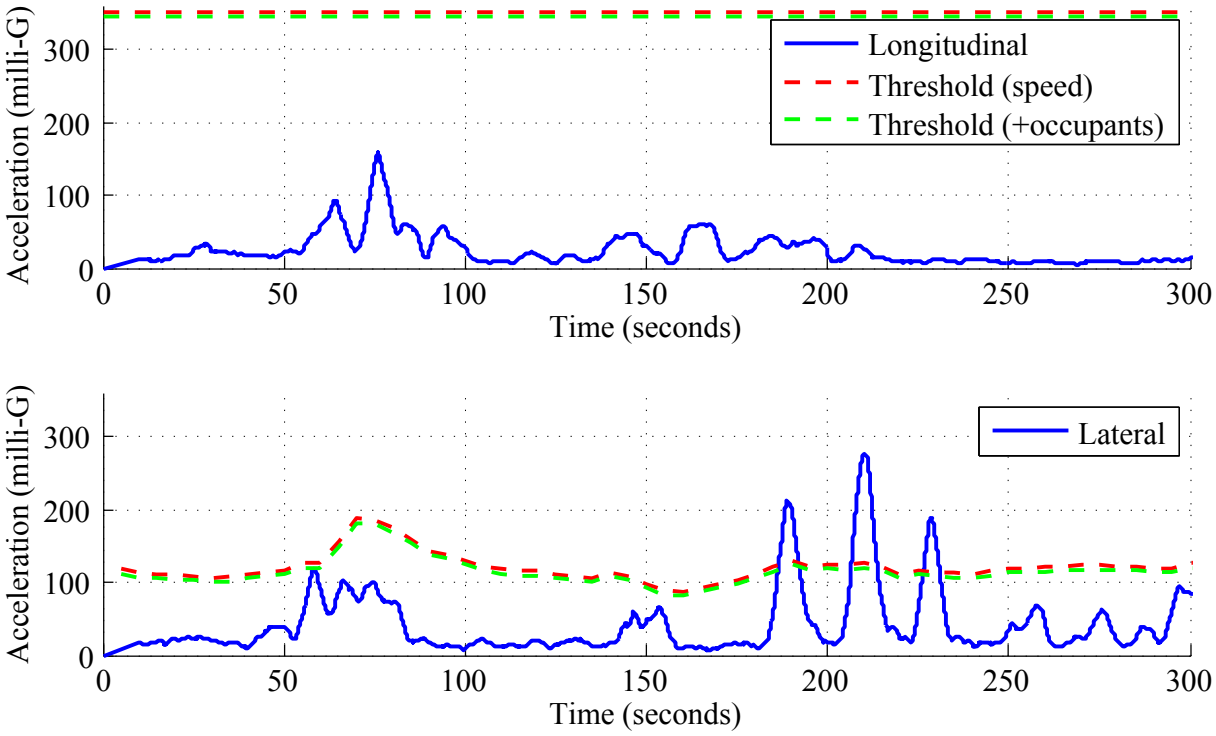

Figure 4.23: Filtered longitudinal and lateral acceleration data of the minibus taxi from Figure 4.16 with the dynamic speed threshold (red) and occupancy dependant threshold (green).

threshold, which includes the occupancy dependant threshold, is shown. Since only two occupants are present in the minibus taxi, the threshold is reduces minimally by 4 milli-G, but results in a detected reckless event at 58 seconds. Although this is a small reckless event, it is picked up and penalised with a level 1 reckless value. Clear erratic events occur at 185 sec, 205 sec, and 225 sec, and result in acceleration differences of 93 milli-G, 151 milli-G and 72 milli-G, leading to penalised level values of 3, 5 and 3, respectively. These values (including the event at 58 sec) add up and increase the total reckless level with 12 penalised points. These results are transmitted to the online platform, from where the responsible parties can be notified of these infringements.

The longitudinal acceleration with the road design erratic driving threshold can also be seen in Figure 4.23. No erratic driving events were identified. Longitudinal erratic events are less often identified on highway data since minibus taxis stop less frequent than in urban regions. From the collected data, the longitudinal reckless events rarely cross the threshold, and only cross the threshold in rash braking situations.

What the results also show is a weakness in the approach of using only an accelerometer threshold, without considering speed, to model reckless driving – the initial peaks in acceleration that is significantly lower than the latter, occur at a high speed, and constitutes to a reckless event.

4.2.5 Reckless driving detection under different scenarios

In this section we investigate the filtered acceleration output from different driving manoeuvres. The manoeuvres include: right turns, left turns, braking, left and right swerving, U-turns and data with an offset. These tests are performed to determine if the model can successfully detect reckless driving manoeuvres in the above events.

A safe road segment was identified that is straight, well tarred and have no other vehicles. The difference between the safe and reckless manoeuvres, for these tests, is that the safe manoeuvre is performed at a lower speed than the reckless manoeuvre. The figures that follow in this section shows the filtered acceleration results of safe (solid blue line) and reckless (dashed red line) events with the longitudinal (top plot) and lateral (bottom plot) threshold for each plot.

Figure 4.24 shows the right turn. We can see that the longitudinal acceleration does not cross the erratic threshold, with a maximum peak of 200 milli-G for the reckless turn. The safe turn has a maximum longitudinal acceleration peak of 150 milli-G. The reckless lateral acceleration crosses the threshold, and has a maximum acceleration of 230 milli-G. The safe event on the same plot shows a maximum peak of 185 milli-G, which is 20 milli-G lower than the threshold. We can therefore see from Figure 4.24 that the filtering model

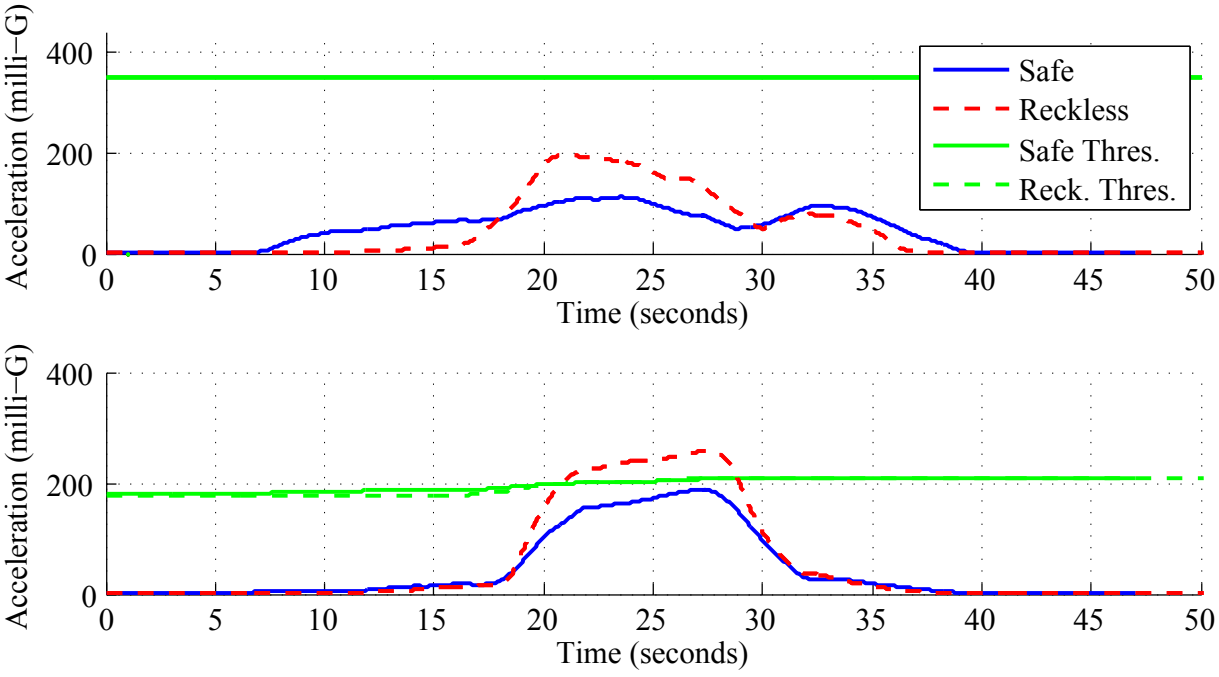

Figure 4.24: Filtered longitudinal (top) and lateral (bottom) acceleration data for a safe and reckless right turn.

results in the distinction between safe and reckless right turns.

Figure 4.25 shows the longitudinal and lateral acceleration of a left turn. The results look similar to that of a right turn with the same acceleration plot form. The safe left turn

shows a lower maximum acceleration peak than the safe right turn. A clear distinction between the safe and reckless left turn is seen.

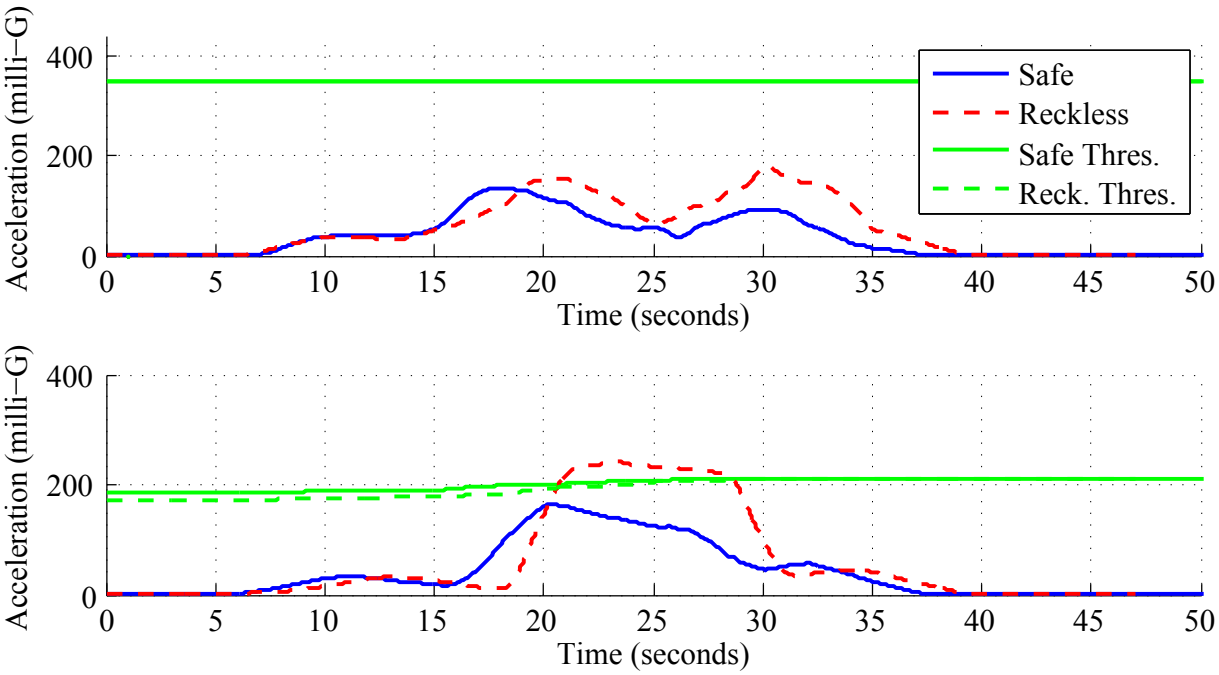

Figure 4.25: Filtered longitudinal (top) and lateral (bottom) acceleration data for a safe and reckless left turn.

The filtered braking acceleration is shown in Figure 4.26. The vehicle was travelling at 50km/h and braked gradually during the safe event. In the reckless event, the vehicle was also travelling at 50km/h, but the brakes were applied sharply, resulting in high acceleration values with a maximum value of 352 milli-G. Since the threshold is static at 350 milli-G, we can see that this braking exceeded the longitudinal threshold. From this data, and previous gathered data, the results show that potential reckless events can occur at lower acceleration values. Since the vehicle was travelling in a straight line, little lateral acceleration was induced. The results show the lifted lateral thresholds following the deceleration of the vehicle.

The plot in Figure 4.27 shows the longitudinal and lateral results for a left (dashed red line) and right (solid blue line) swerving event. Since the vehicle travelled at 60km/h and did not reduce or increase its speed significantly, low longitudinal acceleration values are observed. We can see from the lateral acceleration plot that the left swerving event crosses the lowered threshold; a static threshold at 210 milli-G would have missed the swerving manoeuvre. The right swerving manoeuvre's acceleration values do not cross the threshold, but stays 10 milli-G below the threshold. For safety reasons, swerving was not tested at high speeds. Since the vehicle was travelling at a relatively low speed, this swerving event does not contribute to a high accident risk, but demonstrates the relationship between a lowered threshold, and lateral acceleration. Increasing the vehicle's speed, lowers the threshold and decreases tolerance for swerving events.

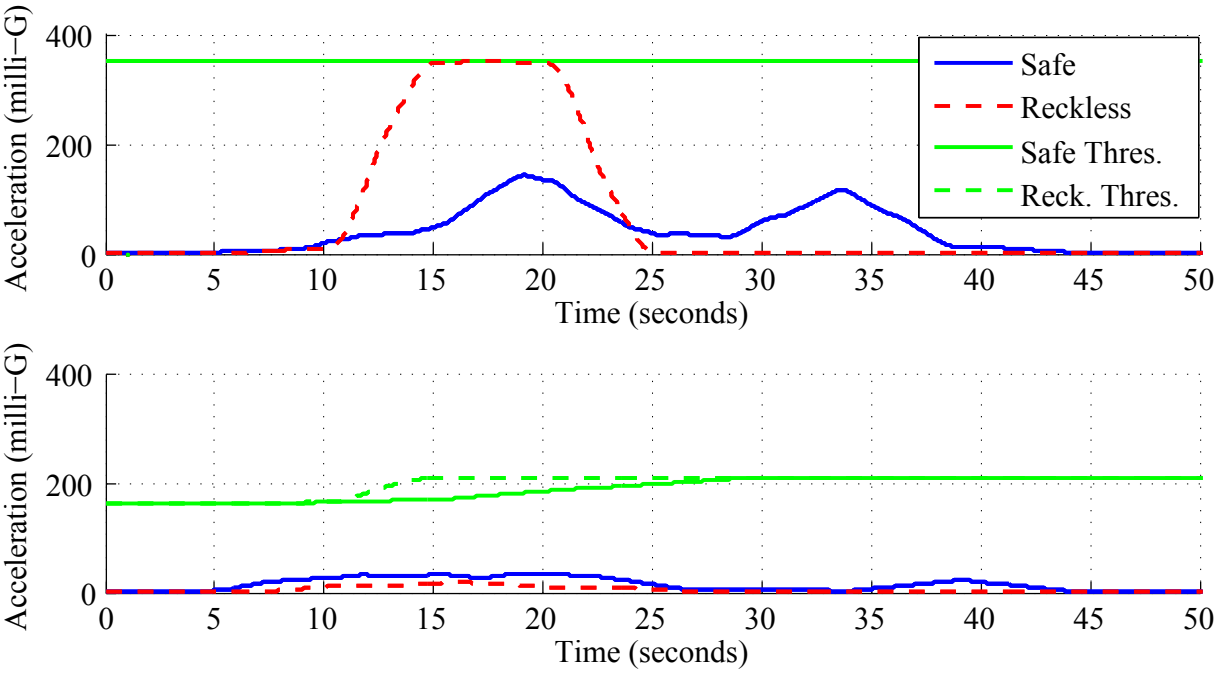

Figure 4.26: Filtered longitudinal (top) and lateral (bottom) acceleration data for a safe and reckless braking event.

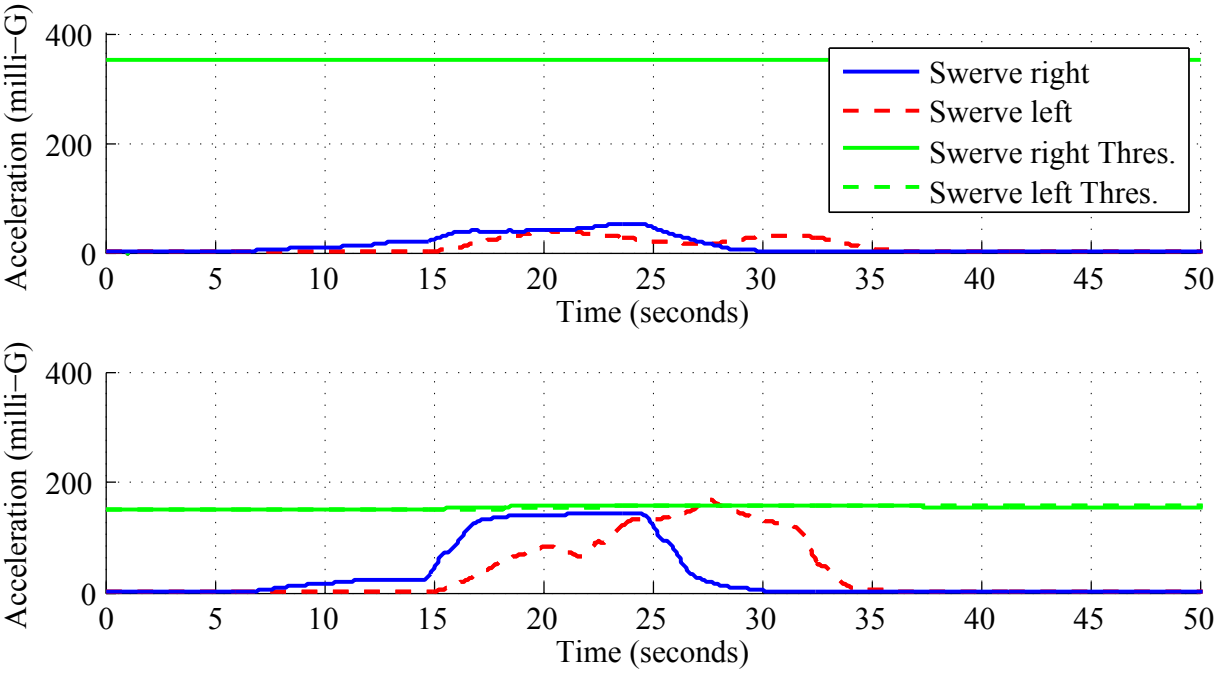

Figure 4.27: Filtered longitudinal (top) and lateral (bottom) acceleration data for a right and left swerving manoeuvre.

Figure 4.28 shows the safe and reckless results of a U-turn manoeuvre. The longitudinal acceleration for the reckless event exceeds the threshold, and the safe event's acceleration stays under the threshold. For the lateral acceleration, both the safe and reckless events exceed the threshold. The reckless event shows very high acceleration

values above the threshold with an erratic level value of 5. The safe lateral event only has small values above the threshold, but is still recognised as a reckless event with an erratic level value of 1. We can therefore see that reckless U-turns are clearly detectable.

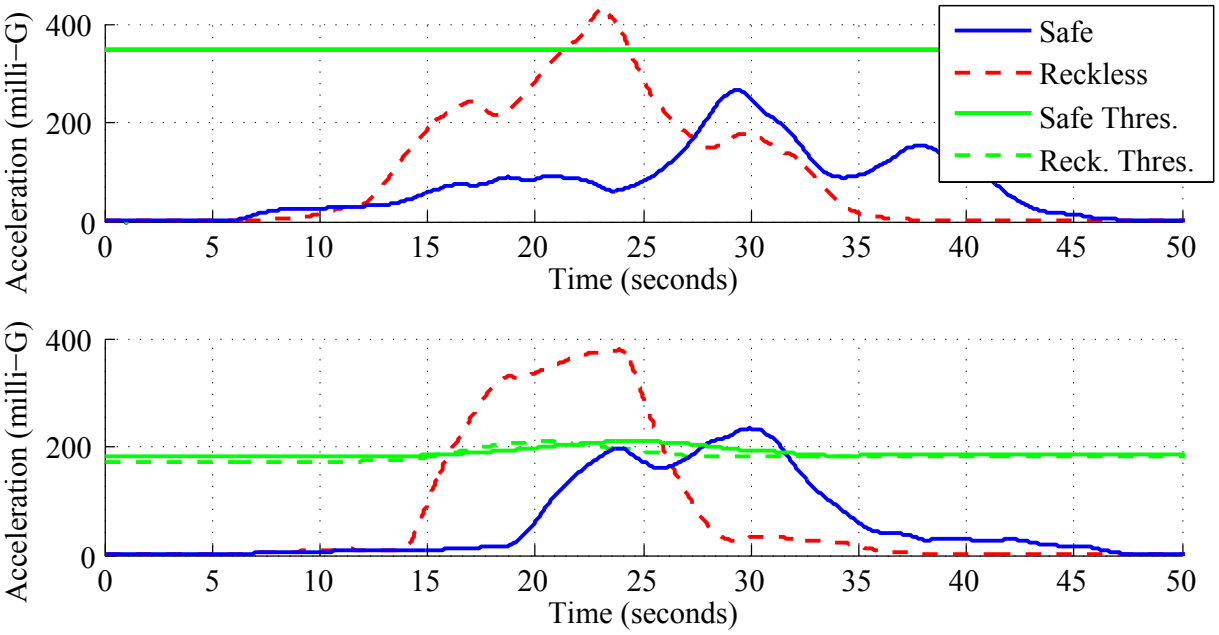

Figure 4.28: Filtered longitudinal (top) and lateral (bottom) acceleration data for a safe and reckless U-turn.

U-turns at low speeds can also be recognised as reckless, and all U-turns are therefore discouraged except if it can be performed at a very low speed.

Figure 4.29 shows data collected in Uganda on a long distance journey in a 14-seater minibus taxi. A high and inconsistent offset is visible for both the longitudinal and lateral acceleration (solid blue line) that was not passed through the high pass filter. This offset is as a result of the prototype resetting and recalibrating after a sudden shock on the device that comes from minibus taxis driving through numerous potholes. Highway and urban roads in Uganda have a high number of potholes. It is visible that the addition of the high pass filter model removes this DC offset (dashed red line) for both lateral and longitudinal acceleration. From the results we can see that without the removed DC offset, a number of false positives are detected for the lateral plot. False positives are readings that trigger the detection of a reckless event, when a reckless event has not occurred. This example was chosen since it gives a clear indication of how the DC offset is removed from data with an inconsistent offset. The removal of the offset also applies for roads with an incline or decline, where gravity induces the offset.

From this section's results, it was seen that the reckless driving detection system can clearly detect right turns, left turns, U-turns, and removes a DC offset in the data. From the swerving results, the detection system demonstrates that reckless manoeuvres are detected at high speeds. The results show that reckless braking events are detected,

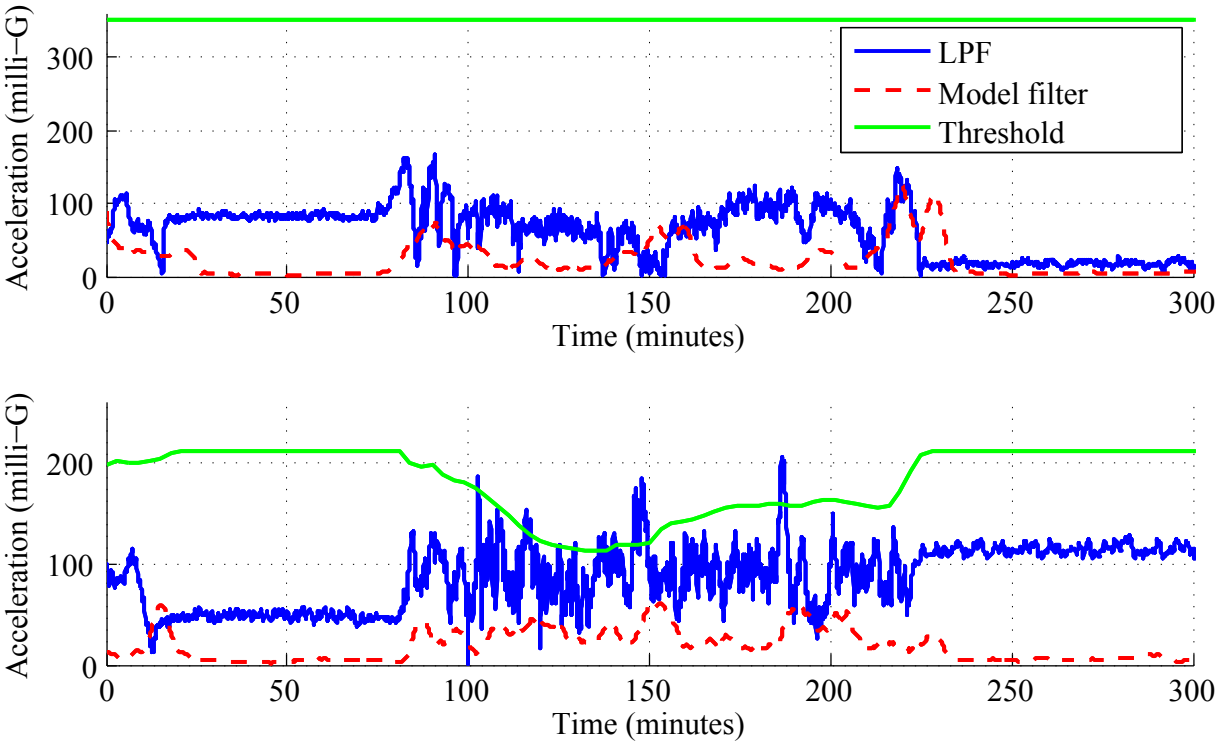

Figure 4.29: Filtered and unfiltered longitudinal (top) and lateral (bottom) acceleration data with an offset.

but potential reckless manoeuvres can occur at lower longitudinal acceleration values. The results also demonstrates the lateral threshold following the longitudinal acceleration curves, which increases the threshold with a decrease in acceleration, as expected, since the speed also decreases.

4.3 Reporting system

The sensing system consists of the occupancy detection and the reckless driving detection system that gathers and processes the collected data, and provides the reporting system with information. The gathered information is then stored on the black box storage device (SD-card), and also uploaded onto an online platform via a GSM modem.

In this section, performance results from the prototype reporting system are discussed. The system's performance is evaluated by investigating the success rate of the uploaded and stored information. The performance results will give us an indication of the reliability of the prototype, and where improvements can be made in the detection system.

For the storage and transmission of occupancy information, the same three-seat sensor setup was used as in Figure 4.2 on page 53. Eight tests were conducted on the seats in the minibus taxi.

For the reckless driving detection system, a road section was identified with seven significant road bends. Five test rounds were conducted. The tests were conducted at a time of day with very low traffic conditions and dry road surface to ensure the safety

of the driver. The driver maintained a speed under the legal speed limit (80km/h), but went into turns without reducing the speed, which resulted in high reckless acceleration values around the road bends. A dynamic acceleration threshold and filtering system was developed in section 3.2. Exceeding the threshold, therefore relates to a reckless driving event. The studied road segment can be seen in Figure 4.30. From the figure, the

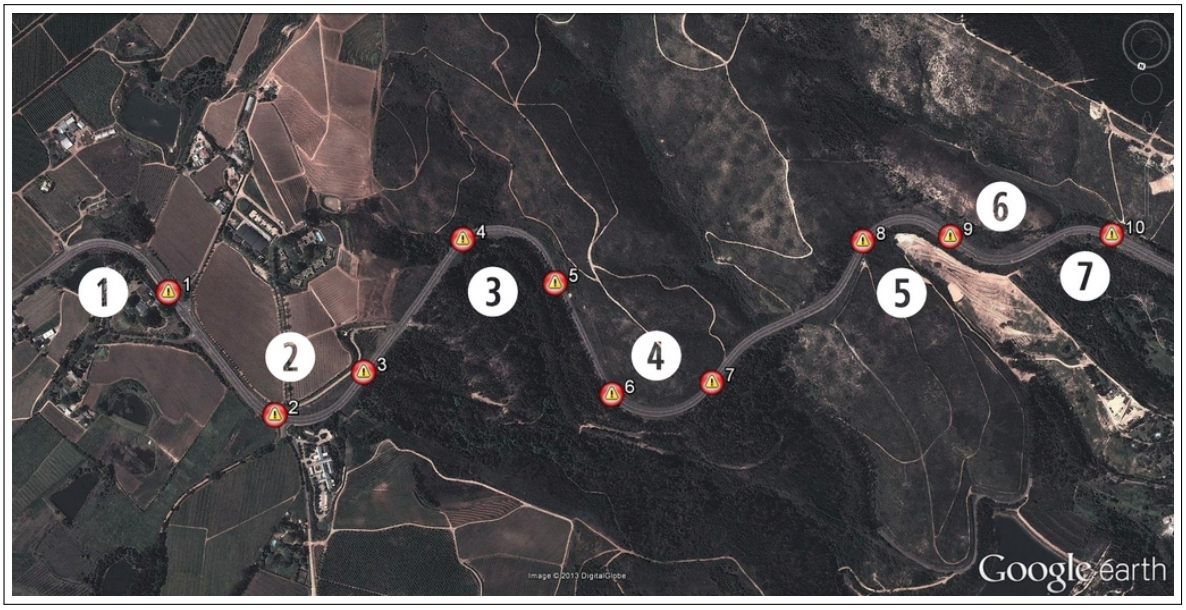

Figure 4.30: Identified road section with seven numbered road bends. The detected reckless events are indicated with red warning symbols.

seven numbered road bends can be seen. The event's duration around bend 3 lasted 28 seconds, travelling at an average speed of 74 km/h. Five of the bends exceed 300m in road length and have similar event durations as bend 3. This results in acceleration durations above the threshold, which lasted for between 10 and 20 seconds. Two erratic events are therefore to be detected at bends: 1, 2, 3, 4 and 5, since high acceleration values are maintained around them for longer than a single event's duration (section 3.3). A buzzer alarm is sounded when the reckless acceleration threshold is exceeded, indicating each event.

In section 4.3.1, the results of the black box storage device is shown and discussed. In section 4.3.2, the performance results of the GSM modem is discussed, where information is transmitted from the prototype's Gateway unit to the online platform. In section 4.3.3, the online dashboard is discussed, which displays the sensing systems information graphically.

4.3.1 Storing information on the black box

The SD-card is used as a black box for the prototype. Sensed events from the system are stored on the black box, which includes occupancy events, and reckless driving events.

The results of stored events on the SD card, for the eight performed tests, are shown in Listing 4.1. The entries in the listing, show an almost exact output of the information on the SD-card. Additional information, that were added after the data has been stored on the SD card (comments), is indicated by '//'. The seat's status combination is given as additional information before and after every changed event. An example of the sequence follows: '001' relates to the seat-status combination: unoccupied sensor 3, unoccupied sensor 2 and occupied sensor 1. A '1' therefore indicates an occupied seat and a '0' an unoccupied seat.

Listing 4.1: Stored occupancy information on black box

```
//000
//Missing status update
//New occupant on seat, 1
//Number of occupants in taxi, 1
//001
Occupant left seat, 1
Minutes on seat, 0
Number of occupants in taxi, 0
//000
New occupant on seat, 2
Number of occupants in taxi, 1
//010
New occupant on seat, 1
Number of occupants in taxi, 2
//011
Occupant left seat, 2
Minutes on seat, 2
Number of occupants in taxi, 1
//001
Occupant left seat, 1
Minutes on seat, 0
Number of occupants in taxi, 0
//000
New occupant on seat, 3
Number of occupants in taxi, 1
//100
New occupant on seat, 1
Number of occupants in taxi, 2
//101
New occupant on seat, 2
Number of occupants in taxi, 3
//111
Occupant left seat, 1
Minutes on seat, 0
Number of occupants in taxi, 2
//110
//Missing status update
//New occupant on seat, 1
```

```
//Number of occupants in taxi, 3
//111
Occupant left seat, 1
Minutes on seat, 3
Number of occupants in taxi, 2
//110
Occupant left seat, 3
Minutes on seat, 6
Number of occupants in taxi, 1
//010
Occupant left seat, 2
Minutes on seat, 5
Number of occupants in taxi, 0
//000
```

It can be seen in the listing that two status update entries are missing from a total of 14 entries. This gives the black box an 86% accuracy for the storage of occupancy events.

The detected reckless driving events, of one tests round, are indicated by red warning symbols, which was shown in Figure 4.30 on page 80. From the figure there can be seen that a reckless driving event is missing at the beginning of bend 1, and the reckless manoeuvre around bend 6 was not detected.

An example of the stored data on the SD card is shown in Listing 4.2. The information in the listing is from the test results of the road section in Figure 4.30. Commented information has been added showing an event number that corresponds with the detected reckless event's warning symbol numbers in the figure. Reckless driving events 5 to 8 are included in the listing.

Listing 4.2: Stored reckless driving information on black box

```
//5
Date, 20130730
Time, 1444
Location, -3392237, 1891559
RDType, lateral
RDLevel, 4
RDLevelTotal, 51
//6
Date, 20130730
Time, 1444
Location, -3392039, 1891360
RDType, lateral
RDLevel, 3
RDLevelTotal, 54
//7
Date, 20130730
Time, 1445
Location, -3392108, 1891120
RDType, lateral
```

```
RDLevel, 3
RDLevelTotal, 57
//8
Date, 20130730
Time, 1445
Location, -3392466, 1890830
RDType, lateral
RDLevel, 3
RDLevelTotal, 60
```

From the above example we can see that the date, time and location are combined into a single number and all the information is separated by commas. This is to simplify the extraction of the data. *RDType* is the reckless driving type that can be either *lateral*, *longitudinal* or *accident*. *RDLevel* is the reckless driving level that was generated by comparing the acceleration above the threshold to the level table in Table 3.3 on page 44, and *RDLevelTotal* is the current cumulated level values.

From the five reckless driving test rounds, 78% of the reckless events were detected. From the detected events, 93% of them was stored successfully, with all the information, on the SD-card.

4.3.2 Uploading information on to the online platform

The GSM modem sends updated information from the prototype, which is stored on an online database. Studying the uploaded information on the database, and comparing it to the commands given to the modem to send the data, gives an indication of the success rate. In this section, the GSM modem's performance is therefore investigated.

Occupancy, location, and speed information is sent every 15 seconds by the GSM modem. During the occupancy tests conducted in a minibus taxi, multiple failed communication attempts were observed. After several failed attempts, the modem resets itself and re-establishes connectivity. The longest update period before connectivity was restore lasted 1 minute. Although the modem showed problems, the occupancy information was not lost, but only delayed.

The GSM modem's performance, for the updating of detected reckless events, was studied on the road segment from Figure 4.30 on page 80. Comparing the reckless events to the information uploaded onto the platform, showed that 81% of the detected events were reported, which relates to 64% of the total reckless events.

Missing occupancy and reckless driving events on the SD-card, is as a result of the GSM modem sending information to the platform at the time of an event. Whenever the modem attempts to establish connectivity and transmit the information, the prototype's sensing system and SD-card storage functions are interrupted, waiting for the modem to complete its action. The prototype's occupancy and reckless driving detection capabilities are therefore temporarily disabled, missing possible reckless events. A software buffer will solve this problem, since new data is temporarily stored while the GSM modem updates.

When reoccurring modem connectivity problems occur, a relay is enabled resetting the modem. A higher success rate is guaranteed if the GSM modem in the system is replaced by one with improved reliability.

4.3.3 Minibus taxi monitoring system dashboard

The information stored on the online database, is made available graphically on an online dashboard. The online dashboard was designed for users to quickly take in the information generated on the sensing system. In this section the dashboard is shown and discussed.

Figure 4.31 and 4.32 shows a screenshot taken of the dashboard during tests. The dashboard can be found online via the following link:
`http://smart.trintel.co.za`.
Username: `taxi`
Password: `taxi`

The dashboard can be viewed from any web browser, and works on mobile devices. An automatic updating function is also available on the dashboard. The following information is available on the dashboard:

- the monitoring system's current state (active or inactive),
- an image of the minibus taxi showing every seat and its current occupied state,
- total number of seats in the minibus taxi (occupied and unoccupied),
- total number of current seated occupants in the minibus taxi,
- current duration that each of the occupants have been on their seat,
- taxi's current location and the previous 10 recorded locations,
- current travelling speed,
- the last time the dashboard was updated with new occupancy information,
- speed history
- reckless event history showing the location of each reckless event,
- maximum travelled speed in last hour
- the time of the previous reckless event
- reckless level of previous event, and
- the current reckless level total.

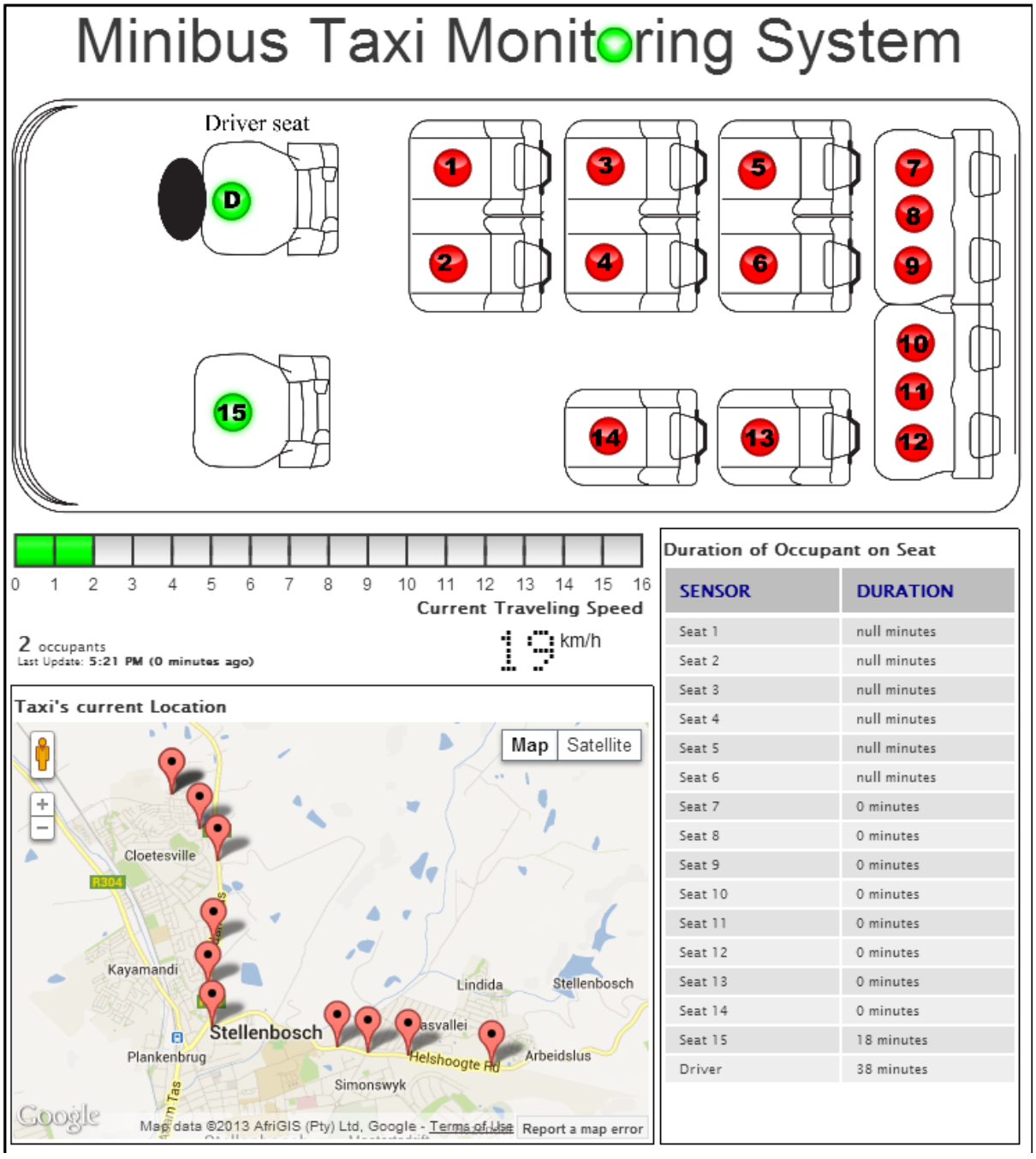

Figure 4.31: Top half of the minibus taxi monitoring system's online dashboard.

In the title, at the top of the dashboard, a green status indicator shows that the modem is currently operational, sensing, and displaying updated information from the sensing system. This can also be seen from the text showing the last time the dashboard was updated with new occupancy information (currently *0 minutes ago*). If the status indicator is red, it means that the sensing system is currently inactive. This dashboard image is an example of sensed information from a typical minibus taxi. The co-driver passenger seat (seat 15), is normally occupied since this passenger handles the money that is collected from the other passengers. In this taxi, there can be seen that the *duration of occupants* on the other seats have durations of 0 minutes since they are unoccupied.

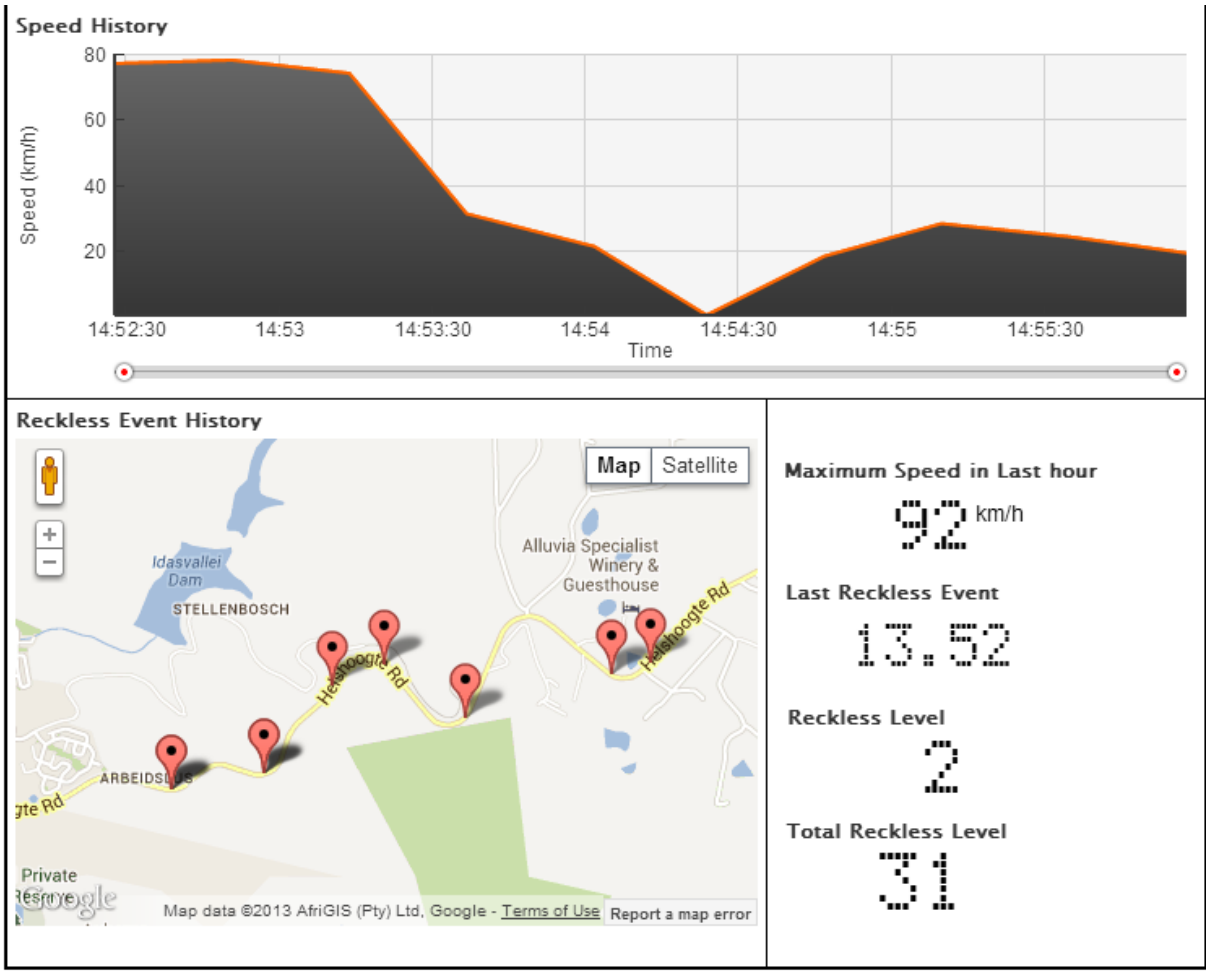

Figure 4.32: Bottom half of the minibus taxi monitoring system's online dashboard.

The current total reckless level is at 31, which means that the minibus taxi driver has been driving very recklessly. The reckless event map also indicates this, since a number of reckless events have been detected.

The designed online dashboard therefore displays information from the sensing and reporting system in user-friendly graphical representation.

Chapter 5

Conclusion

This chapter concludes the work in the manuscript, giving a summary and the motivation behind the work. There is commented on the accomplished objectives, and also possible applications and recommendations for future work discussed.

5.1 Summary of work

This study focuses on the most prominent segment of informal public transport in SSA in general, and in South Africa in particular, namely the minibus taxi sector. In Chapter 1 the need for a safe and reliable public transportation system in SSA was discussed and the main challenges identified: namely, safety and efficiency. A number of ITS solutions have been designed to improve road safety and efficiency, but these systems are mostly aimed at developed countries. Technologies used for improving road safety and efficiency is not always feasible in developing countries – due to the cost of implementation, maintenance and operations, the intermittent supply of electricity, lack of technical skills in the country, and remote roads and distance to cities.

Public transport in SSA is considered dangerous due to the high number of accidents annually, many leading to fatalities. The root cause for the unsafe nature is found in financial incentives, since drivers have a clear incentive to generate as much money as possible – transporting more passengers more frequently, by speeding and performing dangerous driving manoeuvres between destinations. SSA's taxis are mostly demand driven, and the biggest transport inefficiency is the time spent waiting, by both the passengers as well as the drivers. This work therefore presents the design and testing of a sensing and reporting system, for minibus taxis in SSA, to improve its safety and efficiency.

An in-depth analysis of systems developed for improving road safety and detecting occupants in a vehicle were discussed in Chapter 2. Systems developed for improving road safety depend on advanced and expensive technology, and does not provide a sustainable solution, since a high accident risk still remains to other vehicles, cyclists and pedestrians on the road. Many systems have been developed to detect reckless driving manoeuvres, but shortcomings still exist. A study of previously developed occupancy detection systems shows that a number of different systems have been developed and implemented in vehicles. These systems are, however, not viable solutions for implementation in minibus taxis, due to their complexity and/or high cost.

A model and sensing system is developed for the detection of reckless events and multiple occupants in a vehicle. Tests are performed in a Quantum minibus taxi and the results analysed to evaluate the sensing and reporting system. The results are used to validate the designed detection model, and investigate the realisable of the system in SSA. The results are also used to confirm the hypotheses from Chapter 1 in the next section.

5.2 Conclusions

The conclusions in this section are divided into those related to detecting multiple occupants in a minibus taxi, reckless driving detection, and the graphical representation of minibus taxi information. References are made throughout the section to the hypotheses defined in Chapter 1.

5.2.1 Detecting multiple occupants in a minibus taxi

The capacitive occupancy detection system developed in section 3.1 is validated with results from section 4.2. A low-cost sensor system, which uses a single electrode for the detection of an occupant, is placed on a taxi's seat to detect the presence of an occupant.

The developed simplified mathematical model in section 3.1.4 is used for preliminary theoretical analysis in section 3.1.5, which shows that the occupied capacitance is double the unoccupied capacitance on the sensor electrode. This is confirmed in section 4.1.1 where the actual capacitance on the electrode is measured. Although the theoretical and measured capacitance values differ, the occupied/unoccupied ratios are the same. This confirms Hypothesis 1.1 and 1.2.

Hypothesis 1.1:

The capacitive effects of passengers can be modelled mathematically.

Hypothesis 1.2:

There is a significant difference between the capacitance with an occupant present and without an occupant present.

The results from section 4.1.2 show that multiple occupants can be detected with high degree of certainty. A wide range of tests were performed in a Quantum minibus taxi to get the most accurate representation of real-world scenarios. Small, medium and large sized occupants were used to ensure size coverage, and seven occupant-seat scenarios were investigated. The seven tests include: an occupant sits completely on an electrode, partially, and next to it; the occupant touches a large metal object in the taxi while sitting on the sensor; a foreign non-conduction and then conducting object is placed on the electrode; the sensor, when surrounded by water, receives an occupant. The results show a clear distinction between a human body and a non-human body. The results also demonstrate that the occupancy detection system has a robust sensor setup, and can detect multiple occupants in the minibus taxi's heterogeneous environment. This confirms Hypothesis 1.3, 1.4, 1.5, and 1.6.

Hypothesis 1.3:

The presence of multiple bodies can be individually detected using capacitive coupling and sensing.

Hypothesis 1.4:

Multiple passengers can accurately be detected using a low-complexity capacitive sensing system.

Hypothesis 1.5:

Capacitive coupling and sensing can distinguish between a human body and a non-human body (e.g. a bag) on a seat.

Hypothesis 1.6:

A capacitive sensing system can endure the heterogeneous minibus taxi environment.

5.2.2 Reckless driving detection

A reckless driving detection system developed in section 3.2 is validated with results from section 4.2.

Acceleration and speed results collected, on South African and Ugandan roads, show a clear correlation to driving manoeuvres and are used as a measure of recklessness. The designed accelerometer data filtering system in section 3.2.2 is investigated in section 4.2.3. Results show the removal of high frequencies and unwanted offsets. The reckless driving detection system is based on novel techniques used to identify reckless driving manoeuvres in augmenting acceleration data with vehicle speed, and occupancy information. The designed model in section 3.2.3 is based on principles used in road design, which takes into account the relationship between a vehicle's tyres and the road surface,

i.e. the friction coefficient. Two thresholds (lateral and longitudinal) were developed from the model for comparison to the vehicle's inertial acceleration. Results in section 4.2.4 clearly shows the speed dependant lateral threshold, and the longitudinal threshold. This confirms Hypothesis 2.1, 2.2, and 2.3.

Taxis were fitted with a tracking device. The speed results in section 4.2.1 is from a typical minibus taxi journey, which was analysed and very high speed samples observed. More than 50% of the speed samples is above the legal speed limit of 100km/h. This confirms Hypothesis 2.4.

Hypothesis 2.1:
Acceleration and speed provide a measure of recklessness.

Hypothesis 2.2:
Sensors can be sampled fast enough to detect recklessness from accelerometers and GPS speed detection.

Hypothesis 2.3:
Acceleration measurements can be filtered successfully to remove unwanted variances and offsets.

Hypothesis 2.4:
Minibus taxis travel at excessive speeds and ignores the national speed-limit.

In section 3.2.1 it was stated that urban events have shorter acceleration durations, for longitudinal and lateral manoeuvres, than highway events. Results in section 4.2.2 confirms the statement. A number of other differences between minibus taxi drivers' driving on urban and highway roads were also observed, therefore confirming Hypothesis 2.5.

Hypothesis 2.5:
There are substantial differences in the driving patterns of minibus taxis in urban and highway scenarios.

An additional occupancy dependant threshold is designed in section 3.2.4 which deceases the threshold, for both lateral and longitudinal acceleration, with an increase in the number of occupants in the minibus taxi. Results in section 4.2.4 show that, with the addition of the occupancy dependent threshold, which decreases the threshold, more reckless events are detected. The number of passenger in a minibus taxi affects the weight and dynamics of the vehicle. This confirms Hypothesis 2.6.

Hypothesis 2.6:

Occupancy information can be used to improve a reckless driving detection system.

5.2.3 Graphical representation of minibus taxi information

A real-time reporting system was designed in Chapter 3, and validated with results in section 4.3. The reporting system receives occupancy and the reckless driving information from the sensing system, which is then stored on a black box, and uploaded onto Trinity Telecoms' SMART online platform. The prototype in section 3.3 is implemented with the designed system and provided with a GSM modem that uploads the minibus taxi's information onto the online platform. The GSM modem makes use of standard cellular communication means. Results in section 4.3.3 shows the visualised information from the online platform. This confirms Hypothesis 3.1 and 3.2.

Hypothesis 3.1:

The system is integrable with the existing cellular network in SSA.

Hypothesis 3.2:

Minibus taxis can be tracked in real-time, and information of recklessness and occupancy combined with location information.

5.3 Future work

In this section some recommendations and applications are discussed for future work.

Although the system was tested in several minibus taxis and valuable data collected, we recommend more field studies by implementing a number of minibus taxis with the designed system. The prototype must therefore be adapted into a smaller, more manageable device, which can easily be installed in a minibus taxi. It is important that the device maintains high sensitivity and low-cost. A further improvement for the system, is automatic calibration for the accelerometer's axis orientation. Currently the x-axis and y-axis needs to be perfectly aligned for accurate results, but if the device can automatically detect its orientation it would simplify installation. With multiple minibus taxis equipped with the sensing and reporting system, the field study can be expanded to start monitoring the impact of the system on road safety and efficiency. It would be interesting to evaluate feedback from passengers in taxis equipped with the monitoring system, and compare it to passengers' feedback in taxis without the monitoring system.

The occupancy detection system can be expanded to detect overloading. This can probably be accomplished by implementing or measuring the weight on the wheels.

Taxi owners may find the monitoring system of interest, since they can keep close tabs on the number of passengers being transported between locations, and detect if drivers

are abusing vehicles. This would therefore reduce maintenance costs. The motoring data collected is also of academic and government interest, since it can be used to study minibus taxi driver behaviour; improve the deployment of ITS solutions (e.g. for intelligent police and speed camera allocation); to monitor high accident zones and compare it to reckless driving; identifying popular routes, since the number of passengers in the taxi is always known. Finally, it can also be of importance to medical and safety response services. In the event of an accident, the exact number of passengers in the minibus taxi are known, and the reported acceleration and speed readings give an indications of the severity of the collision. The response team can therefore deploy the appropriate number of medical and recovery vehicles to the scene of the accident.

5.4 Concluding remarks

A sensing and reporting system was proposed that detects reckless driving manoeuvres, the number of occupants in the minibus taxi, and visualises the information online. The sensing and reporting system was successfully developed and tested, and could make public transport in Sub-Saharan Africa safe and reliable. The inspiration behind this study was from to the unsafe nature of our South African roads, partially due to the dangerous minibus taxi sector. This study was therefore conducted to help improve our roads, by reducing the potential for accident, and helping people who depend daily on this transit system.

APPENDICES

Appendix A

Detailed Software Setup

The information in this appendix shows the detailed implementation of the software setup. An overview of the software setup was shown in Figure 3.15 on page 49.

In A.1, two flow diagrams for the end device microcontroller are discussed. The functions determine if an occupant is present on the seat, and calculates the occupant's duration on the seat (when occupied). The collected data is then organised into information packets and transmitted wirelessly, which is discussed in the ZigBee function. In A.2, the functions used in the Gateway unit are discussed.

A.1 End device microcontroller

A flow diagram of the process determining when a seat is occupied, is given in Figure A.1. An occupant on the seat increases the capacitance on the electrode (see section 3.1.2), which results in an increased timer value. This timer value is stored in the variable, *sensorReading*, after every charge/discharge cycle. A new *sensorReading* is generated every 20ms. The sensor readings are generated from a function that is based on the *capacitiveSensor* library for Arduino [102]. The sensor readings are filtered with a LPF designed in section 3.1.3. When *sensorReading* exceeds the occupied threshold, a counter (*countOcc*) waits for 5 seconds of *sensorReading* above the threshold before changing the reported seat status to occupied. A sensor reading under the threshold resets the occupied counter (*countOcc*), which ensures that consecutive sensors readings above the threshold have to follow for 5 seconds for the status to change. A timer (*occupiedDuration*) gives the total duration a seat has been occupied, which is reset (set to zero) after each reported status change. Sensor readings under the threshold relate to an occupant not detected on the sensor. The reported status of the seat is also not immediately changed

to unoccupied, since sensors have to be unoccupied for more than 5 seconds to change the reported status to unoccupied. Similarly, a counter *countUnocc* increases its value with every reading below the threshold to calculate the unoccupied duration.

For every new reported state a seat enters, the total number of occupants in the system is updated and a boolean variable (variable that can be ether true or false), *statusChange* is set to true. This boolean variable enables the ZigBee function to transmit the new seat information. Figure A.1 shows ZigBee function. The occupancy information (called

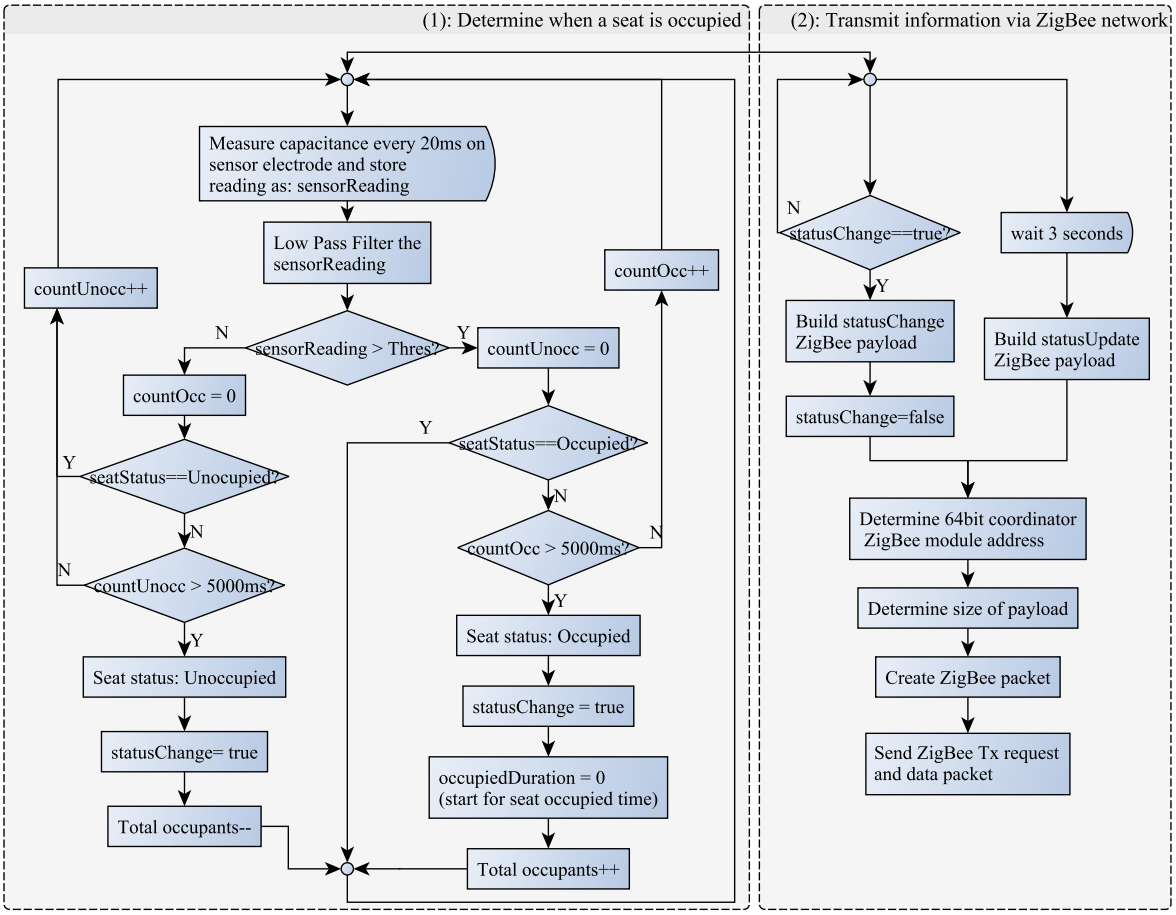

Figure A.1: Occupant detection and ZigBee transmission flow diagram.

the payload) is combined with ZigBee address information (required for communication between the two ZigBee devices) into a ZigBee data packet. Every 3 seconds, the end device transmits status information from all the seat sensors, therefore giving updated information of the durations occupants have been present on the sensor. This information is called status update information. Occupancy information is also sent to the Gateway unit with every reported seat status change in the minibus taxi.

A.2 Gateway unit microcontroller

In this section the Gateway unit's software setup is investigated, which consists of 9 main functions. Information is received, processed, and then stored on a SD-card and sent via a GSM modem.

The Gateway unit waits for a valid ZigBee data packet and then extracts the received occupancy information. An acknowledgement message is transmitted to the end device ZigBee module confirming that the packet was successfully delivered. If the received packet on the Gateway unit contains status update information from the end device, a boolean variable (*sendToModem*) is set as true and enables the GSM modem to transmit the received occupancy information to the online database. Data packets containing information regarding a change in a seat's status, sets the boolean variable, *sendToSD* to true, which enables the SD-card function to store the occupancy event on the SD-card. The flow diagram of the ZigBee function, receiving occupancy information, can be seen in Figure A.2.

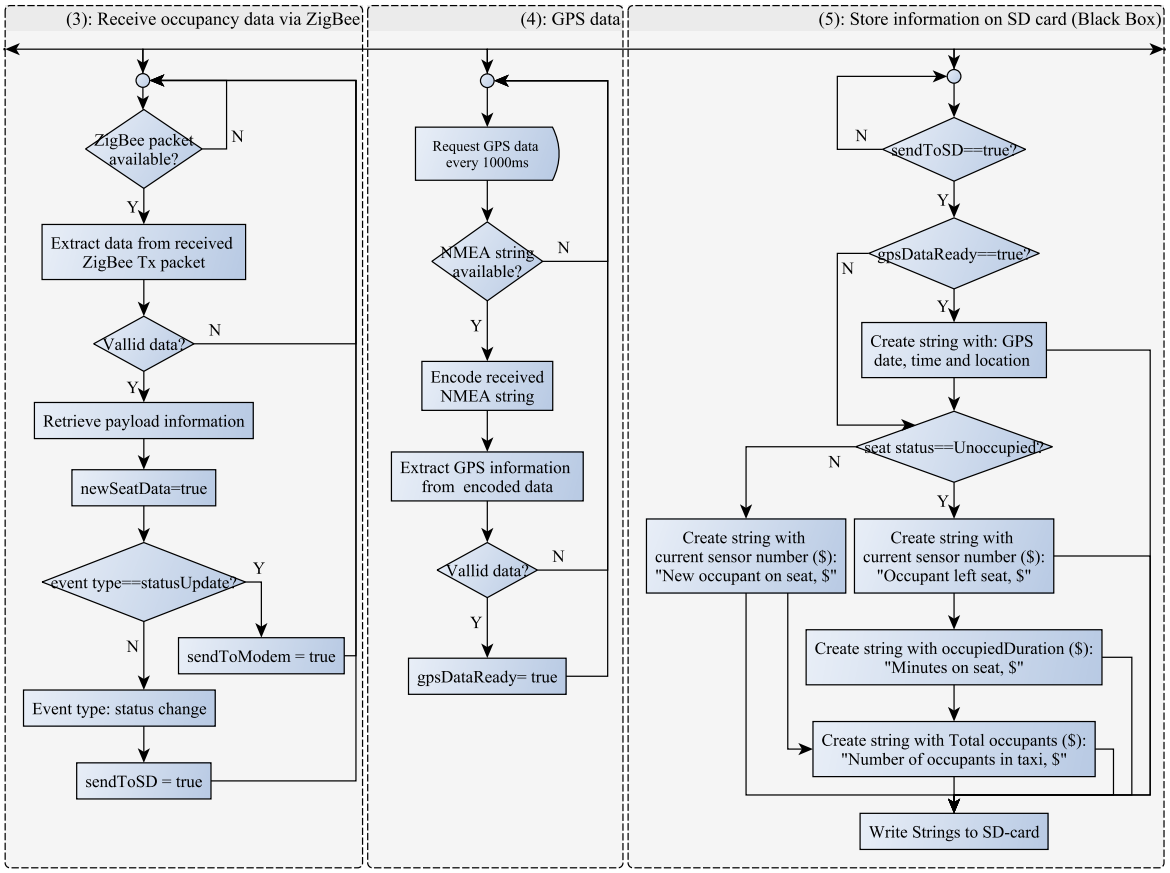

Figure A.2: Flow diagrams from the Gateway unit. Diagram (3) is the function extracting the information from the ZigBee packet, (4) shows the process of requesting and encoding the GPS information, and (5) is the function writing string lines onto a file on the SD-card.

The GPS modem requests GPS data every 1000ms, which is received serially in a

NMEA 0183 data format. The GPS information is made available for the other functions after the received GPS data has been processed on the microcontroller. A variable, *gspDataReady* indicates that GPS information is available and ready.

A SD-card provides the occupancy detection system with black box capability. Every seat-occupancy event is logged on this storage device. When an occupant leaves their seat, the total duration that this occupant was on the seat is stored, including the seat's name and the new number of occupants currently seated in the minibus taxi. The current date, time and location of this event are also included. This black box feature therefore provides a very accurate log for the seats in the minibus taxi. The information and text are separated by commas for easy comma separated extraction. Two examples of how the information is logged on the SD-card are given. In the first example an occupant takes a seat in a taxi with five seats currently occupied:

```
Date, 20130628
Time, 1528
Current location, -3390369, 1859958
New occupant on seat, 2
Number of occupants in taxi, 6
```

The seconds example is an occupant leaving a seat 2 minutes later:

```
Date, 20130628
Time, 1530
Current location, -3390611, 1858490
Occupant left seat, 5
Minutes on seat, 13
Number of occupants in taxi, 5
```

Figure A.3 shows the flow diagram for the acceleration filtering, and threshold calculation functions. Longitudinal (y-axis) and lateral (x-axis) acceleration readings, from the 3-axis accelerometer, are stored in a buffer. The acceleration buffer's last value is checked for a non-zero value to confirm that the buffer is not empty. The buffer is an array of type float with 100 elements, which means that the values can contain decimal places for improved accuracy. A new value is added into the first buffer space and the last value pushed out. The acceleration buffer allows the EMA-jerk function to calculate (see section 3.2.2) the EMA and the jerk from previous values. Since the accelerometer samples at 20Hz, and the jerk window is 5 seconds, W_n is calculated as 100. The calculated values are stored in the EMA-jerk buffer with the same type and size as the acceleration buffer. Before the sum of the jerk values are calculated, the model checks to confirm that the buffer is not empty. The sum of all the values in the EMA-jerk buffer is then calculated and the output made available for the other functions.

The dynamic threshold makes use of GPS speed data (section 3.2.3). The lateral threshold is set as 0.21G if GPS data is unavailable. The longitudinal threshold is set as 0.35G since it is not dependant on the speed. If occupancy data is available, the threshold is reduced according to the total occupants present in the taxi. After the thresholds were

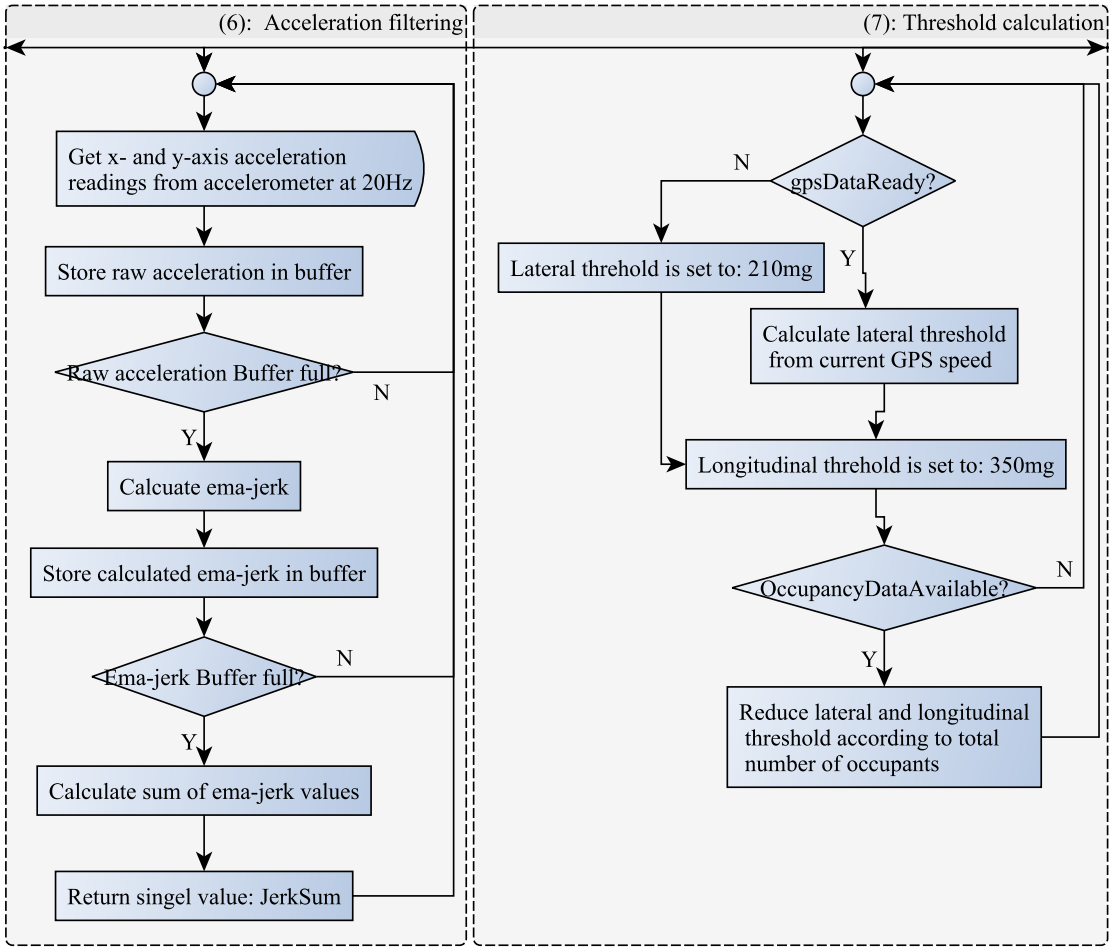

Figure A.3: Acceleration filtering (6) and threshold calculation (7) flow diagram.

calculated, it is made available to the other functions to be used in the reckless detection function shown in Figure A.4.

In the reckless detection function, the filtered acceleration values are firstly compared to an accident threshold (0.8G) and then to the corresponding threshold. The difference between the threshold and the acceleration value is calculated and compared to the reckless driving table (Table 3.3 on page 44) that assigns the reckless level value. From studied data, the results show that new reckless events do not occur after each other in less than 10 seconds. The prototype has therefore been implemented with a function that calculates the maximum reckless level in the 10 seconds interval after the first threshold crossing, in that event. This prevents the system from reading a single event as multiple reckless events. If an event has a very long duration and is still above the threshold after 10 seconds, the event is stored as two reckless events. The highest level value is determined in the 10 seconds by comparing each new level value with the current highest, storing the highest between the two values.

When the acceleration threshold is exceeded, and 10 seconds have passed since the beginning of the previous reckless event, *newErraticEcentAllowed* will be true and the

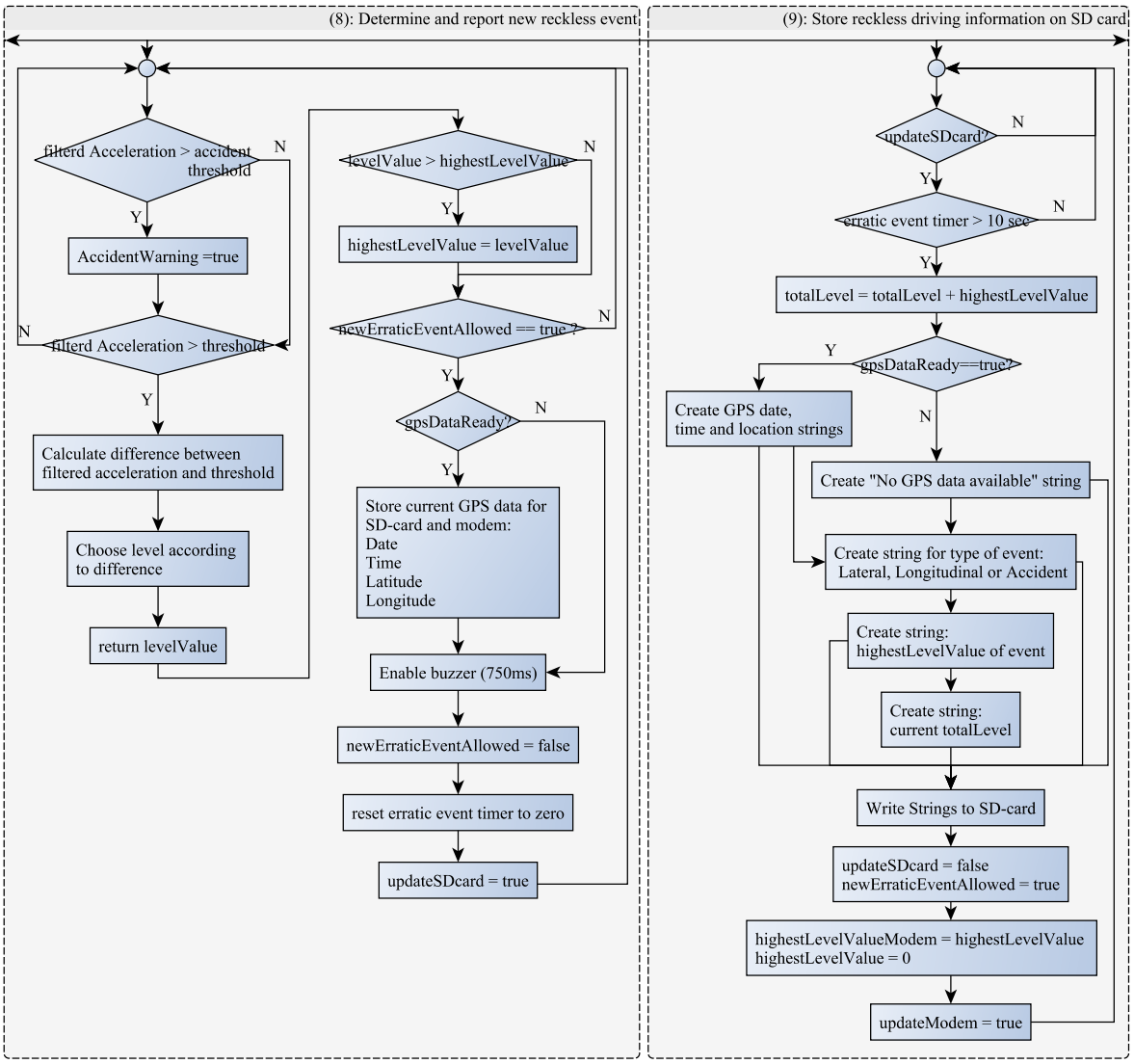

Figure A.4: Function (8) is the flow diagram of the how a reckless event is determined. The left half is when acceleration exceeds the threshold and the right half shows how a new event is handled. Function (9) shows how the information is stored on the SD-card.

current GPS information is stored. The information is stored in two structures: one for the SD-card and the other for the GSM modem. The GPS data included are the current date, time and location. A warning alarm, in the form of a buzzer, gives a warning when the driver is performing an illegal manoeuvre. The *newErraticEcentAllowed* flag is set to false to indicate that the system is currently in a reckless event, and the update SD-card function is enabled (*updateSDcard* = true).

Figure A.4's flow diagram on the right shows the function for the storage of reckless driving information on the SD-card. In this function, the *erraticEventTimer* monitors the elapsed duration of the event, from the beginning of the event when the acceleration first crossed the threshold, as previously discussed. The *erraticEventTimer* therefore grants the function permission to store the information on the SD-card. The GPS information,

stored on the SD-card structure, is converted into strings and written to the SD-card. The following reckless driving information is stored on the SD-card: the type of event (longitudinal or lateral), level (highest level value for the specific event type) and the total level value. The boolean variable, *newErraticEventAllowed*, is set as *true*, to indicate that the event has reached an end, and new reckless events can be detected. Other variables are also reset, preparing for the next reckless driving event. A boolean variable, *updateModem*, grants the modem permission to send the information onto the online platform.

Figure A.5 shows the GSM modem's function, which updates the online platform with information from the sensing system. Figure A.5 is a flow diagram of the Gateway unit's modem function. The GSM modem sends information, in 15 second intervals, to

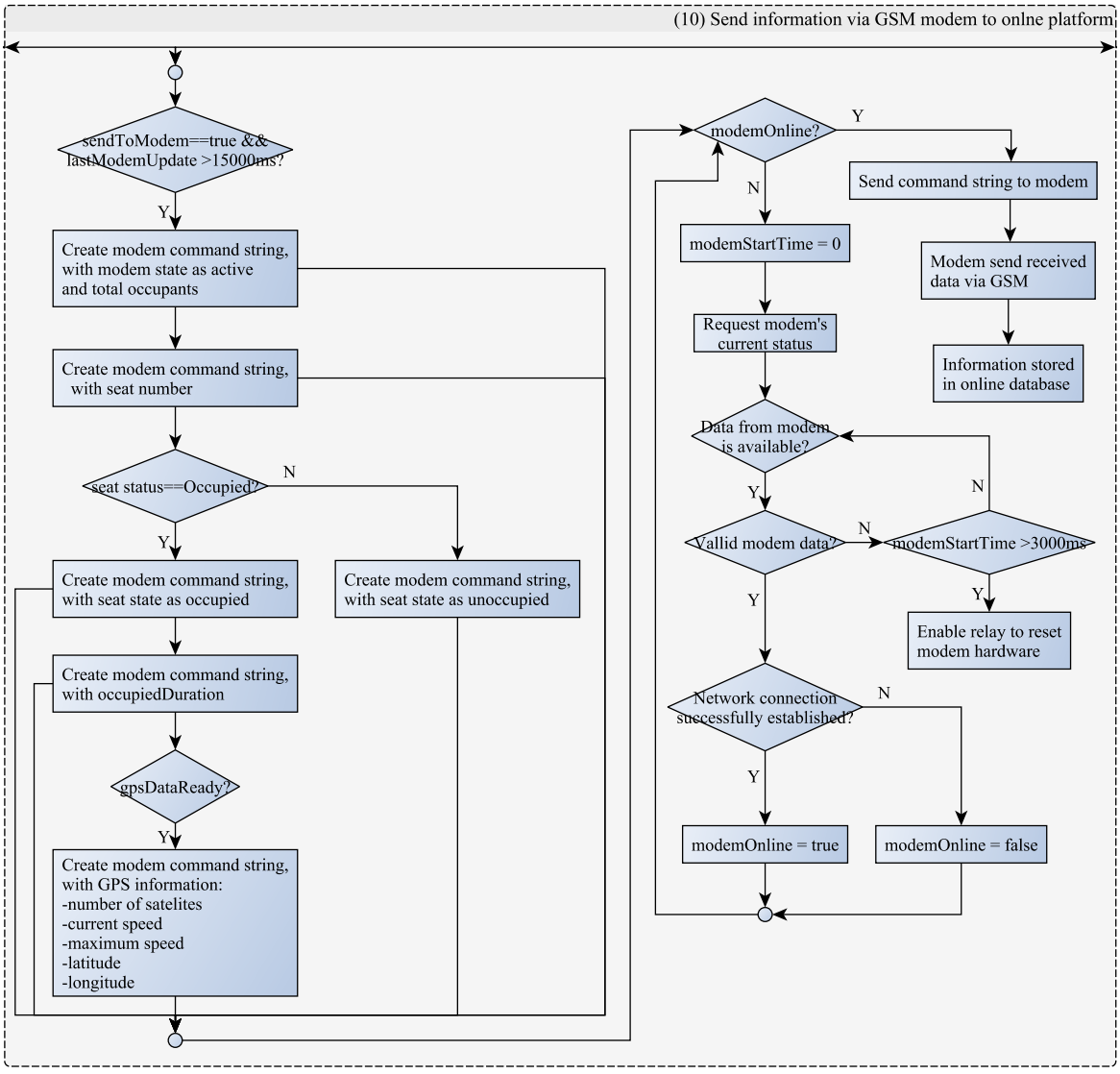

Figure A.5: Flow diagram of the Gateway unit's GSM modem function, which updates the platform with information from the sensing system.

the online platform, which is stored on an online database. The information contains,

modem status, occupancy, location, and travelling speed information. The occupancy information included are the seat number, the seat's state (occupied or unoccupied), and the duration that the seat is currently occupied (when available). The speed information includes the maximum travelling speed and the current travelling speed. The numbers of active satellites in use are also included for development purposes since the satellites gives an idea on the accuracy of the GPS information. The modem will only update if a valid ZigBee packet has arrived with seat status update information. The modem state also informs the online platform that the prototype is active and that new information is available.

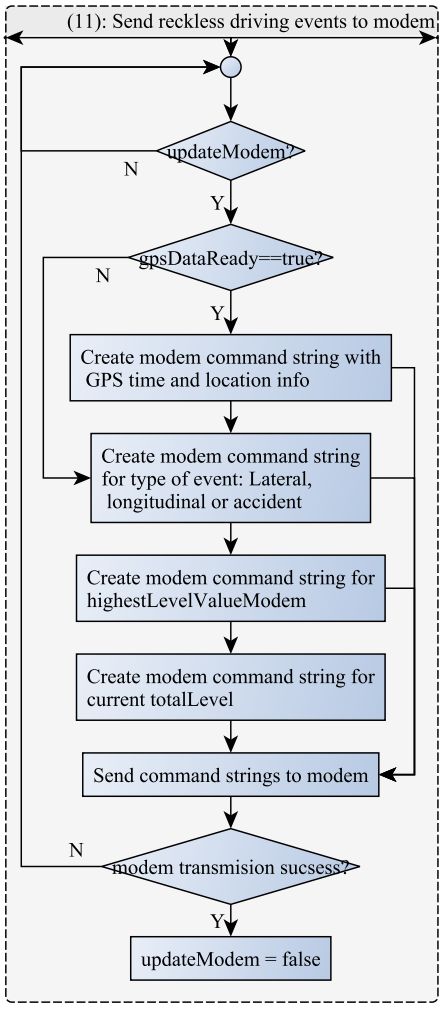

Figure A.6: Flow diagram of the GSM modem function that sends the detected reckless driving events to the online platform.

The flow diagram on the right in Figure A.5, shows the transmission procedure for the GSM modem function. The GSM modem communicates with an online platform where the transmitted data is stored on a database. Data variables were created with an *asset model* to specify the information's storage location on the data base. These variables can

be accessed from the platform, and is used to create the visual online dashboard. If the GSM modem is online (connection established with the online platform), the occupancy and GPS information strings are sent serially to the GSM modem as AT commands (Command Prompt commands). These commands contain the sensed information from the prototype, and its data base storage location defined by the asset model. If the GSM modem is offline an AT command is sent, requesting a status update from the GSM modem in order to re-establish communication. When a network connection is successfully established the information is resent. The modem is reset if no network connection could be established after 3 seconds. In Figure A.6, the GSM modem function can be seen, which sends the detected reckless driving events to the online platform. The enabled GSM modem function checks for available GPS information, which was determined in the GPS function. The GPS information gives the time and location where the reckless event took place. A modem command string is created and sent to the modem, containing the type of event, its level and the current total level. In the case of unsuccessful transmission, the modem will resend the command string ensuring that every new reckless event is stored on the online database.

Appendix B

Circuit Diagram

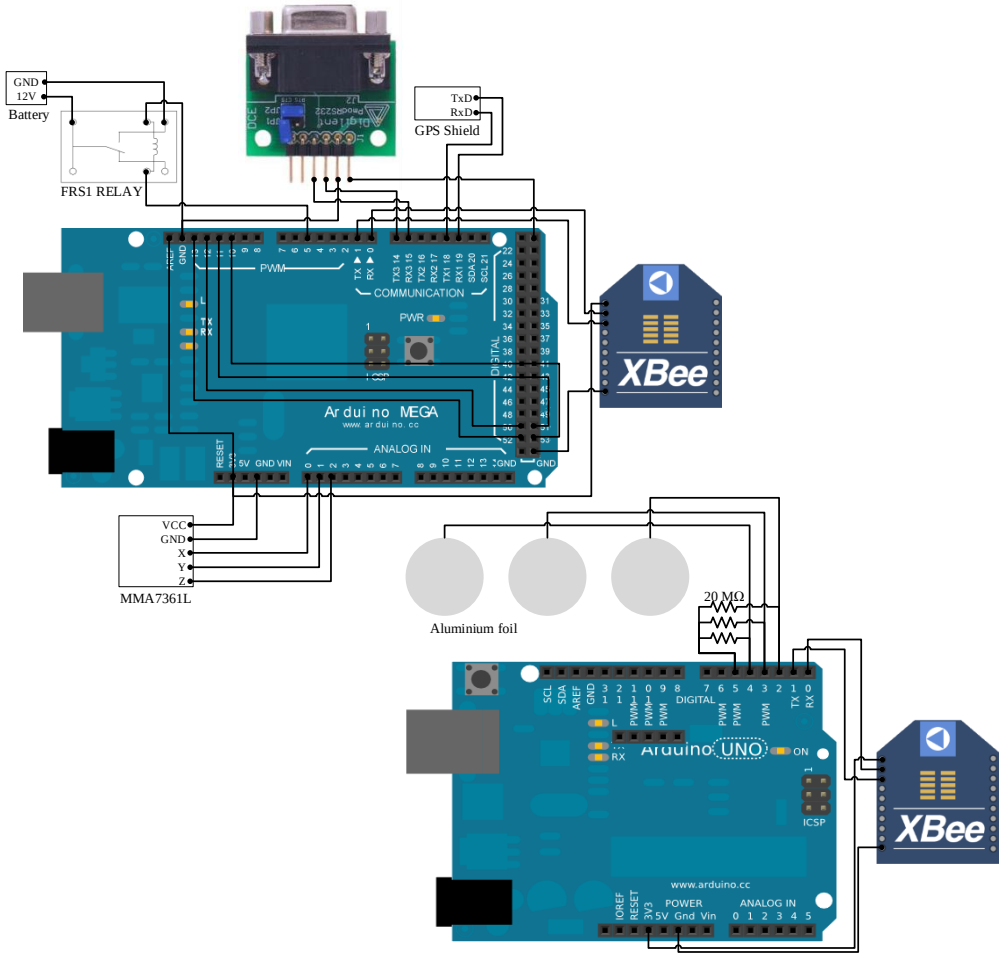

Figure B.1: System circuit diagram.

References

[1] K. Chen and J. C. Miles, "Its handbook 2004: Recommendations from the world road association (piarc)," 2004. 1

[2] W. R. Black, *Sustainable transportation: problems and solutions.* Guilford Press, 2010. 1

[3] L. Figueiredo, I. Jesus, J. Machado, J. Ferreira, and J. de Carvalho, "Towards the development of intelligent transportation systems," in *Intelligent Transportation Systems, 2001. Proceedings. 2001 IEEE*, 2001, pp. 1206–1211. 1

[4] United States, Federal Transit Administration, "Advanced public transportation systems: The state of the art – update 2000," U.S. Department of Transportation, Tech. Rep., 2000. [Online]. Available: http://ntl.bts.gov/lib/jpodocs/repts_te/13583.pdf 1

[5] ISO. (2013, Aug.) ISO/TC 204 Intelligent transport systems. [Online]. Available: http://www.iso.org/iso/iso_technical_committee?commid=54706 1.1

[6] SANRAL, "Gauteng freeway improvement project," http://www.nra.co.za/live/content.php?Category_ID=58. 1.1

[7] Arrive Alive campaign. (2008, Sep.) Minibus taxis and road safety. [Online]. Available: www.arrivealive.co.za/pages.aspx?i=2850 1.1.1

[8] World Health Organization, "Status report on road safety in countries of the who african region," 2009. 1.1.1

[9] E. Kopits and M. Cropper, "Traffic fatalities and economic growth," *Accident Analysis & Prevention*, vol. 37, no. 1, pp. 169–178, 2005. 1.1.1

[10] Koos van Zyl and Jonathan Myers, "Introducing its in unsibsidised public transport." in *12th Conference on Competition and ownership in land passenger transport. Durban, South Africa*, September 2011. 1.1.1

[11] Trans-Africa Consortium, "Overview of public transport in sub-saharan africa," 2008. 1.1.1

[12] Transport Education Training Authority, "Overview," http://www.teta.org.za/Chambers/Taxi/overview.shtml. 1.1.1

[13] Mercatus, "Taxing alternatives: Poverty alleviation and the south african taxi/minibus industry," http://mercatus.org/sites/default/files/publication/Taxi_Policy_Series.pdf. 1.1.1

[14] UK Drivers, "Bus drivers' eu hours rules," www.ukdrivers.com/bus_hours.asp. 1.1.1

[15] A.S. Zeeman, "Video of a trip in an urban taxi." http://goo.gl/X8FP0. 1.1.1

[16] Institute for Road Safety Research, The Netherlands. (2010, Jul.) Swov fact sheet – intelligent transport systems (its) and road safety. [Online]. Available: http://www.swov.nl/rapport/Factsheets/UK/FS_ITS_UK.pdf 1.2

[17] ——. (2010, Feb.) Swov fact sheet – electronic stability control (esc). [Online]. Available: http://www.swov.nl/rapport/Factsheets/UK/FS_ESC_UK.pdf 1.2

[18] K. Persad, C. M. Walton, and S. Hussain, "Electronic vehicle identification: Industry standards, performance, and privacy issues," Tech. Rep., 2007. 1.2

[19] W. H. Taylor, "Collision avoidance system," Sep. 28 1993, uS Patent 5,249,157. 1.2

[20] Y.-L. Chen, B.-F. Wu, H.-Y. Huang, and C.-J. Fan, "A real-time vision system for nighttime vehicle detection and traffic surveillance," *Industrial Electronics, IEEE Transactions on*, vol. 58, no. 5, pp. 2030–2044, 2011. 1.2, 2.1.3

[21] S. G. Klauer, T. A. Dingus, V. L. Neale, J. D. Sudweeks, and D. J. Ramsey, "The impact of driver inattention on near-crash/crash risk: An analysis using the 100-car naturalistic driving study data," Tech. Rep., 2006. 1.2

[22] G. Rill, *Road vehicle dynamics: fundamentals and modeling*. CRC Press, 2012. 1.2

[23] T. Toledo, O. Musicant, and T. Lotan, "In-vehicle data recorders for monitoring and feedback on drivers' behavior," *Transportation Research Part C: Emerging Technologies*, vol. 16, no. 3, pp. 320–331, 2008. 1.2

[24] R. Elvik, P. Christensen, and A. Amundsen, "Speed and road accidents," *An evaluation of the Power Model. TØI report*, vol. 740, p. 2004, 2004. 1.2

[25] L. Aarts and I. van Schagen, "Driving speed and the risk of road crashes: A review," *Accident Analysis & Prevention*, vol. 38, no. 2, pp. 215 – 224, 2006. [Online]. Available: http://www.sciencedirect.com/science/article/pii/S0001457505001247 1.2

[26] N. J. Garber and L. A. Hoel, *Traffic and highway engineering.* Thomson Engineering, 2009. 1.5, 3.2.3.1, 3.11, 3.2.3.1

[27] Institute for Road Safety Research, The Netherlands. (2011, Dec.) Swov fact sheet – alcolock. [Online]. Available: http://www.swov.nl/rapport/Factsheets/UK/FS_Alcolock.pdf 2.1, 2.1.1

[28] International Transport Forum. (2003, Oct.) Road safety: Impact of new technologies. Paris. [Online]. Available: http://www.internationaltransportforum.org/Pub/pdf/03SRnewTech.pdf 2.1, 2.1.3

[29] Transport - European Commission. (2006, Jan.) Cost-benefit assessment and prioritisation of vehicle safety technologies. [Online]. Available: http://ec.europa.eu/transport/roadsafety_library/publications/vehicle_safety_technologies_final_report.pdf 2.1, 2.1.1, 2.1.3

[30] M. Plöchl and J. Edelmann, "Driver models in automobile dynamics application," *Vehicle System Dynamics*, vol. 45, no. 7-8, pp. 699–741, 2007. 2.1, 2.1.4

[31] J. A. Jang, H. S. Kim, and H. B. Cho, "Smart roadside system for driver assistance and safety warnings: Framework and applications," *Sensors*, vol. 11, no. 8, pp. 7420–7436, 2011. 2.1

[32] S. Tokoro, K. Kuroda, A. Kawakubo, K. Fujita, and H. Fujinami, "Electronically scanned millimeter-wave radar for pre-crash safety and adaptive cruise control system," in *Intelligent Vehicles Symposium, 2003. Proceedings. IEEE*, 2003, pp. 304–309. 2.1.2

[33] R. Filjar, K. Vidovic, P. Britvic, and M. Rimac, "ecall: Automatic notification of a road traffic accident," in *MIPRO, 2011 Proceedings of the 34th International Convention.* IEEE, 2011, pp. 600–605. 2.1.2

[34] O. Carsten and F. Tate, "Intelligent speed adaptation: accident savings and cost–benefit analysis," *Accident Analysis & Prevention*, vol. 37, no. 3, pp. 407 – 416, 2005. [Online]. Available: http://www.sciencedirect.com/science/article/pii/S0001457504001174 2.1.3

[35] P. I. Wouters and J. M. Bos, "Traffic accident reduction by monitoring driver behaviour with in-car data recorders," *Accident Analysis & Prevention*, vol. 32, no. 5, pp. 643–650, 2000. 2.1.3

[36] J. Hickman and E. Geller, "Self-management to increase safe driving among short-haul truck drivers," *Journal of Organizational Behavior Management*, vol. 23, no. 4, pp. 1–20, 2005. 2.1.3

[37] D. Johnson and M. Trivedi, "Driving style recognition using a smartphone as a sensor platform," in *Intelligent Transportation Systems (ITSC), 2011 14th International IEEE Conference on*, oct. 2011, pp. 1609 –1615. 2.1.3, 2.1, 2.2, 2.1.4

[38] R. M. Ishtiaq Roufa, H. Mustafaa, S. O. Travis Taylora, W. Xua, M. Gruteserb, W. Trappeb, and I. Seskarb, "Security and privacy vulnerabilities of in-car wireless networks: A tyre pressure monitoring system case study," in *19th USENIX Security Symposium, Washington DC*, 2010, pp. 11–13. 2.1.3

[39] W.-L. Hsu, H.-Y. Liao, B.-S. Jeng, and K.-C. Fan, "Real-time traffic parameter extraction using entropy," *Vision, Image and Signal Processing, IEE Proceedings* -, vol. 151, no. 3, pp. 194–202, 2004. 2.1.3

[40] M.-C. Huang and S.-H. Yen, "A real-time and color-based computer vision for traffic monitoring system," in *Multimedia and Expo, 2004. ICME '04. 2004 IEEE International Conference on*, vol. 3, 2004, pp. 2119–2122 Vol.3. 2.1.3

[41] G. Gritsch, N. Donath, B. Kohn, and M. Litzenberger, "Night-time vehicle classification with an embedded, vision system," in *Intelligent Transportation Systems, 2009. ITSC '09. 12th International IEEE Conference on*, 2009, pp. 1–6. 2.1.3

[42] Y. Wakabayashi and M. Aoki, "Traffic flow measurement using stereo slit camera," in *Intelligent Transportation Systems, 2005. Proceedings. 2005 IEEE*, 2005, pp. 198–203. 2.1.3

[43] R. Grace and S. Steward, "Drowsy driver monitor and warning system," in *International driving symposium on human factors in driver assessment, training and vehicle design*, vol. 8, 2001, pp. 201–208. 2.1.3

[44] F. Sterzer and G. S. Kaplan, "Dual mode automobile collision avoidance radar," Jan. 11 1977, uS Patent 4,003,049. 2.1.3

[45] E. Dagan, O. Mano, G. Stein, and A. Shashua, "Forward collision warning with a single camera," in *Intelligent Vehicles Symposium, 2004 IEEE*, 2004, pp. 37–42. 2.1.3

[46] G. Widman, W. A. Bauson, and S. W. Alland, "Development of collision avoidance systems at delphi automotive systems," in *Proc. Int. Conf. Intelligent Vehicles*. Citeseer, 1998, pp. 353–358. 2.1.3

[47] B. Fleming, "New automotive electronics technologies [automotive electronics]," *Vehicular Technology Magazine, IEEE*, vol. 7, no. 4, pp. 4–12, 2012. 2.1.3

[48] C. T. Chen and Y. S. Chen, "Real-time approaching vehicle detection in blind-spot area," in *Intelligent Transportation Systems, 2009. ITSC '09. 12th International IEEE Conference on*, 2009, pp. 1–6. 2.1.3

[49] S. Glaser, L. Nouveliere, and B. Lusetti, "Speed limitation based on an advanced curve warning system," in *Intelligent Vehicles Symposium, 2007 IEEE*, 2007, pp. 686–691. 2.1.3

[50] D. Shinar and I. Oppenheim, "Review of models of driver behaviour and development of a unified driver behaviour model for driving in safety critical situations," in *Human Modelling in Assisted Transportation*. Springer, 2011, pp. 215–223. 2.1.4

[51] N. Oliver and A. Pentland, "Graphical models for driver behavior recognition in a smartcar," in *Intelligent Vehicles Symposium, 2000. IV 2000. Proceedings of the IEEE*. IEEE, 2000, pp. 7–12. 2.1, 2.2, 2.1.4

[52] N. Dapzol, "Driver's behaviour modelling using the hidden markov model formalism," in *ECTRI Young researchers seminar, The Hague, the Netherlands*, 2005. 2.1, 2.2, 2.1.4

[53] J. M. Nigro and M. Rombaut, "Idres: A rule-based system for driving situation recognition with uncertainty management," *Information Fusion*, vol. 4, no. 4, pp. 309 – 317, 2003. [Online]. Available: http://www.sciencedirect.com/science/article/pii/S1566253503000423 2.1, 2.2, 2.1.4

[54] V. Di Lecce and M. Calabrese, "Nn-based measurements for driving pattern classification," in *Instrumentation and Measurement Technology Conference, 2009. I2MTC'09. IEEE*. IEEE, 2009, pp. 259–264. 2.1, 2.2, 2.1.4

[55] T. Imkamon, P. Saensom, P. Tangamchit, and P. Pongpaibool, "Detection of hazardous driving behavior using fuzzy logic," in *Electrical Engineering/Electronics, Computer, Telecommunications and Information Technology, 2008. ECTI-CON 2008. 5th International Conference on*, vol. 2. IEEE, 2008, pp. 657–660. 2.1, 2.2, 2.1.4

[56] P. Mohan, V. N. Padmanabhan, and R. Ramjee, "Nericell: rich monitoring of road and traffic conditions using mobile smartphones," in *Proceedings of the 6th ACM conference on Embedded network sensor systems*. ACM, 2008, pp. 323–336. 2.1, 2.2, 2.1.4

[57] H. Eren, S. Makinist, E. Akin, and A. Yilmaz, "Estimating driving behavior by a smartphone," in *Intelligent Vehicles Symposium (IV), 2012 IEEE*, june 2012, pp. 234 –239. 2.1, 2.2, 2.1.4

[58] J. Dai, J. Teng, X. Bai, Z. Shen, and D. Xuan, "Mobile phone based drunk driving detection," in *Pervasive Computing Technologies for Healthcare (PervasiveHealth), 2010 4th International Conference on-NO PERMISSIONS*, march 2010, pp. 1 –8. 2.1, 2.2, 2.1.4

[59] J. Castellanos, A. Susin, and F. Fruett, "Embedded sensor system and techniques to evaluate the comfort in public transportation," in *Intelligent Transportation Systems (ITSC), 2011 14th International IEEE Conference on*, oct. 2011, pp. 1858 –1863. 2.1, 2.2, 2.1.4

[60] Z. Zhu, G. Xu, B. Yang, D. Shi, and X. Lin, "Visatram: A real-time vision system for automatic traffic monitoring," *Image and Vision Computing*, vol. 18, no. 10, pp. 781–794, 2000. 2.2

[61] T. J. Schousek, "Vehicle occupant restraint with seat pressure sensor," Dec. 12 1995, uS Patent 5,474,327. 2.2.1

[62] F. Zeidler, V. Petri, R. Mickeler, and M. Meyer, "Device for detecting seat occupancy in a motor vehicle," Mar. 18 1997, uS Patent 5,612,876. 2.2.1

[63] K. Kikuo, K. Kanamori, and R. Masuda, "Distribution type tactile sensor," Apr. 30 1991, uS Patent 5,010,774. 2.2.1

[64] Delphi. (2009, Dec.) Delphi passive occupant detection system-b. [Online]. Available: http://delphi.com/manufacturers/auto/safety/passive/oc/pods/ 2.2.1

[65] M. Devy, A. Giralt, and A. Marin-Hernandez, "Detection and classification of passenger seat occupancy using stereovision," in *Intelligent Vehicles Symposium, 2000. IV 2000. Proceedings of the IEEE*, 2000, pp. 714–719. 2.2.2

[66] S. Wender and O. Loehlein, "A cascade detector approach applied to vehicle occupant monitoring with an omni-directional camera," in *Intelligent Vehicles Symposium, 2004 IEEE*, 2004, pp. 345–350. 2.2.2

[67] H. Kong, Q. Sun, W. Bauson, S. Kiselewich, P. Ainslie, and R. Hammoud, "Disparity based image segmentation for occupant classification," in *Computer Vision and Pattern Recognition Workshop, 2004. CVPRW'04. Conference on.* IEEE, 2004, pp. 126–126. 2.2.2

[68] M. M. Trivedi, S. Y. Cheng, E. M. C. Childers, and S. J. Krotosky, "Occupant posture analysis with stereo and thermal infrared video: Algorithms and experimental evaluation," *Vehicular Technology, IEEE Transactions on*, vol. 53, no. 6, pp. 1698–1712, 2004. 2.2.2

[69] E. N. Dalal, P. Paul, L. K. Mestha, and A. S. Islam, "Vehicle occupancy detection via single band infrared imaging," Jun. 6 2013, uS Patent 20,130,141,574. 2.2.2

[70] P. R. Devarakota, M. Castillo-Franco, R. Ginhoux, B. Mirbach, and B. Ottersten, "Occupant classification using range images," *Vehicular Technology, IEEE Transactions on*, vol. 56, no. 4, pp. 1983–1993, 2007. 2.2.2

[71] J. G. Stanley, R. A. Stopper Jr, and J. G. Mcdonnell, "Occupant sensor," Dec. 24 2008, eP Patent 1,373,030. 2.2.2, 2.2.3

[72] R. Wimmer, "Capacitive sensors for whole body interaction," *Whole Body Interaction*, pp. 121–133, 2011. 2.2.3, 2.2.3

[73] L. K. Baxter, "Capacitive sensors," *Ann Arbor*, vol. 1001, p. 48109, 2000. 2.2.3

[74] J. Smith, T. White, C. Dodge, J. Paradiso, N. Gershenfeld, and D. Allport, "Electric field sensing for graphical interfaces," *Computer Graphics and Applications, IEEE*, vol. 18, no. 3, pp. 54–60, 1998. 2.2.3

[75] P. W. Kithil, "Automobile air bag systems," Feb. 11 1997, uS Patent 5,602,734. 2.2.3

[76] P. W. Kithil, M. H. Barron, and W. C. McIntosh, "Motor vehicle occupant sensing systems," Sep. 1 1998, uS Patent 5,802,479. 2.2.3

[77] C. E. Atkins, "High-discrimination antenna array for capacitance-responsive circuits," Jun. 19 1973, uS Patent 3,740,567. 2.2.3

[78] B. George, H. Zangl, T. Bretterklieber, and G. Brasseur, "Seat occupancy detection based on capacitive sensing," *Instrumentation and Measurement, IEEE Transactions on*, vol. 58, no. 5, pp. 1487 –1494, may 2009. 2.2.3, 2.1, 2.2.3, 2.3

[79] D. Tumpold and A. Satz, "Contactless seat occupation detection system based on electric field sensing," in *Industrial Electronics, 2009. IECON'09. 35th Annual Conference of IEEE*. IEEE, 2009, pp. 1823–1828. 2.2.3

[80] B. George, H. Zangl, T. Bretterklieber, and G. Brasseur, "A combined inductive–capacitive proximity sensor for seat occupancy detection," *Instrumentation and Measurement, IEEE Transactions on*, vol. 59, no. 5, pp. 1463–1470, 2010. 2.2.3

[81] Software Technologies Group, Inc. (2013, Aug.) What is ZigBee. [Online]. Available: http://www.stg.com/wireless/ZigBee_def.html 3

[82] R. Faludi, *Building Wireless Sensor Networks: With ZigBee, XBee, Arduino, and Processing*. O'Reilly Media, Inc., 2010. 3

[83] G. Brasseur, "Design rules for robust capacitive sensors," *Instrumentation and Measurement, IEEE Transactions on*, vol. 52, no. 4, pp. 1261–1265, 2003. 3.1

[84] J. Smith, "Electric field imaging," Ph.D. dissertation, Massachusetts Institute of Technology, 1998. 3.1.1

[85] J. Paradiso and N. Gershenfeld, "Musical applications of electric field sensing," *Computer music journal*, vol. 21, no. 2, pp. 69–89, 1997. 3.1.1, 3.1.1

[86] NIST/SEMATECH. (2012, April) e-Handbook of Statistical Methods. [Online]. Available: http://www.itl.nist.gov/div898/handbook/pmc/section3/pmc324.htm 3.1.3

[87] E. Hoch, "Electrode effects in the measurement of power factor and dielectric constant of sheet insulating materials," *Bell System Technical Journal*, vol. 5, p. 555, 1926. 3.1.4

[88] I. Bahl and D. Trivedi, "A designer's guide to microstrip line," *Microwaves*, vol. 16, no. 5, pp. 174 – 176, 1977. 3.1.4

[89] J. I. Reynolds, L. Chrysler, and I. By, "Automotive cushioning through the ages," 2008. 3.1.5

[90] G. Elert. (2012, Aug.) The Physics Hypertextbook - Dielectrics. [Online]. Available: http://physics.info/dielectrics/ 3.1.5

[91] P. Watson, I. Watson, and R. Batt, "Total body water volumes for adult males and females estimated from simple anthropometric measurements," *The American journal of clinical nutrition*, vol. 33, no. 1, pp. 27–39, 1980. 3.1.5

[92] S. Gabriel, R. Lau, and C. Gabriel, "The dielectric properties of biological tissues: III. Parametric models for the dielectric spectrum of tissues," *Physics in medicine and biology*, vol. 41, p. 2271, 1996. 3.1.5

[93] National Center for Statistics and Analysis. (2012, Jul.) Rural/urban comparison - traffic safety facts. [Online]. Available: http://www-nrd.nhtsa.dot.gov/Pubs/811637.pdf 3.2.1

[94] K. Keay and I. Simmonds, "Road accidents and rainfall in a large australian city," *Accident Analysis & Prevention*, vol. 38, no. 3, pp. 445 – 454, 2006. [Online]. Available: http://www.sciencedirect.com/science/article/pii/S0001457505001880 3.2.3

[95] South African National Roads Agency Limited, *geometric design guidelines*. CSIR, 2003. 3.2.3.1, 3.2.3.1

[96] B. Trach. (2003, Sep.) G force. [Online]. Available: http://newton.dep.anl.gov/askasci/phy99/phy99491.htm 3.2.3.1

[97] A. Aashto, "Policy on geometric design of highways and streets," *American Association of State Highway and Transportation Officials, Washington, DC*, 2001. 3.2.3.2

[98] S. C. Walpole, D. Prieto-Merino, P. Edwards, J. Cleland, G. Stevens, and I. Roberts, "The weight of nations: an estimation of adult human biomass," *BMC Public Health*, vol. 12, no. 1, p. 439, 2012. 3.2.4

[99] (2013, Aug.) Arduion. [Online]. Available: http://arduino.cc/en/Guide/Introduction 3.3

[100] *MMA7361L: XYZ AXIS ACCELEROMETER*, Freescale Semiconductor, 2008. [Online]. Available: http://www.freescale.com/files/sensors/doc/data_sheet/MMA7361L.pdf 3.3

[101] *Atmel 8-bit Microcontroller with 4/8/16/32KBytes In-System Programmable Flash*, Atmel, 2012. [Online]. Available: http://www.freescale.com/files/sensors/doc/data_sheet/MMA7361L.pdf 4.1.1

[102] Paul Badger. (2013, Jul.) Capacitive Sensing Library. [Online]. Available: http://playground.arduino.cc//Main/CapacitiveSensor?from=Main.CapSense A.1